University of the Witwatersrand

Masters Dissertation

Hydraulic fracture with Darcy and non-Darcy flow in a porous medium

Student:
Mathibele Willy Nchabeleng

Supervisor:
Dr. A.G. Fareo

A dissertation submitted to the Faculty of Science, University of the Witwatersrand, in fulfilment of the requirements for the degree of Master of Science.

December 2016

Declaration of Authorship

I, Mathibele Willy Nchabeleng, declare that the work in this dissertation is my own unaided work. It is being submitted to the University of the Witwatersrand, Johannesburg, for the degree of Master of Science. It has not been submitted before for any degree or examination at any other university.

Signed: Mathibele Willy Nchabeleng

Date: 12 December 2016

"If we knew what it was we were doing, it would not be called research, would it?"

Albert Einstein

Abstract

This research is concerned with the analysis of a two-dimensional Newtonian fluid-driven fracture in a permeable rock. The fluid flow in the fracture is laminar and the fracture is driven by the injection of a Newtonian fluid into it. Most of the problems in literature involving fluid flow in permeable rock formation have been modeled with the use of Darcy's law. It is however known that Darcy's model breaks down for flows involving high fluid velocity, such as the flow in a porous rock formation during hydraulic fracturing. The Forchheimer flow model is used to describe the non-Darcy fluid flow in the porous medium. The objective of this study is to investigate the problem of a fluid-driven fracture in a porous medium such that the flow in the porous medium is non-Darcy. Lubrication theory is applied to the system of partial differential equations since the fracture that is considered is thin and its width slowly varies along its length. For this same reason, Perkins-Kern-Nordgren approximation is adopted. The theory of Lie group analysis of differential equations is used to solve the nonlinear coupled system of partial differential equations to obtain group invariant solutions for the fracture half-width, leak-off depth and length of the fracture. The strength of fluid leak-off at the fracture wall is classified into three forms, namely, weak, strong and moderate. A group invariant solution of the traveling wave form is obtained and an exact solution for the case in which there is weak fluid leak-off at the interface is found. A dimensionless parameter, F_0, termed the Forchheimer number was obtained and investigated. Numerical results are obtained for both the case of Darcy and non-Darcy flow. Computer generated graphs are used to illustrate the analytical and numerical results.

Acknowledgements

Firstly, I would like to acknowledge and thank my supervisor, Dr. A.G. Fareo, for his support, his excellent guidance, patience and motivation throughout my dissertation, he was a tremendous mentor to me. I am thankful to Prof J Moitsheki for helping me develop my background in symmetry methods.

I would like to acknowledge my parents who have continously encouraged and inspired me to excel in everything I do. I want to thank my brother, Dr. Molefe Nchabeleng, for being a brother to me at all times. I warmly thank my two lovely sisters, Ntheno Nchabeleng and Hunadi Nchabeleng, for their support. I also like to thank my sister-in-law, Mmaphuthego Sebashe, for her encouragement, and Bokamoso Nchabeleng.

I am grateful to Lungelo Mabuza for the moral support that he gave me throughout my research. I have to offer my special thanks to Vuyelwa Makibelo for her hearty support and encouragement. I also acknowledge my friends, Christopher Nchabeleng, Matete Motubatse, Frank Nchabeleng, Ilish Seema, David Kgokolo and Thato Mashigo for their support. A big thank you to Simphiwe Mazibuko for the good times we shared.

Finally, I am very grateful to DST-NRF Centre of Excellence in Mathematical and Statistical Sciences (CoE-MaSS) and the Nedbank Eyethu Community Trust for the financial support during my research. I am thankful to the School of Computer Science and Applied Mathematics (CSAM) at the University of the Witwatersrand for making it possible for me to complete my dissertation. I cannot terminate without thanking the Almighty God, my creator.

Jeremiah 29:11
"For I know the plans I have for you," declares the Lord,
"plans to prosper you and not to harm you,
plans to give you hope and a future."

Contents

List of Figures

To my parents

Chapter 1

INTRODUCTION

1.1 Introduction

The study of rock fractures has been a great part of petroleum and mining engineering for hundreds of years, but it was only in the mid 1940s that the analysis of rock fractures and other materials were developed into an engineering discipline [1]. Fractures are either man-made created by the injection of a viscous fluid from a bore hole into a subsurface reservoir rock in order to increase the production from gas and oil reservoirs, or natural fractures such as kilometers-long volcanic dykes driven by magma coming from the upper mantle beneath the Earth's crust or fissures in rocks in mining opened up by the use of high pressure water [2]. Fluid-driven fracture is significant for the transport of both magma and hydrothermal fluids [3]. The problem of a fluid-driven hydraulic fracture with non-Darcy fluid flow in the rock-mass media arises in petroleum engineering. Fluid flow in a permeable rock formation is mostly described by Darcy's law but it is however known that Darcy's law breaks down when there is high velocity or turbulence. In this dissertation, the problem of a hydraulic fracture propagating in a permeable rock with Darcy and non-Darcy fluid flow will be investigated.

1.2 Hydraulic fracturing

Hydraulic fracturing is a technique widely used in the petroleum and mining industry to open up fractures in rocks. In this technique, a fracture in a rock is propagated by use of high pressured fluid injected into the fracture. Hydraulic fracturing has many applications in engineering, some of which include reservoir stimulation, drilling cuttings, underground caving operations, and contaminated land remediation [4]. If the injected fluid is water then the process is called hydrofracturing [3].

In the past half century a lot has been done in the mathematical modeling of hydraulic fractures. These mathematical models, which estimate the net fluid pressure, opening, size, leak-off and shape of the fracture given the properties of the rock, injection rate and fluid characteristics, have to consider the primary physical mechanisms involved, namely, fracturing or creation of new rock surfaces, leakage of the fracturing fluid into the encompassing permeable rock-mass and flow of the viscous Newtonian fluid into the fracture. The most widely used leak-off model was developed by Carter [5].

A lot of research has been done on fluid-driven fractures in a porous rock formation. Fluid leak-off into the rock formation as well as fluid flow in the porous rock are important in many areas of reservoir engineering which includes hydraulic fracturing. Therefore, accurate description of fluid flow behaviour in a permeable medium is vital to the success of operations in hydraulic fracturing. In describing fluid flow in a porous media, the two widely used models are Carter's leak-off model and Darcy's model [3, 6–8]. The assumptions under which Carter's leak-off model is useful for modeling flow through the porous rock formation are highlighted in [9]. Our interest lies in Darcy and non-Darcy fluid flow model.

1.2.1 Lubrication theory of rocks

Lubrication theory is the analysis of fluid flow in a geometry in which there is inequality between dimensions, that is, one dimension is much smaller than the others. The most important requirement of lubrication theory is that the characteristic fracture half-width, H, be far less than the characteristic fracture length, L. That is,

$$\frac{H}{L} \ll 1. \tag{1.2.1}$$

It is also assumed that

$$Re\left(\frac{H}{L}\right)^2 \ll 1, \tag{1.2.2}$$

where Re is the Reynolds number defined by

$$Re = \frac{UL}{\nu}. \tag{1.2.3}$$

In (1.2.3), U is characteristic fluid velocity in the direction of propagation of the fracture and ν is the fluid kinematic viscosity. Equation (1.2.3) implies that we can neglect the inertia term in the Navier-Stokes equation. When (1.2.1) and (1.2.2) do not hold, lubrication theory breaks down. Elasticity equations can be applied to rocks but it should be noted that the analogous behaviour of rocks is much more complex than the behaviour observed in metals or other engineering materials. Linear elasticity is the most common used form of the stress-strain relationship [9]. Rocks exhibit elastic behaviour under certain stress levels. During the hydraulic fracturing process a rock will fail in a ductile or brittle manner due to the pressure from the injected fluid. A rock exhibits ductile behaviour if it is able to support an increasing load as it deforms. On the other hand, a rock is said to be brittle if the load supported by the rock decreases as the strain increases. The range of stresses in which a rock shows brittle or ductile behaviour depends heavily on the mineralogy, micro-structure, and also on factors such as temperature [10].

1.3 Literature Review

Hydraulic fracturing was introduced in the 1940s and has become of great economic importance and a viable technique for extraction of oil and natural gas from underground. A number of studies have been done on hydraulic fracturing in the past decades. These studies were motivated by the need to understand the dynamics of hydraulic fracturing. A lot of fracture geometry models have been developed since the inception of hydraulic fracturing. The first two-dimensional fracture model was formulated by Khristianovic and Zheltove [11].

Spence et al. [12] considered a problem of elastohydrodynamic cavity flow. The enlargement of a lens-shaped cavity was studied. Barenblatt [13] was the first to apply fracture mechanics to such problems. The fluid flow is modeled by lubrication theory, which gave a nonlinear differential equation relating the pressure and the cavity shape. Solutions for pressure distribution and shape of two-dimensional cavities of volume proportional to t^{α} or $e^{\alpha t}$ were found. Spence et al. [12] discovered that for constant growth rate, the functions of the fracture half-width and pressure depend on the strength of the singularity at the crack tip [12]. The singularity is a property of the medium into which the fracture is propagating.

Fitt et al. [14] found similarity solution for a pre-existing fluid-driven fracture embedded in an impermeable rock. Fareo and Mason [2] extended the model to a hydraulic fracture propagating in a porous rock with one-dimensional fluid leak-off at the fracture faces. Fareo and Mason [2] showed that when the leak-off velocity is proportional to the half-width of the fracture, there are some regions at which there is extraction of the fluid at the entry of the fracture and inflow of fluid at the fracture interface. The case in which the fracturing fluid is non-Newtonian is also considered by Fareo and Mason [15, 16]. Rubin [17] reviewed the propagation of magma-filled fractures.

Kgatle and Mason [18] studied a pre-existing rock fracture with tortuosity in the fluid flow. The tortuous fracture was replaced with a symmetric open fracture without asperities but with a modified Reynolds flow law and modified stress in the fracture. The Perkins-Kern-Nordgren approximation was used. Group invariant solutions for the volume, fracture half-width and length of the fracture were formulated by use of Lie point symmetry analysis. It was found that tortuosity can remove the singularity in the spatial slope of the half-width at the fracture tip of the model fracture and the increase in tortuosity causes the length of a partially open hydraulic fracture to becomes less dependent on the working conditions at the entry of the fracture.

A criterion for non-Darcy fluid flow in a permeable medium was considered by Zeng and Grigg [19]. In the past, the Reynolds and Forchheimer number were the most used components to identify the beginning of non-Darcy flow. In [19], the Forchheimer number was used as a criterion to identify the non-Darcy fluid flow in porous media. The Forchheimer number was chosen because of its direct relation to the non-Darcy effect. Zeng and Grigg [19] discovered that the superficial velocity in the rock-mass formation increases nonlinearly with the Forchheimer number. A generalized Forchheimer flow in a porous medium was considered by Douglas et al. [20].

Andrade et al. [21] considered the inertial effects on fluid flowing through a disordered permeable medium. The Forchheimer fluid flow model was used to describe the fluid flow in the porous medium. A conversion from linear to nonlinear behavior was observed. This transition occurred at high Reynolds numbers, that is when the inertial effects becomes relevant. It was noted that such conversion can be understood and statistically characterized according to the spatial distribution of kinetic energy in the system. Holditch and Morse [22] investigated the effects of a non-Darcy fluid flow on the behavior of hydraulic fractured gas wells. Analysis of multiphase non-Darcy flow in porous media was considered in [23].

Chai et al. [24] considered non-Darcy fluid flow in disordered porous media. Numerical simulations at pore-scales were carried out with the Reynolds number ranging from 0.02 to 30, which covered the Darcy and non-Darcy flow regimes. Three flow regimes of fluid through porous media are identified. At vanishing Reynolds number, a linear Darcy regime is identified and at low but finite Reynolds number a weak inertial regime is identified. Finally, strong inertial regime is identified for high Reynolds number. Chai et al. [24] concluded that there exists a transitional process from one regime to the other. They also discovered that the microscopic inertial effect was the main factor that led to the deviation from Darcy law. Miguel [25] investigated non-Darcy fluid flow in slip and no-slip regimes.

Macini et al. [26] considered non-Darcy flow coefficients in natural and artificial porous media. Experimental results suggested that the inertial coefficient β is affected by pore structure to some extent. Analytical solutions for two-regime flows in wells were considered in [27].

1.4 Basic concepts

A fluid is a continuous medium which cannot sustain a shear stress.

1.4.1 Viscosity

Viscosity is a measure of a fluid's internal friction. A viscous fluid is a fluid that has internal friction, hence it has high resistance to flow. An inviscid or non-viscous fluid is a fluid that has no internal friction. Inviscid fluids do not exist in practice.

1.4.2 Newtonian and non-Newtonian fluids

A fluid whose viscosity remains constant when the rate of flow changes is called a Newtonian fluid. Some examples of Newtonian fluids include air, water, glycerine, honey and most mineral oils. Newtonian fluids obey Newton's Law of Viscosity, which gives a linear relation between shear stress, τ and shear rate, γ, as [28, 29]

$$\tau = \mu\gamma, \tag{1.4.1}$$

where the constant of proportionality μ is the dynamic viscosity. Fluids which are not Newtonian fluids are termed non-Newtonian fluids. Examples of non-Newtonian fluids include shampoo and blood.

1.4.3 Compressible and incompressible fluids

A fluid is compressible if the fluid density changes when high pressure is applied to it. The conservation of mass for a compressible fluid is given by

$$\frac{\partial \rho}{\partial t} + \nabla.(\rho \mathbf{v}) = 0, \tag{1.4.2}$$

where the fluid density is denoted by ρ and fluid velocity by $\mathbf{v}$. An incompressible fluid is the one in which the density of the fluid does not change as it moves along its path-line.

The incompressibility condition is

$$\nabla.\mathbf{v} = 0. \tag{1.4.3}$$

1.4.4 Steady and unsteady flow

A flow is called steady flow if the conditions (velocity, pressure, etc) do not change with time at any point, that is $\frac{\partial}{\partial t} = 0$. A flow in which the conditions change with time at any point in the fluid is described as unsteady.

1.4.5 Laminar and turbulent flow

Laminar flow: A laminar flow is an undisturbed flow.
Turbulent flow: There are random fluctuations and considerable mixing of the fluid. Fluid vorticity is high. Turbulence is a feature of the fluid flow not of the fluid.

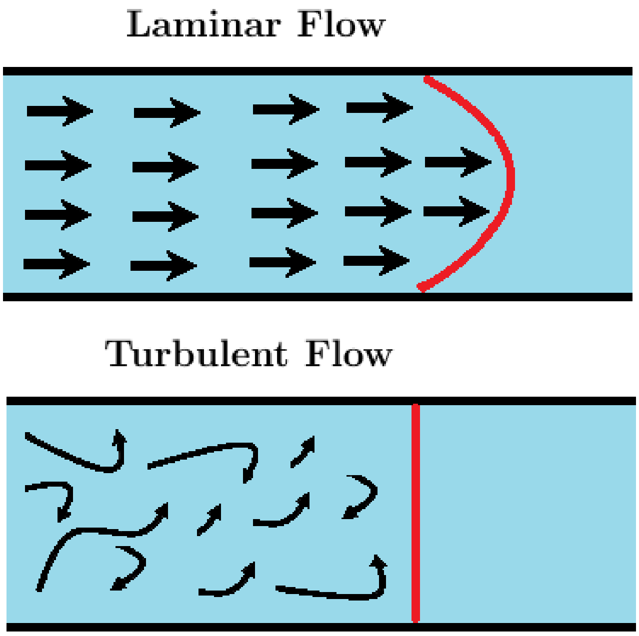

FIGURE 1.4.1: A graphical representation of laminar and turbulent flow.

1.5 Darcy's law and its limitations

Henri Darcy (1856), a French scientist, was concerned with the flow of water through sand filters for water purification. Through his experimental observations he noticed that the flow of fluid is directly proportional to the pressure gradient. Hence, Darcy's law is an empirical relationship based on experimental observations of one-dimensional water flow through packed sands at low velocity. This law aims to describe flow of fluid behavior in a porous medium and according to the law, the pressure gradient driving the flow is linearly proportional to the fluid velocity, denoted volume flux per unit area, in the porous media. Using different theoretical approaches, a lot of effort was made to derive Darcy's law. It was found that Darcy's law is a good approximation in describing fluid flow in a porous media at a limited range of low velocity and low flow rates [9, 30]. Experimentally, fluid flow deviation from Darcy's law have also been noticed [31]. The deviation from Darcy's model is attributed mainly to the effects of inertia, turbulence and other high velocity effects in the porous medium.

In this Masters research, we will extend the analysis of the fluid-driven fracture in a porous medium from the case in which the flow in the porous medium is governed by Darcy's law to the more general case in which the flow in the porous medium is non-Darcy. This research is motivated in light of the non-Darcy behavior of high velocity fluid flow in porous rock media. The first of the two main models for non-Darcy flows is the Brinkman model, which accounts for the microscopic shearing effect between the fluid and the pore walls, given as

$$-\nabla p = \frac{\mu}{\kappa}\mathbf{v} + \mu_e \nabla^2 \mathbf{v}, \qquad \mathbf{v} = (u, v, w), \tag{1.5.1}$$

where p is the fluid pressure, κ is the rock permeability, μ is the dynamic viscosity, μ_e is an effective viscosity and $\mathbf{v}$ is the fluid velocity. The second is the Forchheimer model, accounting for inertial effects and given as

$$-\nabla p = \frac{\mu}{\kappa}\mathbf{v} + \beta\rho\,|\mathbf{v}|\,\mathbf{v}, \qquad |\mathbf{v}| = \sqrt{u^2 + v^2 + w^2}, \tag{1.5.2}$$

where p is the fluid pressure, κ is the rock permeability, μ is the dynamic viscosity, β is the non-Darcy coefficient, $\mathbf{v}$ is the velocity of the fluid and ρ, is the fluid density. In this research, we will focus on the Forchheimer model because of its inertia term.

Various authors have published empirical correlations of the coefficient β with the permeability and porosity of the porous medium [32–34]. It is accepted by most researchers that β is a property of the porous medium. In (1.5.2), when $\beta = 0$, the equation reduce to Darcy's empirical model given by

$$-\nabla p = \frac{\mu}{\kappa}\mathbf{v}. \tag{1.5.3}$$

Equation (1.5.3) will be considered in Chapter 3 to describe the fluid flow in a porous medium with Darcy flow while (1.5.2) will be utilized in Chapter 4 for non-Darcy fluid flow.

1.6 Outline of research

In this dissertation, the aim is to study the problem of a fluid driven hydraulic fracture with Darcy and non-Darcy flow in a porous medium. The two-dimensional PKN model will be used.

In Chapter 2, a brief discussion on the theory of Lie group analysis of differential equations will be made.

In Chapter 3, we study a two-dimensional hydraulic fracture with Darcy flow in the permeable rock mass. We begin the chapter by comparing the order of magnitude of the terms in the Navier-Stokes equation along the x and z direction which allows the simplification of the Navier-Stokes equation. The nonlinear diffusion equation that describes the development of the half-width of the fracture together with the leak-off depth are derived. Dimensionless variables are introduced to non-dimensionalize the system of equations governing the flow of fluid in the fracture. Three cases of fluid leak-off as discussed in [35] are considered. Lie group analysis is used to reduce the system of partial differential equation into a system of ordinary differential equations. Asymptotic behaviour near the tip of the fracture is investigated and numerical solutions for the governing nonlinear ordinary differential equations are obtained and analyzed.

In chapter 4, a two-dimensional hydraulic fracture with non-Darcy fluid flow in the rock-mass media is considered. The Forchheimer flow model is used to describe the fluid flow in the porous medium. The Lie point symmetries and the analysis of the dimensionless system of equations in Chapter 4 are the same as derived in Chapter 3. Numerical solutions for the governing equations are investigated.

Finally, a summary of results and conclusion is given in Chapter 5.

Chapter 2

MATHEMATICAL PRELIMINARIES

2.1 Introduction

The theory of Lie symmetry analysis of differential equations was pioneered by Sophus Lie, a Norwegian mathematician, in the 19th century. This field of study has been extensively studied in the following literature [36–39]. In section 2.2, we briefly look at the theory of Lie symmetry analysis for a system of partial differential equations, an approach that will be used in this dissertation to transform a system of partial differential equations into a system of ordinary differential equations.

2.2 Invariance for a system of partial differential equations

2.2.1 Lie point symmetries

A symmetry of a system of differential equations is a transformation that maps any solution to another solution of the system [36]. We consider a system of N partial differential equations ($N > 1$) with m dependent variables $u = (u^1, u^2, \ldots, u^m)$ and n independent variables $x = (x^1, x^2, \ldots, x^n)$ given by

$$F^{\sigma}(x, u, \partial u, \partial^2 u, \ldots, \partial^k u) = 0, \quad \sigma = 1, 2, \ldots, N, \tag{2.2.1}$$

where $\partial u, \partial^2 u$ up to $\partial^k u$ are collection of all distinct first, second up to kth-order partial derivatives with respect to the n independent variables:

$$\partial u = \left\{ \frac{\partial u^\alpha}{\partial x^j} \right\}, \partial^2 u = \left\{ \frac{\partial^2 u^\alpha}{\partial x^{j_1} \partial x^{j_2}} \right\}, \dots, \partial^k u = \left\{ \frac{\partial^k u^\alpha}{\partial x^{j_1} \partial x^{j_2} \dots \partial x^{j_k}} \right\},$$

where $\alpha = 1, 2, \dots, m$. We look for a one-parameter Lie group of transformations

$$\begin{aligned} \bar{x}^i &= x^i + \epsilon \xi^i(x, u) + O(\epsilon^2), \\ \bar{u}^\alpha &= u^\alpha + \epsilon \eta^\alpha(x, u) + O(\epsilon^2), \end{aligned} \tag{2.2.2}$$

which leaves the system of partial differential equations (2.2.1) invariant. The infinitesimal transformations in (2.2.2) can be represented by the Lie point symmetry generator

$$X = \xi^i(x, u) \frac{\partial}{\partial x^i} + \eta^\alpha(x, u) \frac{\partial}{\partial u^\alpha}. \tag{2.2.3}$$

Equation (2.2.3) is also referred to as the symbol of infinitesimal transformation or infinitesimal operator. To solve the system of partial differential equation (2.2.1), we start by deriving the group invariant solution. We first derive the Lie point symmetry generators of (2.2.1). The Lie point symmetry generators are derived by solving the invariance criterion for the system of partial differential equations (2.2.1), given by

$$X^{[k]} F^\sigma(x, u, \partial u, \partial^2 u, \dots, \partial^k u) \Big|_{\substack{F^1(x,u,\partial u,\partial^2 u,\dots,\partial^k u)=0 \\ \vdots \\ F^\sigma(x,u,\partial u,\partial^2 u,\dots,\partial^k u)=0}} = 0, \tag{2.2.4}$$

for each $\sigma = 1, 2, \dots, N$. Equation (2.2.4) is a system of N determining equations which, after substituting into each, the N partial differential equations (2.2.1) and their differential consequence, are to be solved, for the unknown functions $\xi^i(t, x)$ and $\eta^\alpha(t, x)$. The operator $X^{[k]}$ is called the kth-extended infinitesimal generator of (2.2.3) and it is given by

$$X^{[k]} = \xi^i(x, u) \frac{\partial}{\partial x^i} + \eta^\alpha(x, u) \frac{\partial}{\partial u^\alpha} + \zeta^\alpha_{x^i} \frac{\partial}{\partial u^\alpha_{x^i}} + \dots + \zeta^\alpha_{x^{i_1}, x^{i_2}, \dots, x^{i_k}} \frac{\partial}{\partial u_{x^{i_1}, x^{i_2}, \dots, x^{i_{k-1}}}}, \quad k \geq 1, \tag{2.2.5}$$

where the extended infinitesimals satisfies the following recursion relations

$$\begin{aligned} \zeta^\alpha_{x^i} &= D_{x^i}(\eta^\alpha) - u^\alpha_{x^j} D_{x^i}(\xi^j), \\ \zeta^\alpha_{x^i x^j} &= D_{x^i}(\eta^\alpha) - u^\alpha_{jl} D_{x^i}(\xi^l), \\ \vdots \quad & \quad \vdots \\ \zeta^\alpha_{x^{i_1}, x^{i_2}, \dots, x^{i_k}} &= D_{x^i x^j}(\zeta^\alpha_{x^{i_1}, x^{i_2}, \dots, x^{i_{k-1}}}) - u^\alpha_{x^{i_1}, x^{i_2}, \dots, x^{i_{k-1}}} D_{x^{i_k}}(\xi^l). \end{aligned} \tag{2.2.6}$$

The total derivative operator with respect to the independent variable x is defined by

$$D_i = \frac{\partial}{\partial x^i} + u^\alpha_i \frac{\partial}{\partial u^\alpha} + u^\alpha_{ij} \frac{\partial}{\partial u^\alpha_i} + \dots + u^\alpha_{ii_1, i_2, \dots, i_k} \frac{\partial}{\partial u_{i_1, i_2, \dots, i_k}} + \dots, \quad i = 1, 2, \dots, n. \tag{2.2.7}$$

where

$$u_i^\alpha = \frac{\partial u^\alpha}{\partial x^i}, \quad u_{ij}^\alpha = \frac{\partial^2 u^\alpha}{\partial x^i \partial x^j}, \quad \text{etc.} \tag{2.2.8}$$

The system of determining equations allow us to determine the coefficients $\xi^i(t,x)$ and $\eta^\alpha(t,x)$ of the Lie point symmetry generator. The coefficients of the powers and product of the partial derivatives in each of the partial differential equations in (2.2.4) do not depend on the derivatives of the dependent variable u . Therefore, the determining equations can be separated according to derivatives of the dependent variables u and the coefficient of each derivative set to zero. Typically, the system of q linear homogeneous partial differential equations for the $(n+m)$ coefficient functions ξ^i and η^α is overdetermined since $q > n+m$. Solving the overdetermined system of differential equations produces expressions for the coefficients ξ^i and η^α. These solutions contain a finite number of arbitrary constants. By setting all the constants to zero except one in turn, we obtain all the Lie point symmetry generators admitted by the system of partial differential equations.

2.2.2 Group invariant solution

The symmetry generators found are of the form

$$X_i = \xi_i^1(x,u)\frac{\partial}{\partial x^1} + \cdots + \xi_i^n(x,u)\frac{\partial}{\partial x^n} + \eta_i^1(x,u)\frac{\partial}{\partial u^1} + \cdots + \eta_i^m(x,u)\frac{\partial}{\partial u^m}, \tag{2.2.9}$$

for $i = 1, 2, ..., r$, where r represents the number of Lie point symmetries admitted. A constant multiple of any Lie point symmetry is also a Lie point symmetry, so any linear combination of Lie point symmetries is also a Lie point symmetry. Consider the linear combination of the Lie point symmetry generators in (2.2.9) given by

$$X = c_1 X_1 + c_2 X_2 + c_3 X_3 + ... + c_r X_r, \tag{2.2.10}$$

where $c_i, i = 1, 2, ...r$ are constants. The function $u = \Theta(x^1, x^2, \ldots, x^n)$ is an invariant solution of the system of partial differential equations (2.2.1) if and only if $u = \Theta(x)$ satisfies:

(i) $X(u^\sigma - \Theta^\sigma(x)) = 0$ when $u^\sigma = \Theta^\sigma(x), \quad \sigma = 1, 2, \ldots, m.$

(ii) $F^\sigma(x, u, \partial u, \partial^2 u, \ldots, \partial^k u) = 0$, when $u = \Theta(x), \quad \sigma = 1, 2, \ldots, N.$

We obtain the group invariant solution, $u = \Theta(x^1, x^2, \ldots, x^n)$, by solving the equation

$$X(u^\sigma - \Theta^\sigma(x^1, x^2, \ldots, x^n))\big|_{u^\sigma = \Theta^\sigma(x^1, x^2, \ldots, x^n)} = 0. \tag{2.2.11}$$

The group invariant solution is substituted back into the system of partial differential equations to reduce the system of partial differential equations to a system of ordinary differential equations.

2.3 Conclusion

In this chapter, we briefly introduced the theory of Lie group analysis of differential equations. We will use this method to transform the system of partial differential equations into a system of ordinary differential equations.

Chapter 3

TWO-DIMENSIONAL HYDRAULIC FRACTURE WITH DARCY FLOW IN PERMEABLE ROCK-MASS

3.1 Introduction

In this chapter, we will derive a mathematical model for a two-dimensional fluid-driven fracture propagating in a permeable rock formation. A viscous fluid is injected at high pressure to propagate the fracture and a proportion of the fluid leaks into the encompassing rock at the fracture walls. The strength of leak-off at the fracture walls can either be weak, moderate or strong. The fluid flow into the porous rock formation through the interface is modeled using Darcy's law. The flow of fluid inside the fracture is laminar and the fracturing fluid is a viscous incompressible Newtonian fluid. A review of hydraulic fracture modeling has been given by Mendelsohn [40]. The injected fluid causes the fracture to propagate along the positive x-direction, perpendicular to a far field compressive stress. To construct a mathematical model for the fracturing process, both the mechanics of the fluid inside the fracture and the interaction dynamics with the elasticity of the encompassing rock are considered. Lubrication theory will be used to model the fluid flow inside the thin fracture [28].

3.2 Thin fluid film equations for fluid flow in the fracture

In this section, the thin fluid film equations for the fluid flow in the two-dimensional fracture will be derived. A two-dimensional hydraulic fracture propagating in a permeable elastic medium is considered. Figure 3.2.1 gives a two-dimensional hydraulic fracture with leak-off depth $b(t,x)$. The two-dimensional fracture is symmetrical about the x-axis and identical in every plane y=constant and evolves under plane strain. The fracture boundaries are given by $z = -h(t,x)$ at the lower surface and $z = h(t,x)$ at the upper surface. The flow of fluid inside the fracture is described by the conservation of

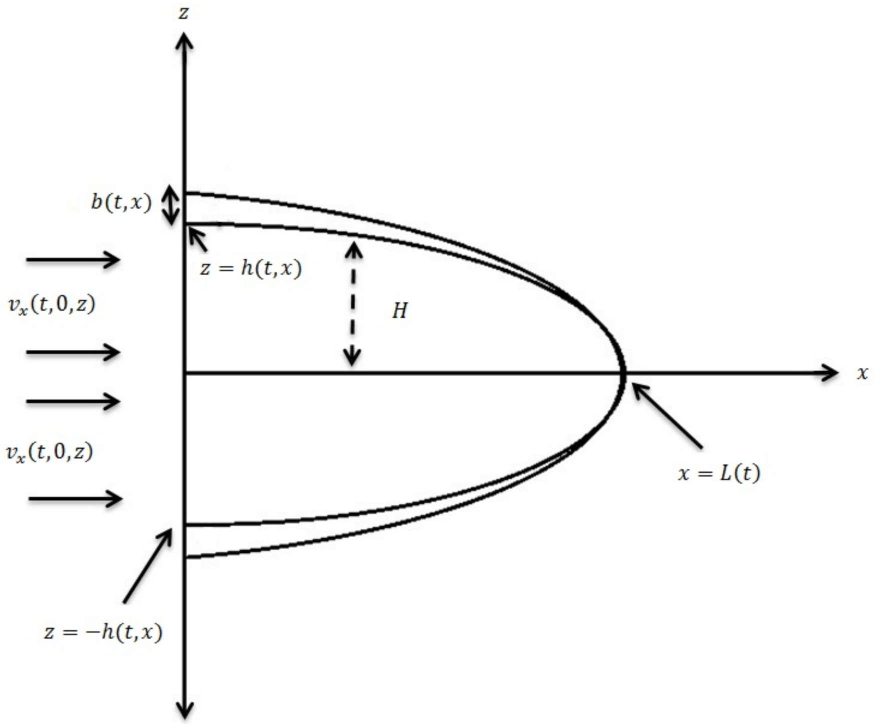

FIGURE 3.2.1: A schematic representation of a hydraulic fracture in an elastic porous medium, where $b(t,x)$ represents the fluid leak-off depth, $h(t,x)$ the fracture half-width and $L(t)$ the fracture length.

mass equation

$$\nabla.\mathbf{v} = 0, \tag{3.2.1}$$

and the Navier-Stokes equation

$$\rho\frac{\partial \mathbf{v}}{\partial t} + \rho(\mathbf{v}\cdot\nabla)\mathbf{v} = -\nabla p + \mu\nabla^2\mathbf{v}, \tag{3.2.2}$$

where ρ is the fluid density, $\mathbf{v} = (v_x(t,x,z), 0, v_z(t,x,z))$ is the fluid velocity, $p(t,x,z)$ is the fluid pressure, and μ, the viscosity. The body force is neglected. To simplify (3.2.1) and (3.2.2) for a fracture whose width is much less than its length we compare the order of magnitude of the terms in the Navier-Stokes equation along the x and z-direction. To compare the order of magnitude, we first introduce characteristic quantities and their justification:

- the characteristic length of the fracture L
- the characteristic fracture half-width H
- the characteristic fluid velocity along the fracture U
- the characteristic fluid velocity across the fracture $W = \frac{UH}{L}$
- the characteristic penetration depth of the fluid in the porous medium B
- the characteristic fluid pressure $P = \frac{\mu UL}{H^2}$
- the characteristic time of the process T

We first justify the expression for the characteristic velocity across the fracture. We express (3.2.1) in Cartesian form as

$$\frac{\partial v_x}{\partial x} + \frac{\partial v_z}{\partial z} = 0. \tag{3.2.3}$$

The order of magnitude of the conservation of mass equation (3.2.3) is given by

$$\frac{U}{L} + \frac{W}{H} \sim 0. \tag{3.2.4}$$

Thus, we can express W as

$$W \sim \frac{UH}{L}. \tag{3.2.5}$$

Consider the x-component of the Navier-Stokes equation, given by

$$\rho \frac{Dv_x}{Dt} = -\frac{\partial p}{\partial x} + \mu \left[\frac{\partial^2 v_x}{\partial x^2} + \frac{\partial^2 v_x}{\partial z^2} \right]. \tag{3.2.6}$$

The orders of magnitude of the viscous terms and inertial term are

$$\frac{\partial^2 v_x}{\partial x^2} \sim \frac{U}{L^2}, \qquad \frac{\partial^2 v_x}{\partial z^2} \sim \frac{U}{H^2} \qquad \text{and} \qquad \frac{Dv_x}{Dt} \sim \frac{U}{T}. \tag{3.2.7}$$

Therefore, the order of magnitude of the terms in (3.2.6) is

$$\rho \frac{U}{T} \sim -\frac{P}{L} + \mu \left(\frac{U}{L^2} + \frac{U}{H^2} \right). \tag{3.2.8}$$

Since $H \ll L$ from equation (1.2.1), then

$$\frac{U}{L^2} \ll \frac{U}{H^2}. \tag{3.2.9}$$

Therefore, we can approximate the viscous term to be $\frac{\mu U}{H^2}$ and equation (3.2.8) can be written as

$$\rho \frac{U}{T} \sim -\frac{P}{L} + \frac{\mu U}{H^2}. \tag{3.2.10}$$

The ratio of the order of magnitude of the inertial term and the viscous term is

$$\frac{\text{inertial term}}{\text{viscous term}} = \frac{\rho U}{T} \div \frac{\mu U}{H^2} = \frac{U^2}{L} \times \frac{H^2}{\nu U} = Re \cdot \left(\frac{H}{L}\right)^2 \cdot \frac{L}{TU}. \tag{3.2.11}$$

Since U is the characteristic fluid speed in the fracture, regardless of whether the interface is permeable or not, the characteristic time of the hydraulic fracture process is taken to be the fracture opening time, which, if the fluid leak-off through the interface is ignored, is $T = \frac{L}{U}$. If, however, the fluid leak-off at the fracture interface cannot be ignored, as in the present case, we have $T \gg \frac{L}{U}$ [35]. Equation (3.2.10) therefore reduces to

$$P \sim \frac{\mu U L}{H^2}. \tag{3.2.12}$$

Hence the inertial term can be ignored and the Navier-Stokes equation along the x-direction in dimensional form becomes

$$\frac{1}{\rho}\frac{\partial p}{\partial x} = \nu \frac{\partial^2 v_x}{\partial z^2}. \tag{3.2.13}$$

Consider now the Navier-Stokes equation along z-direction

$$\rho \frac{D v_z}{Dt} = -\frac{\partial p}{\partial z} + \mu \left[\frac{\partial^2 v_z}{\partial x^2} + \frac{\partial^2 v_z}{\partial z^2}\right]. \tag{3.2.14}$$

The order of magnitude of the partial derivative expressions in the viscous term is given by

$$\frac{\partial^2 v_z}{\partial x^2} \sim \frac{W}{L^2} = \frac{UH}{L^3} = \frac{U}{L^2} \times \left(\frac{H}{L}\right) \qquad \text{and} \qquad \frac{\partial^2 v_z}{\partial z^2} \sim \frac{W}{H^2} = \frac{UH}{LH^2} = \frac{U}{H^2} \times \left(\frac{H}{L}\right). \tag{3.2.15}$$

Since (1.2.1) is satisfied, $\frac{U}{L^2} \ll \frac{U}{H^2}$. The order of magnitude of the pressure gradient is now compared to the order of magnitude of the inertial term and the dominant viscous term. That is,

$$\frac{\text{inertial term}}{\text{pressure gradient term}} = \frac{\rho U}{T} \div \frac{\mu U L}{H^3} = Re \cdot \left(\frac{H}{L}\right)^2 \cdot \frac{H}{UT} \leq Re \cdot \left(\frac{H}{L}\right)^3. \tag{3.2.16}$$

Since either $UT \sim L$ or $UT \gg L$, the ratio is $\mathcal{O}\left(\frac{H}{L}\right)^3$. Similarly,

$$\frac{\text{viscous term}}{\text{pressure gradient term}} = \frac{\mu U H}{LH^2} \div \frac{\mu U L}{H^3} = \left(\frac{H}{L}\right)^2 \ll 1. \tag{3.2.17}$$

Hence, along the z-direction,

$$\frac{\partial p}{\partial z} = 0. \tag{3.2.18}$$

The Navier-Stokes and continuity equations in dimensional form reduce to

$$\frac{\partial v_x}{\partial x} + \frac{\partial v_z}{\partial z} = 0, \tag{3.2.19}$$

$$\frac{\partial p}{\partial x} = \mu \frac{\partial^2 v_x}{\partial z^2}, \tag{3.2.20}$$

$$\frac{\partial p}{\partial z} = 0. \tag{3.2.21}$$

The two-dimensional conservation of mass equation remains unchanged after utilization of the thin fluid film approximation. Equations (3.2.20) and (3.2.21) are the x-component and z-component of the Navier-Stokes equation in the thin fluid film approximation in dimensional form.

3.3 Governing equations

3.3.1 Elasticity model

At the interface $z = h(t, x)$, from Cauchy's formula relating the stress vector to the stress tensor, we have for the lubrication approximation,

$$\sigma_{zz} = -p_f(t, x) + 2\mu \frac{\partial v_z}{\partial z} \qquad \text{on} \qquad z = h(t, x). \tag{3.3.1}$$

Expressed in terms of dimensionless variables,

$$\bar{\sigma}_{zz} = -\bar{p}_f + 2\left(\frac{H}{L}\right)^2 \frac{\partial \bar{v}_z}{\partial \bar{z}} \qquad \text{on} \qquad \bar{z} = \bar{h}(t, x). \tag{3.3.2}$$

Neglecting the term of order $\left(\frac{H}{L}\right)^2$, we have for the lubrication approximation in dimensional form

$$\sigma_{zz}(t, x, z) = -p_f(t, x) \qquad \text{on} \qquad z = h(t, x). \tag{3.3.3}$$

That is, the normal stress at the crack wall, which is negative, is supported entirely by the fluid pressure $p_f(t, x)$. Fitt et al. [41] when considering geothermal reservoir, used the relation due to Spence and Sharp [12]:

$$\sigma_{zz} - \sigma_{zz}^{\infty} = \frac{G}{\pi(1-\nu)} \int_{-L(t)}^{L(t)} \frac{\partial h(t, s)}{\partial s} \frac{\mathrm{d}s}{(s - x)}, \tag{3.3.4}$$

where σ_{zz} is the elastic normal stress along the fracture walls, σ_{zz}^{∞} is the normal stress at infinity within the rock-mass, G is the elastic shear modulus, ν is the Poisson's ratio and $\frac{G}{(1-\nu)}$ is defined as the elastic stiffness of the rock, a measure of resistance of rock to deformation. For a one-sided fracture propagating along the positive x-direction where $0 \leq x \leq L(t)$, we will use the Perkins-Kern-Nordgren approximation [8] which is used widely in the petroleum industry and given as:

$$p = \Lambda h, \qquad \Lambda = \frac{E_0}{(1-\sigma_1^2)B_0}, \tag{3.3.5}$$

where E_0 is the Young's modulus, σ_1 is the Poisson ratio and B_0 is the unit breadth along the y-direction. The net pressure of the fluid

$$p = p_f + \sigma_{zz}^{\infty}, \tag{3.3.6}$$

must be positive for the fracture to propagate. In (3.3.6), p_f is the pressure of the fluid inside the fracture and $-\sigma_{zz}^{\infty}$ is the far field compressive stress.

3.3.2 Fluid flow in the porous medium

The flow of fluid through a permeable medium was derived by Darcy and is called Darcy's equation. In the equation, Darcy relates the flux of fluid per unit area to the pressure gradient. If Q is the volume flow rate and A is the cross-sectional area, then

$$\frac{Q}{A} = -\frac{\kappa}{\mu}\nabla p_d, \tag{3.3.7}$$

where μ is the dynamic viscosity, κ is the rock permeability and p_d is the fluid pressure driving the fluid that has leaked-off through the interface. Equation (3.3.7) in the $z-$direction, given that $\frac{Q}{A} = v_\ell = \frac{\partial b}{\partial t}$, becomes

$$\frac{\partial p_d}{\partial z} = -\frac{\mu}{\kappa}\frac{\partial b}{\partial t}. \tag{3.3.8}$$

The leak-off depth $b(t,x)$ is measured relative to the interface. The velocity of the interface is small compared with the leak-off velocity and is neglected in (3.3.8). Integrating (3.3.8) with respect to z from h to $h+b$, we obtain

$$p_d(t,x,h+b) - p_d(t,x,h) = -\frac{\mu}{\kappa}b\frac{\partial b}{\partial t}. \tag{3.3.9}$$

Using the boundary condition for pressure, given as

$$p_d(t,x,h+b) = 0 \qquad \text{and} \qquad p_d(t,x,h) = p(t,x) = \Lambda h, \tag{3.3.10}$$

equation (3.3.9) becomes

$$\frac{\partial b}{\partial t} = \frac{\Lambda\kappa}{\mu}\frac{h}{b}. \tag{3.3.11}$$

3.3.3 Boundary and Initial conditions

Boundary conditions

The boundary conditions at the fracture interface are the no-slip condition for a viscous fluid at a solid boundary and the leak-off condition. The velocity of leaked-off fluid at the interface is denoted by $\frac{\partial b}{\partial t}$ and is measured relative to the fracture interface in the perpendicular direction to the interface. We refer to $\frac{\partial b}{\partial t}$ as the leak-off velocity. The boundary conditions are as follows:

No-slip condition

$$z = h(t,x): \qquad v_x(t,x,h(t,x)) = 0, \tag{3.3.12}$$

$$z = -h(t,x): \qquad v_x(t,x,-h(t,x)) = 0. \tag{3.3.13}$$

Leak-off condition

$$z = h(t,x): \quad v_z(t,x,h(t,x)) = \frac{\partial h}{\partial t} + v_x(t,x)\frac{\partial h}{\partial x} + v_l(t,x) = \frac{\partial h}{\partial t} + \frac{\partial b}{\partial t}, \tag{3.3.14}$$

$$z = -h(t,x): \quad v_z(t,x,-h(t,x)) = -\frac{\partial h}{\partial t} - v_x(t,x)\frac{\partial h}{\partial x} - v_l(t,x) = -\left(\frac{\partial h}{\partial t} + \frac{\partial b}{\partial t}\right), \tag{3.3.15}$$

since $v_x(t,\pm h(t,x)) = 0$ from the no slip boundary condition (3.3.12) and (3.3.13). Also, at $z = 0$

$$\frac{\partial v_x}{\partial z} = 0. \tag{3.3.16}$$

Initial conditions

The initial conditions are

$$t = 0: \qquad L(0) = 1, \qquad h(0,0) = 1. \tag{3.3.17}$$

The initial conditions in (3.3.17) are imposed because the length scale along the fracture is the initial length of the fracture and that across the fracture is the initial half-width at the fracture entry. The rock-mass has a pre-existing fracture:

$$t = 0: \qquad h(0,x) = h_0(x), \qquad h_0(0) = 1, \qquad b(0,x) = b_0(x), \qquad 0 \le x \le L(t). \tag{3.3.18}$$

At the fracture nose

$$x = L(t): \qquad h(t, L(t)) = 0, \qquad b(t, L(t)) = 0. \tag{3.3.19}$$

In the next section, we will derive the nonlinear partial differential equation relating the fracture half-width $h(t, x)$ and the leak-off velocity $\frac{\partial b}{\partial t}$ by using equations governing the fluid flow in the fracture (3.2.19)-(3.2.21), the equation describing the fluid flow in the porous medium (3.3.11) and the boundary conditions (3.3.12)-(3.3.15).

3.4 Nonlinear diffusion equation

The governing equations together with the boundary equations are in dimensional form. From equation (3.2.21), $p = p(x, t)$. We derive the expression for $v_x(x, z, t)$ from (3.2.20) using the no-slip conditions (3.3.12)-(3.3.13). By integrating equation (3.2.20) twice with respect to z, we obtain

$$\mu v_x = \frac{1}{2}\frac{\partial p}{\partial x} z^2 + \Upsilon(t, x) z + \Phi(t, x), \tag{3.4.1}$$

where $\Upsilon(t, x)$ and $\Phi(t, x)$ are arbitrary functions. Applying the no-slip boundary conditions (3.3.12) and (3.3.13) gives the following expression:

$$v_x(t, x, z) = \frac{1}{2\mu}\frac{\partial p}{\partial x}\left[z^2 - h^2\right]. \tag{3.4.2}$$

The width-averaged fluid velocity, $\bar{v}_x(t, x)$, is defined by

$$\bar{v}_x(t, x) = \frac{1}{2h}\int_{-h}^{h} v_x(t, x, z) \mathrm{d}z. \tag{3.4.3}$$

Substituting (3.4.2) into (3.4.3), we obtain

$$\bar{v}_x = -\frac{h^2}{3\mu}\frac{\partial p}{\partial x}. \tag{3.4.4}$$

Integrating the conservation of mass equation (3.2.19) with respect to z from $z = -h$ to $z = h$ gives

$$v_z(t, x, h) - v_z(t, x, -h) + \int_{-h}^{h} \frac{\partial v_x(t, x, z)}{\partial x} \mathrm{d}z = 0. \tag{3.4.5}$$

Applying the leak-off conditions (3.3.14) and (3.3.15) on equation (3.4.5), we obtain

$$2\left(\frac{\partial h}{\partial t} + \frac{\partial b}{\partial t}\right) + \int_{-h}^{h} \frac{\partial v_x(t, x, z)}{\partial x} \mathrm{d}z = 0. \tag{3.4.6}$$

Using the Leibnitz integral rule [42] and the no-slip boundary conditions (3.3.12) and (3.3.13), the integral term of equation (3.4.6), is

$$\int_{-h}^{h} \frac{\partial \upsilon_x(t,x,z)}{\partial x} dz = \frac{\partial}{\partial x} \int_{-h}^{h} \upsilon_x(t,x,z)\mathrm{d}z. \tag{3.4.7}$$

Equations (3.4.6) becomes, using (3.4.3)

$$\frac{\partial h}{\partial t} + \frac{\partial}{\partial x}(h\bar{\upsilon}_x) = -\frac{\partial b}{\partial t}. \tag{3.4.8}$$

Substituting the PKN approximation (3.3.5) into (3.4.4) yields

$$\bar{\upsilon}_x = -\frac{\Lambda h^2}{3\mu}\frac{\partial h}{\partial x}. \tag{3.4.9}$$

The equations governing the fluid flow in the fracture with Darcy flow into the rock-mass formation, in dimensional form, are given by, using (3.4.9)

$$\frac{\partial h}{\partial t} - \frac{\Lambda}{3\mu}\frac{\partial}{\partial x}\left(h^3\frac{\partial h}{\partial x}\right) = -\frac{\Lambda\kappa}{\mu}\frac{h}{b}, \tag{3.4.10}$$

$$\frac{\partial b}{\partial t} = \frac{\Lambda\kappa}{\mu}\frac{h}{b}. \tag{3.4.11}$$

3.5 Analysis of the dimensionless system of equations

We introduce the following dimensionless variables

$$\bar{x} = \frac{x}{L}, \qquad \bar{z} = \frac{z}{H}, \qquad \bar{t} = \frac{t}{T}, \qquad \bar{\bar{\upsilon}}_x = \frac{\bar{\upsilon}_x}{U}, \qquad \bar{\upsilon}_z = \frac{L}{HU}\upsilon_z, \qquad \bar{h} = \frac{h}{H},$$
$$\bar{b} = \frac{b}{B}, \qquad \bar{p} = \frac{pH^2}{\mu L U}, \qquad \bar{V} = \frac{V}{HL}, \tag{3.5.1}$$

where, as defined in Section 3.2, L is the characteristic length of the fracture, H is the characteristic fracture width and U is the characteristic fluid velocity along the fracture. A new length scale, denoted by B, is the characteristic leak-off depth of the fluid.

Consider first equation (3.4.9), which when non-dimensionalized yields

$$\bar{\bar{\upsilon}}_x = -\frac{\Lambda}{3\mu}\frac{H^3}{UL}\bar{h}^2\frac{\partial \bar{h}}{\partial \bar{x}}. \tag{3.5.2}$$

By choosing $U = \frac{\Lambda}{\mu}\frac{H^3}{L}$, (3.5.2) becomes, dropping the overhead bars,

$$\bar{\upsilon}_x = -\frac{1}{3}h^2\frac{\partial h}{\partial x}. \tag{3.5.3}$$

Using the fact that $U = \frac{\Lambda}{\mu}\frac{H^3}{L}$ and by substituting the dimensionless variables in (3.5.1) into (3.4.10) and (3.4.11), equations (3.4.10) and (3.4.11) in dimensionless form become

$$\Omega\frac{\partial h}{\partial t} - \frac{\partial}{\partial x}\left(h^3\frac{\partial h}{\partial x}\right) + \frac{1}{\Gamma}\frac{h}{b} = 0, \tag{3.5.4}$$

$$\frac{\partial b}{\partial t} - \frac{h}{b} = 0, \tag{3.5.5}$$

where

$$\Omega = \frac{3HL}{UTH}, \quad \Gamma = \frac{UTH}{3BL} \quad \text{and} \quad B = \left[\frac{\Lambda\kappa}{\mu}HT\right]^{\frac{1}{2}}. \tag{3.5.6}$$

In the dimensionless parameter Ω, $\frac{HL}{UTH}$ is equal to the ratio of the fracture volume to the volume of the fluid that enters into the fracture during the characteristic time of the process and in the dimensionless parameter Γ, $\frac{UTH}{BL}$ can be taken as the ratio of the characteristic volume flow rate into the fracture to the characteristic volume flow rate of the fluid that leaks out at the fracture faces into the porous medium. In [43], Fareo and Mason derived a nonlinear diffusion equation with a leak-off term v_ℓ. The form of this leak-off velocity is determined from the invariance of the nonlinear diffusion equation under a one-parameter Lie group of transformation. Equation (3.5.5) for the leak-off velocity $\frac{\partial b}{\partial t}$ agrees with the form for v_ℓ derived in [43]. We now consider the following three cases [35]:

I. Weak fluid leak-off at the interface: $\Omega \sim 1$ and $\Gamma \gg 1$. Then there will be no term containing the dimensionless parameter Γ in (3.5.4), hence b will not be considered in (3.5.4). However b remains moderate and defined by (3.5.5).
II. Strong fluid leak-off at the interface: $\Omega \ll 1$ and $\Gamma \sim 1$. In this case, (3.5.4) does not contain a term with the dimensionless number Ω.
III. Moderate fluid leak-off at the interface: $\Omega \sim 1$ and $\Gamma \sim 1$. This is the general case for consideration.

From (3.5.1), the characteristic pressure is

$$P = \frac{\mu LU}{H^2}. \tag{3.5.7}$$

In (3.5.2), we chose

$$U = \frac{\Lambda}{\mu}\frac{H^3}{L}. \tag{3.5.8}$$

Then, by substituting (3.5.8) into (3.5.7), we obtain another expression for the characteristic pressure P, given as

$$P = \Lambda H. \tag{3.5.9}$$

Equation (3.3.5) in non-dimensional form is

$$P\bar{p} = \Lambda H\bar{h}, \tag{3.5.10}$$

which after using (3.5.9) becomes, dropping the overhead bars

$$p(t,x) = h(t,x). \tag{3.5.11}$$

We now derive the global mass balance equation. The global mass balance equation relates the rate of change of the total volume of the fracture to the volume of fluid injected into the fracture and the volume of fluid that has leaked-off at the fracture interface. The total volume of the fracture , $V(t)$, is

$$V(t) = 2\int_0^{L(t)} h(t,x)\ \mathrm{d}x, \tag{3.5.12}$$

and the total volume flux of the fluid in the x-direction along the fracture, $q_1(t,x)$, is

$$q_1(t,x) = 2\int_0^{h(t,x)} v_x(t,x,z)\mathrm{d}z. \tag{3.5.13}$$

At the fracture entry, $x = 0$, the rate of fluid flow into the fracture is given by

$$q_1 = \int_{-h(t,0)}^{h(t,0)} v_x(t,0,z)\mathrm{d}z = 2\int_0^{h(t,0)} v_x(t,0,z)\mathrm{d}z. \tag{3.5.14}$$

The flow rate of the fluid that has leaked-off is given by

$$q_2 = 2\int_0^{L(t)} v_\ell(t,x)\mathrm{d}x. \tag{3.5.15}$$

The global mass balance equation can be written as

$$\begin{aligned} \frac{dV}{dt} &= q_1 - q_2 \\ &= 2\int_0^{h(t,0)} v_x(t,0,z)\mathrm{d}z - 2\int_0^{L(t)} v_\ell(t,x)\mathrm{d}x \end{aligned} \tag{3.5.16}$$

where $\frac{dV}{dt}$ is the rate of change of the total volume of the fracture. Using (3.4.3) and (3.5.3), (3.5.16) becomes

$$\begin{aligned} \frac{dV}{dt} &= -2h^3(t,0)\frac{\partial h(t,0)}{\partial x} - 2\int_0^{L(t)} \frac{\partial b}{\partial t}\mathrm{d}x \\ &= -2h(t,0)\bar{v}_x(t,0) - 2\int_0^{L(t)} \frac{\partial b}{\partial t}\mathrm{d}x \end{aligned} \tag{3.5.17}$$

Substituting the dimensionless variables in (3.5.1) into (3.5.17), we obtain

$$\frac{HL}{T}\frac{d\bar{V}}{d\bar{t}} = -2UH\bar{v}_x\bar{h} - 2\frac{BL}{T}\int_0^{\bar{L}(\bar{t})}\frac{\partial\bar{b}}{\partial\bar{t}}\mathrm{d}\bar{x}. \tag{3.5.18}$$

Dividing through by UH and dropping the overhead bars, we obtain

$$\Omega\frac{dV}{dt} = -2h^3(t,0)\frac{\partial h(t,0)}{\partial x} - 2\left(\frac{1}{\Gamma}\right)\int_0^{L(t)}\frac{\partial b}{\partial t}\mathrm{d}x. \tag{3.5.19}$$

We are to solve the following system of equations

$$\Omega\frac{\partial h}{\partial t} - \frac{\partial}{\partial x}\left(h^3\frac{\partial h}{\partial x}\right) + \frac{1}{\Gamma}\frac{h}{b} = 0, \tag{3.5.20}$$

$$\frac{\partial b}{\partial t} = \frac{h}{b}, \tag{3.5.21}$$

for $h(t,x)$ and $b(t,x)$ subject to the boundary conditions at the tip of the fracture

$$h(t,L(t)) = 0, \qquad b(t,L(t)) = 0, \tag{3.5.22}$$

and the mass balance law

$$\Omega\frac{dV}{dt} = -2h^3(t,0)\frac{\partial h(t,0)}{\partial x} - 2\left(\frac{1}{\Gamma}\right)\int_0^{L(t)}\frac{\partial b}{\partial t}\mathrm{d}x. \tag{3.5.23}$$

At the fracture tip,

$$q_1(t,L(t)) = -2h^3(t,L(t))\frac{\partial h}{\partial x}(t,L(t)). \tag{3.5.24}$$

The total volume flux may not vanish at the tip of the fracture since there is fluid leak-off into the rock-mass. In Section 3.6, the group invariant solution for the fracture half-width $h(t,x)$ and the leak-off depth $b(t,x)$ will be derived using Lie symmetry analysis.

3.6 Lie point symmetries and group invariant solutions

The group invariant solution of the system of partial differential equations (3.5.20) and (3.5.21) is the solution left invariant under a continuous one-parameter symmetry group. The Lie point symmetry generator

$$X = \xi^1(t,x,b,h)\frac{\partial}{\partial t} + \xi^2(t,x,b,h)\frac{\partial}{\partial x} + \eta^1(t,x,b,h)\frac{\partial}{\partial b} + \eta^2(t,x,b,h)\frac{\partial}{\partial h}, \tag{3.6.1}$$

of the system of partial differential equations (3.5.20) and (3.5.21) is derived by solving the determining equations

$$X^{[2]}\left(\Omega h_t - h^3 h_{xx} - 3h^2(h_x)^2 + \frac{1}{\Gamma}\frac{h}{b}\right)\Bigg|_{\substack{\Omega h_t - h^3 h_{xx} - 3h^2(h_x)^2 + \frac{1}{\Gamma}\frac{h}{b}=0 \\ b_t - \frac{h}{b}=0}} = 0, \tag{3.6.2}$$

$$X^{[2]}\left(b_t - \frac{h}{b}\right)\Bigg|_{\substack{\Omega h_t - h^3 h_{xx} - 3h^2(h_x)^2 + \frac{1}{\Gamma}\frac{h}{b}=0 \\ b_t - \frac{h}{b}=0}} = 0, \tag{3.6.3}$$

for ξ^1, ξ^2, η^1 and η^2 where $X^{[2]}$ is the second prolongation of the Lie point symmetry generator X, given by

$$\begin{aligned} X^{[2]} = X + \zeta_1^1\frac{\partial}{\partial b_t} + \zeta_2^1\frac{\partial}{\partial b_x} + \zeta_{12}^1\frac{\partial}{\partial b_{tx}} + \zeta_{11}^1\frac{\partial}{\partial b_{tt}} + \zeta_{22}^1\frac{\partial}{\partial b_{xx}} + \dots \\ \zeta_1^2\frac{\partial}{\partial h_t} + \zeta_2^2\frac{\partial}{\partial h_x} + \zeta_{12}^2\frac{\partial}{\partial h_{tx}} + \zeta_{11}^2\frac{\partial}{\partial h_{tt}} + \zeta_{22}^2\frac{\partial}{\partial h_{xx}}. \end{aligned} \tag{3.6.4}$$

Partial differentiation is denoted by subscripts, where

$$\begin{aligned} \zeta_i^1 &= D_i(\eta^1) - b_t D_i(\xi^1) - b_x D_i(\xi^2) \qquad i = 1,2 \\ \zeta_i^2 &= D_i(\eta^2) - h_t D_i(\xi^1) - h_x D_i(\xi^2) \qquad i = 1,2 \\ \zeta_{i,j}^1 &= D_j(\zeta_i^1) - b_{it} D_j(\xi^1) - b_{ix} D_j(\xi^2) \qquad i,j = 1,2 \\ \zeta_{i,j}^2 &= D_j(\zeta_i^2) - h_{it} D_j(\xi^1) - h_{ix} D_j(\xi^2) \qquad i,j = 1,2 \end{aligned} \tag{3.6.5}$$

and

$$\begin{aligned} D_1 = D_t &= \frac{\partial}{\partial t} + b_t\frac{\partial}{\partial b} + h_t\frac{\partial}{\partial h} + b_{tx}\frac{\partial}{\partial b_x} + h_{tx}\frac{\partial}{\partial h_x} + b_{tt}\frac{\partial}{\partial b_t} + h_{tt}\frac{\partial}{\partial h_t} + \dots \\ D_2 = D_x &= \frac{\partial}{\partial x} + b_x\frac{\partial}{\partial b} + h_x\frac{\partial}{\partial h} + b_{xt}\frac{\partial}{\partial b_t} + h_{xt}\frac{\partial}{\partial h_t} + b_{xx}\frac{\partial}{\partial b_x} + h_{xx}\frac{\partial}{\partial h_x} + \dots \end{aligned} \tag{3.6.6}$$

We calculate only ζ_1^1, ζ_1^2, ζ_2^2 and ζ_{22}^2 since the partial differential equations in (3.6.2) and (3.6.3) depend on h, b, b_t, h_t, h_x and h_{xx} . By solving the determining equations in (3.6.2) and (3.6.3), we obtain

$$\begin{aligned} X &= (c_2 + c_3 t)\frac{\partial}{\partial t} + (c_1 + 2c_3 x)\frac{\partial}{\partial x} + c_3 b\frac{\partial}{\partial b} + c_3 h\frac{\partial}{\partial h} \\ &= c_2 X_1 + c_1 X_2 + c_3 X_3 \end{aligned} \tag{3.6.7}$$

where c_1, c_2 and c_3 are constants and

$$\begin{aligned} X_1 &= \frac{\partial}{\partial t} \\ X_2 &= \frac{\partial}{\partial x} \\ X_3 &= t\frac{\partial}{\partial t} + 2x\frac{\partial}{\partial x} + b\frac{\partial}{\partial b} + h\frac{\partial}{\partial h}. \end{aligned} \tag{3.6.8}$$

A complete derivation of the Lie point symmetry generator is given in Appendix A. Two cases of interest will now be discussed. The case $c_3 \neq 0$ and the case $c_3 = 0$. When $c_3 = 0$, the group invariant solution obtained are of the traveling wave form. This is discussed in detail later in Section 3.6.

Case: $c_3 \neq 0$

The group invariant solution $h(t, x)$ and $b(t, x)$ of the system of partial differential equations (3.5.20) and (3.5.21) is obtained by solving

$$\begin{aligned} X(h - \phi(t,x))|_{h=\phi(t,x)} &= 0, \\ X(b - \psi(t,x))|_{b=\psi(t,x)} &= 0, \end{aligned} \tag{3.6.9}$$

that is

$$(c_2 + c_3 t)\frac{\partial \phi}{\partial t} + (c_1 + 2c_3 x)\frac{\partial \phi}{\partial x} = c_3\phi, \tag{3.6.10}$$

$$(c_2 + c_3 t)\frac{\partial \psi}{\partial t} + (c_1 + 2c_3 x)\frac{\partial \psi}{\partial x} = c_3\psi. \tag{3.6.11}$$

The system of first order differential equations of the characteristic curves of (3.6.10) and (3.6.11) are

$$\frac{dt}{c_2 + c_3 t} = \frac{dx}{c_1 + 2c_3 x} = \frac{d\phi}{c_3\phi} = \frac{d\psi}{c_3\psi}, \tag{3.6.12}$$

which equivalently can be written as

$$\frac{dt}{c_2 + c_3 t} = \frac{dx}{c_1 + 2c_3 x}, \quad \frac{dt}{c_2 + c_3 t} = \frac{d\phi}{c_3\phi}, \quad \frac{dt}{c_2 + c_3 t} = \frac{d\psi}{c_3\psi}. \tag{3.6.13}$$

On integrating each of the differential equation in (3.6.13), the invariants are

$$I_1 = \frac{c_1 + 2c_3 x}{2c_3(c_2 + c_3 t)^2}, \quad I_2 = \frac{\phi}{c_2 + c_3 t}, \quad I_3 = \frac{\psi}{c_2 + c_3 t}. \tag{3.6.14}$$

We refer to the constants I_1, I_2 and I_3 as the basis of invariants. The general solutions of (3.6.10) and (3.6.11) are

$$I_2 = F(I_1) \qquad \text{and} \qquad I_3 = G(I_1), \tag{3.6.15}$$

where F and G are arbitrary functions. Hence

$$\phi(t,x) = (c_2 + c_3 t)F(\xi), \tag{3.6.16}$$

$$\psi(t,x) = (c_2 + c_3 t)G(\xi), \tag{3.6.17}$$

where

$$\xi = \frac{c_1 + 2c_3 x}{2c_3(c_2 + c_3 t)^2}. \tag{3.6.18}$$

But since $h(t,x) = \phi(t,x)$ and $b(t,x) = \psi(t,x)$, then (3.6.16) and (3.6.17) becomes

$$h(t,x) = (c_2 + c_3 t)F(\xi), \tag{3.6.19}$$

$$b(t,x) = (c_2 + c_3 t)G(\xi). \tag{3.6.20}$$

We now express the system of differential equations and the boundary equations in terms of variable ξ and the functions $F(\xi)$ and $G(\xi)$. We substitute (3.6.19) and (3.6.20) into (3.5.20) and (3.5.21) for $h(t,x)$ and $b(t,x)$. The system of partial differential equations (3.5.20) and (3.5.21) becomes a system of ordinary differential equation

$$\Omega\left(c_3 F(\xi) - 2c_3\xi\frac{dF(\xi)}{d\xi}\right) - \frac{d}{d\xi}\left(F^3(\xi)\frac{dF(\xi)}{d\xi}\right) + \frac{1}{\Gamma}\frac{F(\xi)}{G(\xi)} = 0, \tag{3.6.21}$$

$$c_3 G(\xi) - 2c_3\xi\frac{dG(\xi)}{d\xi} = \frac{F(\xi)}{G(\xi)}. \tag{3.6.22}$$

We note that both equation (3.6.21) and (3.6.22) do not depend on c_1. Therefore, we can choose $c_1 = 0$ such that $\xi = 0$ when $x = 0$. Equation (3.6.18) becomes

$$\xi = \frac{x}{(c_2 + c_3 t)^2}. \tag{3.6.23}$$

From boundary condition (3.5.22a), for the fracture half-width,

$$F(C) = 0 \qquad \text{where} \qquad C(t) = \frac{L(t)}{(c_2 + c_3 t)^2}. \tag{3.6.24}$$

Differentiating (3.6.24) with respect to t, we obtain

$$\frac{dF}{dC}\frac{dC}{dt} = 0. \tag{3.6.25}$$

Since $F(C)$ is not a constant function, it follows that

$$\frac{dC}{dt} = 0, \tag{3.6.26}$$

which implies

$$C(t) = \frac{L(t)}{(c_2 + c_3 t)^2} = \xi_0, \tag{3.6.27}$$

where ξ_0 is a arbitrary constant. Using the initial condition (3.3.17a), we obtain

$$L(t) = \left(1 + \frac{c_3}{c_2} t\right)^2. \tag{3.6.28}$$

Consider now the mass balance law (3.5.23). Substituting (3.6.19) and (3.6.20) into (3.5.23) and using (3.6.28) gives

$$\Omega \frac{dV}{dt} = -2(c_2 + c_3 t)^2 F^3(0) \frac{dF(0)}{d\xi} - 6c_3 (c_2 + c_3 t)^2 \left(\frac{1}{\Gamma}\right) \int_0^{\frac{1}{c_2^2}} G(\xi) \mathrm{d}\xi. \tag{3.6.29}$$

We now consider the left hand side of the mass balance equation (3.6.29). Using (3.6.19), (3.5.12) becomes

$$V(t) = 2(c_2 + c_3 t)^3 \int_0^{\frac{1}{c_2^2}} F(\xi) \mathrm{d}\xi, \tag{3.6.30}$$

and therefore

$$\frac{dV}{dt} = 6c_3 (c_2 + c_3 t)^2 \int_0^{\frac{1}{c_2^2}} F(\xi) \mathrm{d}\xi. \tag{3.6.31}$$

With (3.6.31), (3.6.29) becomes

$$F^3(0) \frac{dF(0)}{d\xi} = -3c_3 \left[\Omega \int_0^{\frac{1}{c_2^2}} F(\xi) \mathrm{d}\xi + \left(\frac{1}{\Gamma}\right) \int_0^{\frac{1}{c_2^2}} G(\xi) \mathrm{d}\xi\right]. \tag{3.6.32}$$

The mathematical formulation of the problem is summarized as follows

$$\Omega \left(c_3 F(\xi) - 2c_3 \xi \frac{dF(\xi)}{d\xi}\right) - \frac{d}{d\xi}\left(F^3(\xi) \frac{dF(\xi)}{d\xi}\right) + \frac{1}{\Gamma} \frac{F(\xi)}{G(\xi)} = 0, \tag{3.6.33}$$

$$c_3 G(\xi) - 2c_3 \xi \frac{dG(\xi)}{d\xi} = \frac{F(\xi)}{G(\xi)}, \tag{3.6.34}$$

$$F\left(\frac{1}{c_2^2}\right) = 0, \qquad G\left(\frac{1}{c_2^2}\right) = 0, \tag{3.6.35}$$

$$F^3(0) \frac{dF(0)}{d\xi} = -3c_3 \left[\Omega \int_0^{\frac{1}{c_2^2}} F(\xi) \mathrm{d}\xi + \left(\frac{1}{\Gamma}\right) \int_0^{\frac{1}{c_2^2}} G(\xi) \mathrm{d}\xi\right], \tag{3.6.36}$$

$$L(t) = \left(1 + \frac{c_3}{c_2} t\right)^2, \tag{3.6.37}$$

$$V(t) = 2c_2^3 \left(1 + \frac{c_3}{c_2} t\right)^3 \int_0^{\frac{1}{c_2^2}} F(\xi) \mathrm{d}\xi, \tag{3.6.38}$$

$$h(t, x) = c_2 \left(1 + \frac{c_3}{c_2} t\right) F(\xi), \tag{3.6.39}$$

$$b(t,x) = c_2\left(1+\frac{c_3}{c_2}t\right)G(\xi), \tag{3.6.40}$$

$$p_f(t,x) = \sigma_{zz}^{\infty} + h(t,x), \tag{3.6.41}$$

where $0 < \xi < \frac{1}{c_2^2}$.

We now make change of variables to simplify the mathematical formulation of the problem. We simplify equations (3.6.33)-(3.6.41) by making a change of variables

$$u = \frac{x}{L(t)}, \quad \xi = \frac{1}{c_2^2}u, \quad F(\xi) = AS(u), \quad G(\xi) = BR(u), \tag{3.6.42}$$

where $0 \leq u \leq 1$ and A and B are constants. Substituting the expressions for $F(\xi)$ and $G(\xi)$ in (3.6.42) into (3.6.33) and (3.6.34), we obtain

$$F(\xi) = \left(\frac{c_3}{c_2^4}\right)^{\frac{1}{3}} S(u) \qquad \text{and} \qquad G(\xi) = \frac{1}{c_3}R(u). \tag{3.6.43}$$

The problem is to solve for $S(u)$ and $R(u)$, the system of nonlinear ordinary differential equations

$$\Omega\left(S(u) - 2u\frac{dS(u)}{du}\right) - \frac{d}{du}\left(S^3(u)\frac{dS(u)}{du}\right) + \frac{1}{\Gamma}\frac{S(u)}{R(u)} = 0, \tag{3.6.44}$$

$$R(u) - 2u\frac{dR}{du}(u) = \left(\frac{c_3}{c_2}\right)^{\frac{4}{3}}\frac{S(u)}{R(u)}, \tag{3.6.45}$$

subject to

$$S(1) = 0, \quad R(1) = 0, \tag{3.6.46}$$

$$S^3(0)\frac{dS(0)}{du} = -3\left[\Omega\int_0^1 S(u)\mathrm{d}u + \left(\frac{1}{\Gamma}\right)\left(\frac{c_3}{c_2}\right)^{-\frac{4}{3}}\int_0^1 R(u)\mathrm{d}u\right]. \tag{3.6.47}$$

Once $S(u)$ and $R(u)$ are obtained, $L(t)$, $V(t)$, $h(t,x)$ and $b(t,x)$ takes the form

$$L(t) = \left(1+\frac{c_3}{c_2}t\right)^2, \tag{3.6.48}$$

$$V(t) = 2\left(\frac{c_3}{c_2}\right)^{\frac{1}{3}}\left(1+\frac{c_3}{c_2}t\right)^3\int_0^1 S(u)\mathrm{d}u, \tag{3.6.49}$$

$$h(t,x) = \left(\frac{c_3}{c_2}\right)^{\frac{1}{3}}\left(1+\frac{c_3}{c_2}t\right)S(u), \tag{3.6.50}$$

$$b(t,x) = \left(\frac{c_3}{c_2}\right)^{-1}\left(1+\frac{c_3}{c_2}t\right)R(u). \tag{3.6.51}$$

The fluid pressure is then given by

$$p_f(t,x) = \sigma_{zz}^{\infty} + h(t,x). \tag{3.6.52}$$

We have now completed the mathematical formulation for a hydraulic fracture with Darcy fluid flow in the rock-mass. We notice that the solutions to equations (3.6.44) to (3.6.51) depend only on the ratio $\frac{c_3}{c_2}$ and not on the constants individually. We will solve (3.6.44) and (3.6.45) numerically subject to the boundary conditions (3.6.46) and (3.6.47). The ratio $\frac{c_3}{c_2}$ is obtained as part of the solution using the condition $h(0,0) = 1$. Since $h(0,0) = 1$,

$$S(0) = \left(\frac{c_3}{c_2}\right)^{-\frac{1}{3}}. \tag{3.6.53}$$

Therefore

$$p_f(0,t) = \left(1 + \frac{c_3}{c_2}t\right) + \sigma_{zz}^{\infty}. \tag{3.6.54}$$

The operating condition associated with the mathematical formulation is therefore that the fluid pressure at the fracture entry is a linear time function.

3.6.1 Weak leak-off at the interface: $\Omega \sim 1$ and $\Gamma \gg 1$

Consider now the case of weak leak-off. The boundary value problem becomes

$$\Omega\left[S(u) - 2u\frac{dS(u)}{du}\right] - \frac{d}{du}\left(S^3(u)\frac{dS(u)}{du}\right) = 0, \tag{3.6.55}$$

$$R(u) - 2u\frac{dR(u)}{du} = \left(\frac{c_3}{c_2}\right)^{\frac{4}{3}}\frac{S(u)}{R(u)}, \tag{3.6.56}$$

$$S(1) = 0, \quad R(1) = 0, \tag{3.6.57}$$

$$S^3(0)\frac{dS(0)}{du} = -3\int_0^1 S(u)\mathrm{d}u. \tag{3.6.58}$$

Using (3.6.53), the invariant solutions are

$$L(t) = \left(1 + \frac{c_3}{c_2}t\right)^2, \tag{3.6.59}$$

$$V(t) = V_0\left(1 + \frac{c_3}{c_2}t\right)^3, \qquad V_0 = 2\left(\frac{c_3}{c_2}\right)^{\frac{1}{3}}\int_0^1 S(u)\mathrm{d}u, \tag{3.6.60}$$

$$h(t,x) = \left(1 + \frac{c_3}{c_2}t\right)\frac{S(u)}{S(0)}, \tag{3.6.61}$$

$$b(t,x) = \left(1 + \frac{c_3}{c_2}t\right)S^3(0)R(u), \tag{3.6.62}$$

$$p_f(t,x) = \sigma_{zz}^{\infty} + h(t,x). \tag{3.6.63}$$

The system of differential equations (3.6.55) and (3.6.56) admits the two Lie point symmetries given by

$$X_1 = 3u\frac{\partial}{\partial u} + R\frac{\partial}{\partial R} + 2S\frac{\partial}{\partial S}, \quad X_2 = \frac{u}{R}\frac{\partial}{\partial R} \tag{3.6.64}$$

and therefore, the integration of the system subject to boundary conditions (3.6.57) and (3.6.58) to obtain an exact analytical solution is not possible since more symmetries are required to transform the system of differential equations (3.6.55) and (3.6.56). We will therefore seek to obtain the solution numerically.

We seek to understand the behaviour of $S(u)$ and $R(u)$ as $u \to 1$ since (3.6.55) and (3.6.56) have a singularity at $u = 1$. We will determine the asymptotic solutions of (3.6.55) and (3.6.56) of the form

$$S(u) \sim a_1(1-u)^{s_1}, \qquad R(u) \sim b_1(1-u)^{r_1} \qquad \text{as} \qquad u \to 1, \tag{3.6.65}$$

where a_1, b_1, $s_1$and r_1 are constants. Substituting (3.6.65) into (3.6.55) and (3.6.56) gives

$$a_1(1-2s_1)\Omega(1-u)^{s_1} + 2a_1 s_1 \Omega(1-u)^{s_1-1} - a_1^4 s_1(4s_1-1)(1-u)^{4s_1-2} \sim 0, \tag{3.6.66}$$

$$(1-2r_1)b_1(1-u)^{r_1} + 2b_1 r_1(1-u)^{r_1-1} - \left(\frac{c_3}{c_2}\right)^{\frac{4}{3}}\left(\frac{6^{\frac{1}{3}}}{b_1}\right)(1-u)^{\frac{1}{3}-r_1} \sim 0, \tag{3.6.67}$$

as $u \to 1$. In order for the dominant terms in (3.6.66) to balance each other it is required that

$$4s_1 - 2 = s_1 - 1, \tag{3.6.68}$$

which implies that $s_1 = \frac{1}{3}$. Substituting the s_1 value into (3.6.66) gives

$$\frac{1}{3}a_1\Omega(1-u)^{\frac{1}{3}} + \frac{2}{3}a_1\Omega(1-u)^{-\frac{2}{3}} - \frac{1}{9}a_1^4(1-u)^{-\frac{2}{3}} \sim 0, \tag{3.6.69}$$

as $u \to 1$, simplifying to

$$\frac{1}{3}a_1\Omega(1-u) + \frac{2}{3}a_1\Omega - \frac{1}{9}a_1^4 \sim 0, \tag{3.6.70}$$

as $u \to 1$. By setting $u = 1$, we obtain $a_1 = 6^{\frac{1}{3}}\Omega^{\frac{1}{3}}$. In order for the dominant terms in (3.6.67) to balance each other it is required that

$$r_1 - 1 = \frac{1}{3} - r_1, \tag{3.6.71}$$

which implies that $r_1 = \frac{2}{3}$. Equation (3.6.67) becomes

$$-\frac{1}{3}b_1(1-u)^{\frac{2}{3}} + \frac{4}{3}b_1(1-u)^{-\frac{1}{3}} - \left(\frac{c_3}{c_2}\right)^{\frac{4}{3}}\left(\frac{6^{\frac{1}{3}}}{b_1}\right)(1-u)^{-\frac{1}{3}} \sim 0, \tag{3.6.72}$$

as $u \to 1$, and therefore

$$-\frac{1}{3}b_1(1-u) + \frac{4}{3}b_1 - \left(\frac{c_3}{c_2}\right)^{\frac{4}{3}}\left(\frac{6^{\frac{1}{3}}\Omega^{\frac{1}{3}}}{b_1}\right) \sim 0, \tag{3.6.73}$$

as $u \to 1$. By setting $u = 1$, we obtain

$$b_1 = \left(\frac{81\Omega}{32}\right)^{\frac{1}{6}}\left(\frac{c_3}{c_2}\right)^{\frac{2}{3}}.$$

Thus, for weak leak-off, the asymptotic solutions of (3.6.55) and (3.6.56) as $u \to 1$, which are true for any value of $\frac{c_3}{c_2} > 0$ are

$$S(u) \sim (6\Omega)^{\frac{1}{3}}(1-u)^{\frac{1}{3}}, \tag{3.6.74}$$

$$R(u) \sim \left(\frac{81\Omega}{32}\right)^{\frac{1}{6}}\left(\frac{c_3}{c_2}\right)^{\frac{2}{3}}(1-u)^{\frac{2}{3}}. \tag{3.6.75}$$

The numerical integration of (3.6.55) and (3.6.56) subject to (3.6.57) and (3.6.58) is done by a nonlinear shooting method. The asymptotic behaviour of $S(u)$ and $R(u)$ obtained in (3.6.74) and (3.6.75) is required to start the integration, thereby overcoming the difficulty posed by the singularity of the differential equation (3.6.55) and (3.6.56) at the fracture tip where $S = R = 0$. Using (3.6.74), it can be shown that

$$S^3(u)\frac{dS}{du} = -2\Omega\left[6\Omega(1-u)\right]^{\frac{1}{3}} = -2\Omega S(u) \to 0 \quad \text{as} \quad u \to 1. \tag{3.6.76}$$

Hence, the fluid flux vanishes at the fracture tip and there is no sink of the fluid there. The lubrication approximation used to simplify the Navier Stokes equation breaks down at the fracture tip since

$$\frac{dS}{du} \sim -\left(\frac{2\Omega}{9}\right)^{\frac{1}{3}}(1-u)^{-\frac{2}{3}} \quad \text{as} \quad u \to 1, \tag{3.6.77}$$

and hence from (3.6.61)

$$\frac{dh}{dx} \to -\infty \quad \text{as} \quad x \to L(t). \tag{3.6.78}$$

The condition $\frac{H}{L} \ll 1$ is therefore invalid near the fracture tip. The system of equations (3.6.55) and (3.6.56) is transformed to a system of three first order differential equations

$$\frac{dS}{du} = y_2, \tag{3.6.79}$$

$$\frac{dy_2}{du} = -\frac{1}{y_1^3}\left[3y_1^2 y_2^2 + \Omega(2uy_2 - y_1)\right], \tag{3.6.80}$$

$$\frac{dy_3}{du} = -\frac{1}{2u}\left[y_3 - \left(\frac{c_3}{c_2}\right)^{\frac{4}{3}} \frac{y_1}{y_3}\right], \tag{3.6.81}$$

subject to the initial and boundary conditions

$$y_1(1) = 0, \qquad y_3(1) = 0, \qquad y_1(0) = \left(\frac{c_3}{c_2}\right)^{-\frac{1}{3}}, \tag{3.6.82}$$

where $y_1 = S(u)$ and $y_3 = R(u)$ and the ratio $\frac{c_3}{c_2}$ is to be determined. The system of first order differential equations (3.6.79)-(3.6.81) were solved using the IVP solver ODE23s of Matlab which is a one-step solver based on the modified Rosenbrock formula of order 2. The difficulty posed by the singularity at $u = 1$ in both (3.6.55) and (3.6.56) was overcome with the use of the asymptotic solutions of both $S(u)$ and $R(u)$ as $u \to 1$ given in (3.6.74) and (3.6.75). The method was used by Fareo and Mason [2] to derive numerical solutions of a hydraulic fracture propagated by a Newtonian fluid in a permeable medium.

We use asymptotic solutions to solve the system of equations governing the propagation of the half-width fracture and the leak-off depth using the shooting method. The value of $\frac{c_3}{c_2}$ is obtained directly from the boundary value problem. Backward integration was initiated at an $\varepsilon-$neighbourhood of the point $u = 1$ with the asymptotic solutions as initial conditions. For rapid convergence of the solutions $S(u)$ and $R(u)$, we iterated based on the bisection algorithm until the condition $S(0) = \left(\frac{c_3}{c_2}\right)^{-\frac{1}{3}}$ was satisfied. After obtaining the solutions for $S(u)$ and $R(u)$, we substitute back into the original functions $h(t,x)$ and $b(t,x)$ as given in (3.6.61) and (3.6.62), respectively. To check accuracy of the numerical solutions, the mass balance law was exercised. Since the mass balance was satisfied, we conclude that the numerical method and solutions are reliable.

3.6.1.1 Fracture half-width and leak-off depth

The half-width of the fracture $h(t,x)$ for the case of weak leak-off at the fracture interface is plotted in Figure 3.6.1. The fracture half-width increases with time t. It is clear from Figure 3.6.1 that the rate of growth of the fracture half-width is strong for the case of weak fluid leak-off at the interface. There is strong rate of growth of the half-width of the fracture for the case of weak fluid leak-off since at the fracture interface only a slight amount of the injected fluid is lost into the rock-mass formation. In Figure 3.6.2, the

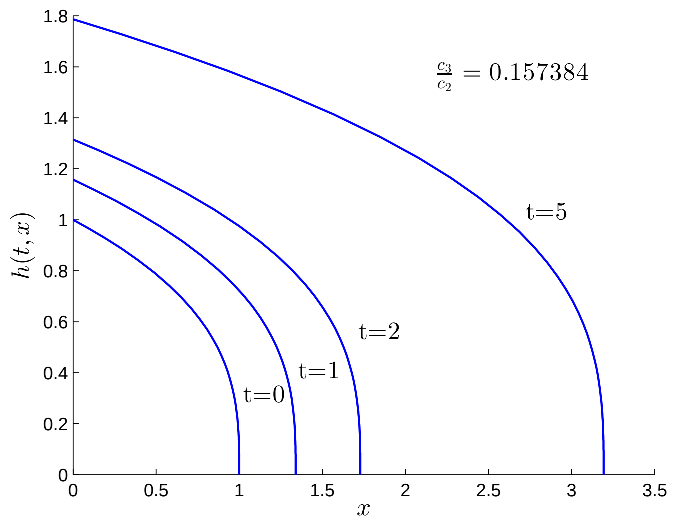

FIGURE 3.6.1: Fracture half-width given by (3.6.61) plotted against x at $t = 0, 1, 2, 5$ when $\Omega = 1$, $c_3 \neq 0$ and weak leak-off at the interface.

leak-off depth $b(t, x)$ given by (3.6.62) is depicted. The leak-off depth of fluid in the permeable medium when there is weak leak-off at the fluid-rock interface is expected to be small since only a inconsiderable proportion of the injected fluid is lost at the interface.

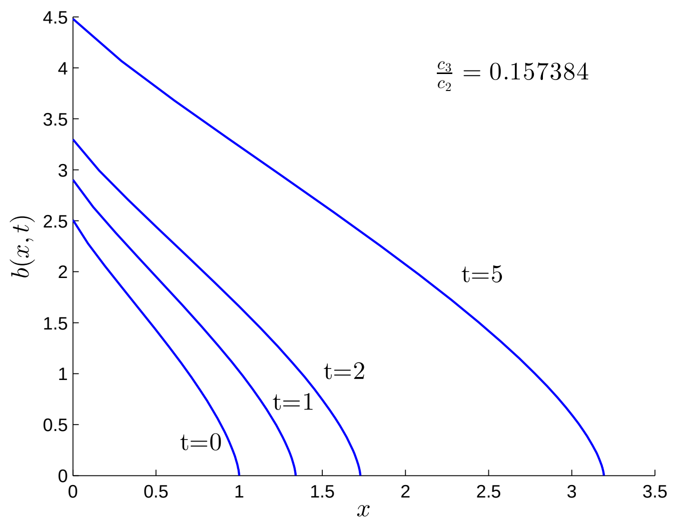

FIGURE 3.6.2: Leak-off depth given by (3.6.62) plotted against x at $t = 0, 1, 2, 5$ when $\Omega = 1$, $c_3 \neq 0$ and weak leak-off at the interface.

3.6.2 Strong leak-off at the interface: $\Omega \ll 1$ and $\Gamma \sim 1$

We now investigate the case of strong leak-off into the rock-mass. The boundary value problem becomes

$$\frac{d}{du}\left(S^3(u)\frac{dS(u)}{du}\right) - \frac{1}{\Gamma}\frac{S(u)}{R(u)} = 0, \tag{3.6.83}$$

$$R(u) - 2u\frac{dR(u)}{du} = \left(\frac{c_3}{c_2}\right)^{\frac{4}{3}}\frac{S(u)}{R(u)}, \tag{3.6.84}$$

$$S(1) = 0, \quad R(1) = 0, \tag{3.6.85}$$

$$S^3(0)\frac{dS(0)}{du} = -3\left(\frac{c_3}{c_2}\right)^{-\frac{4}{3}}\int_0^1 R(u)\mathrm{d}u. \tag{3.6.86}$$

The solution $L(t)$, $V(t)$, $h(t,x)$ and $b(t,x)$ are obtained, once $S(u)$ and $R(u)$ are calculated, as

$$L(t) = \left(1 + \frac{c_3}{c_2}t\right)^2, \tag{3.6.87}$$

$$V(t) = V_0\left(1 + \frac{c_3}{c_2}t\right)^3, \qquad V_0 = 2\left(\frac{c_3}{c_2}\right)^{\frac{1}{3}}\int_0^1 S(u)\mathrm{d}u, \tag{3.6.88}$$

$$h(t,x) = \left(1 + \frac{c_3}{c_2}t\right)\frac{S(u)}{S(0)}, \tag{3.6.89}$$

$$b(t,x) = \left(1 + \frac{c_3}{c_2}t\right)S^3(0)R(u), \tag{3.6.90}$$

$$p_f(t,x) = \sigma_{zz}^{\infty} + h(t,x), \tag{3.6.91}$$

where $0 \le u \le 1$.

The strong leak-off case requires numerical integration and also presents a singularity problem at the tip of the fracture.

We seek the asymptotic solutions of (3.6.83) and (3.6.84) as $u \to 1$. The asymptotic solutions are of the form

$$S(u) \sim a_2(1-u)^{s_2} \qquad \text{as} \qquad u \to 1, \tag{3.6.92}$$

$$R(u) \sim b_2(1-u)^{r_2} \qquad \text{as} \qquad u \to 1, \tag{3.6.93}$$

where a_2, s_2, b_2 and r_2 are constants. Substituting (3.6.92) and (3.6.93) into (3.6.83) and (3.6.84) gives

$$a_2^4 s_2(4s_2 - 1)(1-u)^{4s_2-2} - \left(\frac{1}{\Gamma}\right)\left(\frac{a_2}{b_2}\right)(1-u)^{s_2-r_2} \sim 0, \tag{3.6.94}$$

$$b_2(1-2r_2)(1-u)^{r_2} + 2b_2 r_2 (1-u)^{r_2-1} - \left(\frac{c_3}{c_2}\right)^{\frac{4}{3}} \left(\frac{a_2}{b_2}\right)(1-u)^{s_2-r_2} \sim 0, \qquad (3.6.95)$$

as $u \to 1$. In order for the dominant terms in (3.6.94) and (3.6.95) to balance each other it is required that

$$4s_2 - 2 = s_2 - r_2 \quad \text{and} \quad r_2 - 1 = s_2 - r_2. \qquad (3.6.96)$$

Solving for s_2 and r_2 yields $r_2 = \frac{5}{7}$ and $s_2 = \frac{3}{7}$. Using the values of r_2 and s_2 in (3.6.94) and (3.6.95), the values of b_2 and a_2 are obtained as

$$b_2 = \left(\frac{7}{10}a_2\right)^{\frac{1}{2}} \left(\frac{c_3}{c_2}\right)^{\frac{2}{3}} \quad \text{and} \quad a_2 = \left(\frac{686}{45}\right)^{\frac{1}{7}} \left(\frac{c_3}{c_2}\right)^{-\frac{4}{21}} \left(\frac{1}{\Gamma}\right)^{\frac{2}{7}}. \qquad (3.6.97)$$

Then the function $S(u)$ and $R(u)$ as $u \to 1$ can therefore be written as

$$S(u) \sim \left(\frac{686}{45}\right)^{\frac{1}{7}} \left(\frac{c_3}{c_2}\right)^{\frac{4}{21}} \left(\frac{1}{\Gamma}\right)^{\frac{2}{7}} (1-u)^{\frac{3}{7}}, \qquad (3.6.98)$$

$$R(u) \sim \left(\frac{7}{10}\right)^{\frac{1}{2}} \left(\frac{686}{45}\right)^{\frac{1}{14}} \left(\frac{c_3}{c_2}\right)^{\frac{12}{21}} \left(\frac{1}{\Gamma}\right)^{\frac{1}{7}} (1-u)^{\frac{5}{7}}. \qquad (3.6.99)$$

3.6.2.1 Fracture half-width and leak-off depth

In the case of strong fluid leak-off at the interface, the fluid volume entering the fracture is much more than the volume of the fracture and much of this fluid entering the fracture is lost at the fracture walls. Because of this phenomenon the rate of growth for the fracture half-width when there is strong leak-off at the fluid-rock interface is small. This can be seen in Figure 3.6.3. The leak-off depth plotted in Figure 3.6.4 for strong fluid leak-off is

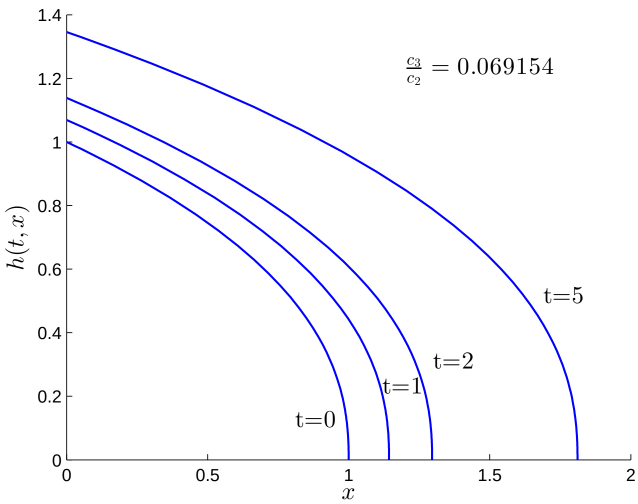

FIGURE 3.6.3: Fracture half-width given by (3.6.89) plotted against x at $t = 0, 1, 2, 5$ when $\Gamma = 1$, $c_3 \neq 0$ and strong leak-off at the interface.

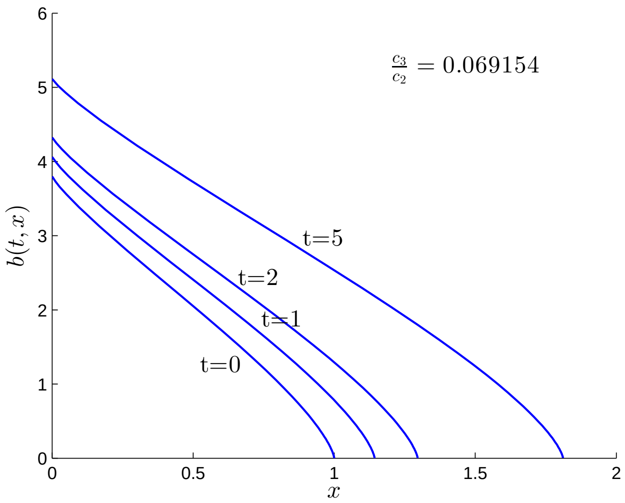

FIGURE 3.6.4: Leak-off depth given by (3.6.90) plotted against x at $t = 0, 1, 2, 5$ when $\Gamma = 1$, $c_3 \neq 0$ and strong leak-off at the interface.

however greater than the leak-off depth for weak fluid leak-off since the amount of fluid lost at the fracture walls when there is strong leak-off is greater than the amount of fluid lost when there is weak leak-off. Furthermore, for the case of strong fluid leak-off, the fluid entering the fracture is met by an approximately equal leak-off flux at the fracture walls.

3.6.3 Moderate leak-off at the interface: $\Omega \sim 1$ and $\Gamma \sim 1$

Consider the case of moderate leak-off into the rock-mass. This is the general case of fluid leak-off. The boundary value problem becomes

$$\Omega\left[S(u) - 2u\frac{dS(u)}{du}\right] - \frac{d}{du}\left(S^3(u)\frac{dS(u)}{du}\right) + \frac{1}{\Gamma}\frac{S(u)}{R(u)} = 0, \qquad (3.6.100)$$

$$R(u) - 2u\frac{dR(u)}{du} = \left(\frac{c_3}{c_2}\right)^{\frac{4}{3}}\frac{S(u)}{R(u)}, \qquad (3.6.101)$$

$$S(1) = 0, \quad R(1) = 0, \qquad (3.6.102)$$

$$S^3(0)\frac{dS(0)}{du} = -3\left[\int_0^1 S(u)\mathrm{d}u + \left(\frac{c_3}{c_2}\right)^{-\frac{4}{3}}\int_0^1 R(u)\mathrm{d}u\right]. \qquad (3.6.103)$$

Once $S(u)$ and $R(u)$ are obtained, the solutions $L(t)$, $V(t)$, $h(t,x)$ and $b(t,x)$ are

$$L(t) = \left(1 + \frac{c_3}{c_2}t\right)^2, \qquad (3.6.104)$$

$$V(t) = V_0\left(1 + \frac{c_3}{c_2}t\right)^3, \qquad V_0 = 2\left(\frac{c_3}{c_2}\right)^{\frac{1}{3}}\int_0^1 S(u)\mathrm{d}u, \qquad (3.6.105)$$

$$h(t,x) = \left(1 + \frac{c_3}{c_2}t\right)\frac{S(u)}{S(0)}, \tag{3.6.106}$$

$$b(t,x) = \left(1 + \frac{c_3}{c_2}t\right)S^3(0)R(u), \tag{3.6.107}$$

$$p_f(t,x) = \sigma_{zz}^{\infty} + h(t,x), \tag{3.6.108}$$

where $0 \leq u \leq 1$.

As with weak and strong leak-off case, we proceed numerically since exact solutions are not obtainable. We therefore seek to understand the behaviour of both $S(u)$ and $R(u)$ as $u \to 1$.

We seek the asymptotic solutions of (3.6.100) and (3.6.101) as $u \to 1$. The asymptotic solutions are of the form

$$S(u) \sim a_3(1-u)^{s_3} \qquad \text{as} \qquad u \to 1, \tag{3.6.109}$$

$$R(u) \sim b_3(1-u)^{r_3} \qquad \text{as} \qquad u \to 1, \tag{3.6.110}$$

where a_3, s_3, b_3 and r_3 are constants. Substituting (3.6.109) and (3.6.110) into (3.6.100) and (3.6.101) gives

$$a_3(1-2s_3)\Omega(1-u)^{s_3}+2a_3s_3\Omega(1-u)^{s_3-1}-a_3^4s_3(4s_3-1)(1-u)^{4s_3-2}+\left(\frac{a_3}{b_3}\right)\frac{1}{\Gamma}(1-u)^{s_3-r_3} \sim 0, \tag{3.6.111}$$

$$b_3(1-2r_3)(1-u)^{r_3} + 2b_3r_3(1-u)^{r_3-1} + \left(\frac{c_3}{c_2}\right)^{\frac{4}{3}}\left(\frac{a_3}{b_3}\right)(1-u)^{s_3-r_3} \sim 0, \tag{3.6.112}$$

as $u \to 1$. In order for the dominant terms in (3.6.111) to balance each other it is required that

$$4s_3 - 2 = s_3 - 1, \tag{3.6.113}$$

which implies that $s_3 = \frac{1}{3}$. Similarly, it is required that $r_3 = \frac{2}{3}$ for dominant terms in (3.6.112) to balance each other. Substituting the values of s_3 and r_3 into (3.6.111) and (3.6.112), the values of a_3 and b_3 are obtained as

$$a_3 = 6^{\frac{1}{3}}\Omega^{\frac{1}{3}} \quad \text{and} \quad b_3 = \left(\frac{81\Omega}{32}\right)^{\frac{1}{3}}\left(\frac{c_3}{c_2}\right)^{\frac{2}{3}}. \tag{3.6.114}$$

The asymptotic solutions of (3.6.100) and (3.6.101) as $u \to 1$ are

$$S(u) \sim 6^{\frac{1}{3}}\Omega^{\frac{1}{3}}(1-u)^{\frac{1}{3}}, \tag{3.6.115}$$

$$R(u) \sim \left(\frac{81\Omega}{32}\right)^{\frac{1}{3}} \left(\frac{c_3}{c_2}\right)^{\frac{2}{3}} (1-u)^{\frac{2}{3}}. \tag{3.6.116}$$

3.6.3.1 Fracture half-width and leak-off depth

The fracture half-width $h(t,x)$ for moderate fluid leak-off case is plotted in Figure 3.6.5. For this case, the volume of the fracturing fluid entering the fracture is approximately equal to the volume of the fracture. In addition, the fluid that is lost at the fracture interface is approximately equal to the fluid injected into the fracture. The rate of growth for the moderate fluid leak-off case is very small since only a limited amount of the fracturing fluid is usable to drive the fracture propagation. Figure 3.6.6 illustrates the leak-off depth for when there is moderate fluid leak-off. The unexpected result is that the leak-off depth when there is moderate fluid leak-off at the fracture walls is greater than the leak-off depth for the case of strong fluid leak-off at the fluid-rock interface. This is unexpected since for strong leak-off, the fluid flux entering the fracture is much more than the volume of the fracture while for moderate fluid leak-off the fluid flux is approximately equal to the fracture volume. This phenomenon might be due to changes in permeability or fluid pressure in the area adjacent to the fracture interface in the case of strong fluid leak-off in response to the large volume of fluid entering the porous media.

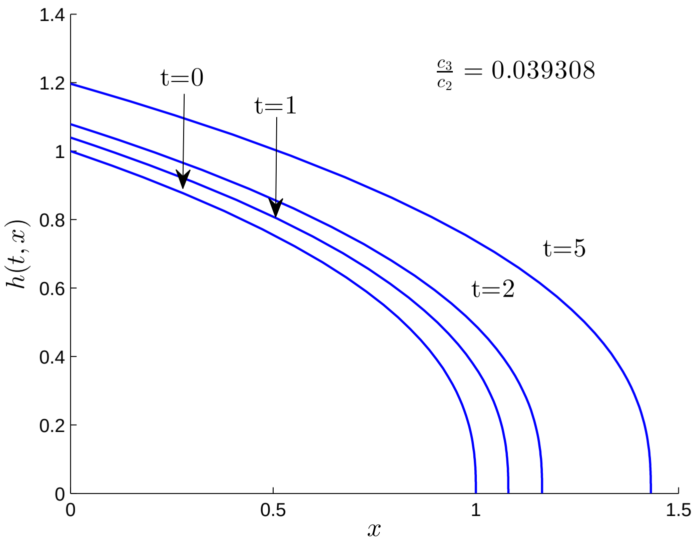

FIGURE 3.6.5: Fracture half-width given by (3.6.106) plotted against x at $t = 0, 1, 2, 5$ when $\Omega = \Gamma = 1$, $c_3 \neq 0$ and moderate leak-off at the interface.

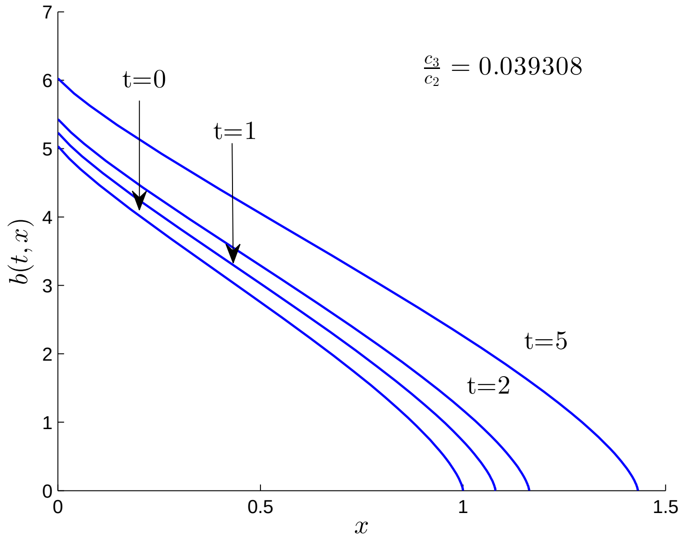

FIGURE 3.6.6: Leak-off depth given by (3.6.107) plotted against x at $t = 0, 1, 2, 5$ when $\Omega = \Gamma = 1$, $c_3 \neq 0$ and moderate leak-off at the interface.

3.6.4 Length of the fracture

In all three cases considered, the fracture length, $L(t)$, grows quadratically with time, the rate of growth depending on the ratio $\frac{c_3}{c_2} > 0$. The ratio $\frac{c_3}{c_2}$ was obtained numerically. It has the least value for the case of moderate fluid leak-off, and the highest value for weak leak-off. In Figure 3.6.7, the graph of $L(t)$ for the three distinct cases are plotted. As shown, the graph of the fracture length given by Figure 3.6.7 and plotted in (i) grows the strongest, since there is weak leak-off at the interface. When there is strong leak-off at the fluid-rock interface, the growth of the fracture length with time is depicted in (ii). It is seen that the length of the fracture increases with time, even when there is strong leak-off at the fluid-rock interface. The growth of the fracture length when there is moderate fluid leak-off at the interface is plotted in (iii). For this case, the rate of growth of the fracture length is the smallest, with $L(t)$ behaving almost linear with time t because only a small range of time is considered. For sufficiently large time range it will behave quadratically. The rate of growth of the length of the fracture when there is weak leak-off at the fluid-rock interface is expected to be greater than that of strong leak-off since for the strong leak-off case, more fluid is lost at the fracture interface and only a proportion of the injected fluid is responsible for driving the propagation of the fracture. Similarly, it is expected that the rate of growth of the fracture length when there is strong leak-off is greater than that of moderate leak-off since the volume of the fracturing fluid is approximately equal to the fracture volume while the fluid flux entering the fracture is matched by an approximate leak-off flux at the fracture interface.

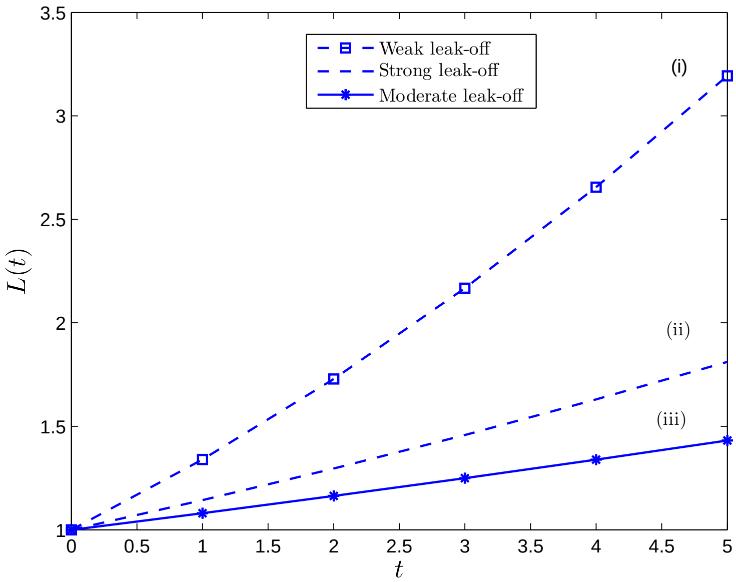

FIGURE 3.6.7: Length of the fracture $L(t)$ plotted against t for (i) weak fluid leak-off, (ii) strong fluid leak-off and (iii) moderate leak-off of fluid at the interface.

Case: $c_3 = 0$

When $c_3 = 0$, the Lie point symmetry generator (3.6.7) becomes

$$X = c_2 X_1 + c_1 X_2, \tag{3.6.117}$$

where

$$X_1 = \frac{\partial}{\partial t}, \quad X_2 = \frac{\partial}{\partial x}. \tag{3.6.118}$$

Newman [44] first made this observation for a turbulent hydraulic fracture. The solutions $h(t,x)$ and $b(t,x)$ of the partial differential equation (3.5.20) and (3.5.21) is obtained by solving

$$X(h - \phi(t,x))|_{h=\phi(t,x)} = 0, \tag{3.6.119}$$

$$X(b - \psi(t,x))|_{b=\psi(t,x)} = 0, \tag{3.6.120}$$

that is

$$c_2 \frac{\partial \phi}{\partial t} + c_1 \frac{\partial \phi}{\partial x} = 0, \tag{3.6.121}$$

$$c_2 \frac{\partial \psi}{\partial t} + c_1 \frac{\partial \psi}{\partial x} = 0. \tag{3.6.122}$$

The basis for invariants corresponding to (3.6.121) and (3.6.122) are constructed by solving the following characteristic equations

$$\frac{dt}{c_2} = \frac{dx}{c_1} = \frac{d\phi}{0} = \frac{d\psi}{0}. \tag{3.6.123}$$

The characteristic equations in (3.6.123) can be written equivalently as

$$\frac{dt}{c_2} = \frac{dx}{c_1}, \qquad \frac{dt}{c_2} = \frac{d\phi}{0}, \qquad \frac{dt}{c_2} = \frac{d\psi}{0}. \tag{3.6.124}$$

Therefore, the invariants are

$$K_1 = x - \frac{c_1}{c_2}t, \quad K_2 = \phi, \quad K_3 = \psi. \tag{3.6.125}$$

The general solutions for (3.6.121) and (3.6.122) are

$$K_2 = F(K_1) \qquad \text{and} \qquad K_3 = G(K_1). \tag{3.6.126}$$

where F and G are arbitrary functions. Hence

$$\phi(t,x) = F(\xi), \tag{3.6.127}$$

$$\psi(t,x) = G(\xi), \tag{3.6.128}$$

where

$$\xi = x - \frac{c_1}{c_2}t. \tag{3.6.129}$$

But we have that $h(t,x) = \phi(t,x)$ and $b(t,x) = \psi(t,x)$, then (3.6.127) and (3.6.128) become

$$h(t,x) = F(\xi), \tag{3.6.130}$$

$$b(t,x) = G(\xi), \tag{3.6.131}$$

where F and G are an arbitrary functions of ξ. The system of partial differential equations (3.5.20) and (3.5.21), after substituting (3.6.130) and (3.6.131), becomes

$$\Omega\frac{c_1}{c_2}\frac{dF(\xi)}{d\xi} + \frac{d}{d\xi}\left(F^3(\xi)\frac{dF(\xi)}{d\xi}\right) - \frac{1}{\Gamma}\frac{F(\xi)}{G(\xi)} = 0, \tag{3.6.132}$$

$$\frac{c_1}{c_2}\frac{dG(\xi)}{d\xi} + \frac{F(\xi)}{G(\xi)} = 0. \tag{3.6.133}$$

Now, by substituting (3.6.130) and (3.6.131) into (3.5.22) we get

$$F(\xi) = 0, \quad G(\xi) = 0 \quad \text{at} \quad \xi = L(t) - \frac{c_1}{c_2}t. \tag{3.6.134}$$

To obtain the functional form of the fracture length, $L(t)$, we consider the boundary condition

$$F\left(L(t) - \frac{c_1}{c_2}t\right) = G\left(L(t) - \frac{c_1}{c_2}t\right) = 0. \tag{3.6.135}$$

Letting $Y(t) = L(t) - \frac{c_1}{c_2}t$, we have

$$\frac{dF}{dt} = \frac{dF}{dY}\frac{dY}{dt} = 0. \tag{3.6.136}$$

Since F is not a constant function, $\frac{dF}{dY} \neq 0$. Therefore

$$\frac{dY}{dt} = 0 \Longrightarrow Y = Y_0, \tag{3.6.137}$$

a constant. Hence

$$L(t) = Y_0 + \frac{c_1}{c_2}t. \tag{3.6.138}$$

Using the initial condition (3.3.17), we get

$$L(0) = 1 = Y_0. \tag{3.6.139}$$

Hence, (3.6.138) becomes

$$L(t) = 1 + \frac{c_1}{c_2}t. \tag{3.6.140}$$

The boundary conditions in (3.6.135) therefore become

$$F(1) = 0, \qquad G(1) = 0. \tag{3.6.141}$$

The system of equations (3.6.132) and (3.6.133) admit only one symmetry

$$X = c\frac{\partial}{\partial \xi}. \tag{3.6.142}$$

Hence, we cannot integrate to obtain $F(\xi)$ and $G(\xi)$. It will only be possible to integrate once. The general asymptotic solution can be derived for equations (3.6.132) and (3.6.133) as $\xi \to 1$. This asymptotic solution is required when deriving the numerical solution for $F(\xi)$ and $G(\xi)$. We look for an asymptotic solution of the form

$$F(\xi) \sim a(\alpha - \xi)^s, \quad G(\xi) \sim b(\beta - \xi)^r \quad \text{as} \quad \xi \to 1, \tag{3.6.143}$$

where a, b, α, β, s and r are all real constants. The boundary condition (3.6.141) gives $\alpha = \beta = 1$ and therefore

$$F(\xi) \sim a(1 - \xi)^s, \quad G(\xi) \sim b(1 - \xi)^r \quad \text{as} \quad \xi \to 1. \tag{3.6.144}$$

We substitute (3.6.144) into (3.6.132) and (3.6.133) to obtain

$$-\Omega\frac{c_1}{c_2}as(1-\xi)^{s-1} + a^4 s(4s-1)(1-\xi)^{4s-2} - \frac{1}{\Gamma}\frac{a}{b}(1-\xi)^{s-r} \sim 0, \tag{3.6.145}$$

$$-\frac{c_1}{c_2}br(1-\xi)^{r-1}+\left(\frac{a}{b}\right)(1-\xi)^{s-r}\sim 0, \tag{3.6.146}$$

as $\xi \to 1$. The dominant terms balance each other in (3.6.145) and (3.6.146) provided

$$s-1=4s-2 \quad \text{and} \quad r-1=s-r, \tag{3.6.147}$$

that is, provided

$$s=\frac{1}{3} \quad \text{and} \quad r=\frac{2}{3}. \tag{3.6.148}$$

Equations (3.6.145) and (3.6.146) become

$$-\frac{a}{3}\Omega\frac{c_1}{c_2}+\frac{a^4}{9}-\frac{1}{\Gamma}\frac{a}{b}(1-\xi)^{\frac{1}{3}}\sim 0 \quad \text{as} \quad \xi\to 1, \tag{3.6.149}$$

$$-\frac{2}{3}\frac{c_1}{c_2}b+\frac{a}{b}\sim 0 \quad \text{as} \quad \xi\to 1. \tag{3.6.150}$$

Letting $\xi \to 1$ and solving for a and b yield

$$a=\left[3\Omega\frac{c_1}{c_2}\right]^{\frac{1}{3}}, \quad b=\left(\frac{81\Omega}{8}\right)^{\frac{1}{6}}\left(\frac{c_1}{c_2}\right)^{-\frac{1}{3}}. \tag{3.6.151}$$

The asymptotic solutions are

$$F(\xi)\sim\left(3\Omega\frac{c_1}{c_2}\right)^{\frac{1}{3}}(1-\xi)^{\frac{1}{3}}, \quad G(\xi)\sim\left[\frac{81\Omega}{8}\right]^{\frac{1}{6}}\left(\frac{c_1}{c_2}\right)^{-\frac{1}{3}}(1-\xi)^{\frac{2}{3}} \quad \text{as} \quad \xi\to 1. \tag{3.6.152}$$

From (3.6.152),

$$F^3\frac{dF}{d\xi}\sim-\left(3^{\frac{1}{4}}\Omega\frac{c_1}{c_2}\right)^{\frac{4}{3}}(1-\xi)^{\frac{1}{3}}. \tag{3.6.153}$$

Therefore, $F^3\frac{dF}{d\xi}\to 0$ as $\xi\to 1$ and the flux of fluid vanishes at the tip of the fracture. The problem is therefore to solve the system of nonlinear ordinary differential equations

$$\Omega\frac{c_1}{c_2}\frac{dF(\xi)}{d\xi}+\frac{d}{d\xi}\left(F^3(\xi)\frac{dF(\xi)}{d\xi}\right)-\frac{1}{\Gamma}\frac{F(\xi)}{G(\xi)}=0, \tag{3.6.154}$$

$$\frac{c_1}{c_2}\frac{dG(\xi)}{d\xi}+\frac{F(\xi)}{G(\xi)}=0, \tag{3.6.155}$$

subject to

$$F(1)=0, \quad G(1)=0, \quad F^3\frac{dF}{d\xi}\to 0 \quad \text{as} \quad \xi\to 1, \tag{3.6.156}$$

where

$$L(t)=1+\frac{c_1}{c_2}t, \tag{3.6.157}$$

$$h(t,x)=F(\xi), \tag{3.6.158}$$

$$b(t,x)=G(\xi), \tag{3.6.159}$$

$$p(t,x) = F(\xi) + \sigma_{zz}^{\infty}. \tag{3.6.160}$$

Again, three cases of strength of fluid leak-off are now discussed. We first note that in deriving the asymptotic results in (3.6.152) the least dominant term is that from leak-off, that is, the term containing the ratio $\frac{F(\xi)}{G(\xi)}$. A balance is then made between the two remaining terms in (3.6.132). This means that the general asymptotic result in (3.6.152) will also hold for the case of weak leak-off and moderate fluid leak-off. We only need to determine the asymptotic results for the strong leak-off case.

3.6.5 Weak leak-off at the interface: $\Omega \sim 1$ and $\Gamma \gg 1$

When $\Omega \sim 1$ and $\Gamma \gg 1$, exact analytical solution can be derived for the half-width and leak-off depth. Equations (3.6.154)-(3.6.156) become

$$\Omega \frac{c_1}{c_2} \frac{dF(\xi)}{d\xi} + \frac{d}{d\xi}\left(F^3(\xi)\frac{dF(\xi)}{d\xi}\right) = 0, \tag{3.6.161}$$

$$\frac{c_1}{c_2}\frac{dG(\xi)}{d\xi} + \frac{F(\xi)}{G(\xi)} = 0, \tag{3.6.162}$$

$$F(1) = G(1) = 0, \quad F^3\frac{dF}{d\xi} \to 0 \quad \text{as} \quad \xi \to 1. \tag{3.6.163}$$

Integrating (3.6.161) once with respect to ξ gives

$$\Omega\frac{c_1}{c_2}F + F^3\frac{dF}{d\xi} = c, \tag{3.6.164}$$

where c is a constant. Imposing the boundary condition (3.6.163) gives $c = 0$, and therefore (3.6.164) becomes a variable separable ordinary differential equation

$$F^2\frac{dF}{d\xi} = -\Omega\frac{c_1}{c_2}. \tag{3.6.165}$$

Thus,

$$F^3 = -3\Omega\frac{c_1}{c_3}\xi + k. \tag{3.6.166}$$

Since $F(1) = 0$, $k = 3\Omega\frac{c_1}{c_3}$, and therefore

$$F(\xi) = (3\Omega)^{\frac{1}{3}}\left(\frac{c_1}{c_2}\right)^{\frac{1}{3}}(1-\xi)^{\frac{1}{3}}. \tag{3.6.167}$$

Equation (3.6.162) becomes

$$\frac{1}{2}\frac{c_1}{c_2}\frac{dG^2(\xi)}{d\xi} = -3^{\frac{1}{3}}\left(\Omega\frac{c_1}{c_2}\right)^{\frac{1}{3}}(1-\xi)^{\frac{1}{3}}, \tag{3.6.168}$$

Integrating (3.6.168) yields

$$\frac{1}{2}\frac{c_1}{c_2}G^2(\xi) = \frac{3^{\frac{4}{3}}}{4}\left(\Omega\frac{c_1}{c_2}\right)^{\frac{1}{3}}(1-\xi)^{\frac{4}{3}} + k_1. \tag{3.6.169}$$

Imposing (3.6.163) yield $k_1 = 0$. Hence

$$G(\xi) = \left(\frac{81\Omega}{8}\right)^{\frac{1}{6}}\left(\frac{c_1}{c_2}\right)^{-\frac{1}{3}}(1-\xi)^{\frac{2}{3}}. \tag{3.6.170}$$

Since $\xi = x - \frac{c_1}{c_2}t$, $1-\xi = L(t) - x$, and therefore

$$h(t,x) = (3\Omega)^{\frac{1}{3}}\left(\frac{c_1}{c_2}\right)^{\frac{1}{3}} L^{\frac{1}{3}}(t)\left[1 - \frac{x}{L(t)}\right]^{\frac{1}{3}}, \tag{3.6.171}$$

$$b(t,x) = \left(\frac{81\Omega}{8}\right)^{\frac{1}{6}}\left(\frac{c_1}{c_2}\right)^{-\frac{1}{3}} L^{\frac{2}{3}}(t)\left[1 - \frac{x}{L(t)}\right]^{\frac{2}{3}}. \tag{3.6.172}$$

Now, since $h(0,0) = 1$, we obtain from (3.6.171)

$$\frac{c_1}{c_2} = \frac{1}{3\Omega}. \tag{3.6.173}$$

Hence,

$$h(t,x) = L^{\frac{1}{3}}(t)\left[1 - \frac{x}{L(t)}\right]^{\frac{1}{3}}. \tag{3.6.174}$$

In Table 3.1, a comparison is made between the results obtained from numerical computation and exact analytical solution at time $t = 0$ for the case of hydraulic fracture with weak leak-off into the porous rock mass where $\Omega = 1$. This comparison helps validate the results from the numerical computation.

3.6.5.1 Fracture half-width and leak-off depth

The analytical solutions (3.6.171) and (3.6.172) for $h(t,x)$ and $b(t,x)$ are plotted in Figure 3.6.8 and Figure 3.6.9, respectively. The analytical solutions are the exact solutions in the limit $\Gamma \to \infty$ for the hydraulic fracture half-width and leak-off depth when there is weak leak-off at the interface. It is noted in Table 3.1 that the exact and numerical solutions are similar up to 2 decimal places except when x is equal to 0.2 and 0.4. Hence, it is expected that the exact and numerical plots will overlap. Similar to the case $c_3 \neq 0$ for weak leak-off, when $c_3 = 0$, the fluid entering the fracture is approximately equal to the volume of the fracture and the leak-off flux is far less than the fluid flux entering the fracture. However, the growth rate of the fracture half-width $h(t,x)$ for the traveling

x	Fracture Half-width $h(t,x)$		Leak-off depth $b(t,x)$	
	Exact	Numerical	Exact	Numerical
0.000	1.000000	1.000000	2.121320	2.123552
0.200	0.928318	0.928346	1.828098	1.830037
0.400	0.843433	0.843486	1.509062	1.510674
0.600	0.736806	0.736876	1.151630	1.152865
0.800	0.584804	0.584864	0.725481	0.726256
0.900	0.464159	0.464206	0.457025	0.457516
0.920	0.430887	0.430936	0.393852	0.394272
0.940	0.391487	0.391527	0.325118	0.325465
0.960	0.341995	0.342030	0.248111	0.248376
0.980	0.271442	0.271470	0.156300	0.156468
0.982	0.262074	0.262101	0.145698	0.145854
0.984	0.251984	0.252013	0.134695	0.134839
0.986	0.241014	0.241041	0.123223	0.123355
0.988	0.228943	0.228966	0.111189	0.111308
0.990	0.215443	0.215468	0.098463	0.098568
0.992	0.200000	0.200020	0.084853	0.084944
0.994	0.181712	0.181731	0.070044	0.070120
0.996	0.158740	0.158757	0.053454	0.053511
0.998	0.125992	0.126007	0.033674	0.033710
1.000	0.000000	0.000099	0.000000	0.000000

TABLE 3.1: Comparison of the analytical and numerical solutions at time t=0 for the case in which there is weak fluid leak-off at the interface.

wave solution is small compared to when $c_3 \neq 0$. This characteristic is also observed for the growth rate of the leak-off depth $b(t,x)$.

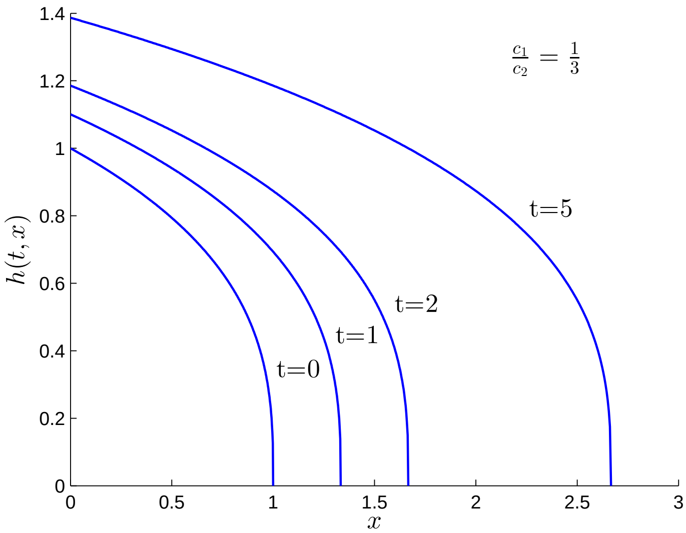

FIGURE 3.6.8: Fracture half-width given by (3.6.158) plotted against x at $t = 0, 1, 2, 5$ when $\Omega = 1$, $c_3 = 0$ and weak leak-off at the interface.

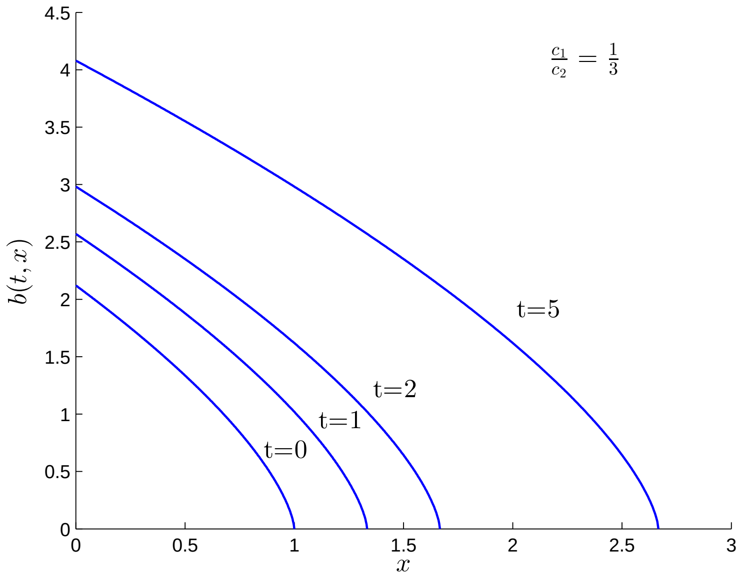

FIGURE 3.6.9: Leak-off depth given by (3.6.159) plotted against x at $t = 0, 1, 2, 5$ when $\Omega = 1$, $c_3 = 0$ and weak leak-off at the interface.

3.6.6 Strong leak-off at the interface: $\Omega \ll 1$ and $\Gamma \sim 1$

We now investigate the case of strong leak-off into the rock-mass. The boundary value problem becomes

$$\frac{d}{d\xi}\left(F^3(\xi)\frac{dF(\xi)}{d\xi}\right) - \frac{1}{\Gamma}\frac{F(\xi)}{G(\xi)} = 0, \tag{3.6.175}$$

$$\frac{c_1}{c_2}\frac{dG(\xi)}{d\xi} + \frac{F(\xi)}{G(\xi)} = 0, \tag{3.6.176}$$

$$F(1) = 0, \quad G(1) = 0, \quad F^3\frac{dF}{d\xi} \to 0 \quad \text{as} \quad \xi \to 1. \tag{3.6.177}$$

The invariant solutions are

$$L(t) = 1 + \frac{c_1}{c_2}t, \tag{3.6.178}$$

$$h(t,x) = F(\xi), \tag{3.6.179}$$

$$b(t,x) = G(\xi), \tag{3.6.180}$$

$$p(t,x) = F(\xi) + \sigma_{zz}^{\infty}. \tag{3.6.181}$$

The strong fluid leak-off case requires numerical integration hence we look for an asymptotic behaviour of $F(\xi)$ and $G(\xi)$ as $\xi \to 1$ of the form

$$F(\xi) \sim a_5(1-\xi)^{s_5} \qquad \text{as} \qquad \xi \to 1, \tag{3.6.182}$$

$$G(\xi) \sim b_5(1-\xi)^{r_5} \qquad \text{as} \qquad \xi \to 1. \tag{3.6.183}$$

Substituting (3.6.182) and (3.6.183) into (3.6.175), we obtain

$$a_5^4 s_5(4s_5-1)(1-\xi)^{4s_5-2} - \frac{1}{\Gamma}\left(\frac{a_5}{b_5}\right)(1-\xi)^{s_5-r_5} \sim 0, \tag{3.6.184}$$

as $\xi \to 1$. In order for the dominant terms in (3.6.184) to balance each other, it is required that

$$4s_5 - 2 = s_5 - r_5, \tag{3.6.185}$$

which implies

$$r_5 = 2 - 3s_5. \tag{3.6.186}$$

Using (3.6.182) and (3.6.183), (3.6.176) becomes

$$-\frac{c_1}{c_2} b_5 r_5 (1-\xi)^{r_5-1} + \left(\frac{a_5}{b_5}\right)(1-\xi)^{s_5-r_5} \sim 0, \tag{3.6.187}$$

as $\xi \to 1$. In order for the dominant terms in (3.6.187) to balance each other, it is required that

$$r_5 - 1 = s_5 - r_5, \tag{3.6.188}$$

which, after substituting (3.6.186), gives

$$s_5 = \frac{3}{7} \qquad \text{and} \qquad r_5 = \frac{5}{7}. \tag{3.6.189}$$

Solving for a_5 and b_5 in (3.6.184) and (3.6.187), using (3.6.189), we obtain

$$a_5 = \left(\frac{343}{45}\right)^{\frac{1}{7}} \left(\frac{c_1}{c_2}\right)^{\frac{1}{7}} \left(\frac{1}{\Gamma}\right)^{\frac{2}{7}} \qquad \text{and} \qquad b_5 = \left(\frac{7^5}{3\times 5^4}\right)^{\frac{1}{7}} \left(\frac{c_1}{c_2}\right)^{-\frac{3}{7}} \left(\frac{1}{\Gamma}\right)^{\frac{1}{7}}. \tag{3.6.190}$$

The asymptotic solutions of (3.6.175) and (3.6.176) as $\xi \to 1$ are

$$F(\xi) \sim \left(\frac{343}{45}\right)^{\frac{1}{7}} \left(\frac{c_1}{c_2}\right)^{\frac{1}{7}} \left(\frac{1}{\Gamma}\right)^{\frac{2}{7}} (1-\xi)^{\frac{3}{7}}, \tag{3.6.191}$$

$$G(\xi) \sim \left(\frac{7^5}{3\times 5^4}\right)^{\frac{1}{7}} \left(\frac{c_1}{c_2}\right)^{-\frac{3}{7}} \left(\frac{1}{\Gamma}\right)^{\frac{1}{7}} (1-\xi)^{\frac{5}{7}}. \tag{3.6.192}$$

3.6.6.1 Fracture half-width and leak-off depth

In Figure (3.6.10), the half-width of the fracture given by (3.6.179) for strong fluid leak-off at the fracture interface is plotted. In agreement with the case $c_3 \neq 0$, when $c_3 = 0$, the rate of growth of the half-width of the fracture when there is strong leak-off is smaller than when there is weak leak-off at the fracture interface. The leak off depth given by (3.6.180) when there is strong leak-off is plotted in Figure 3.6.11. The fluid dynamics for the fracture propagation remains the same as when $c_3 \neq 0$ for strong fluid leak-off at the fracture interface. Thus, a small proportion of the injected fluid is responsible for the propagation of the fracture when there is strong leak-off of fluid at the fracture walls, which in turn, leads to weak growth rate of the fracture half-width.

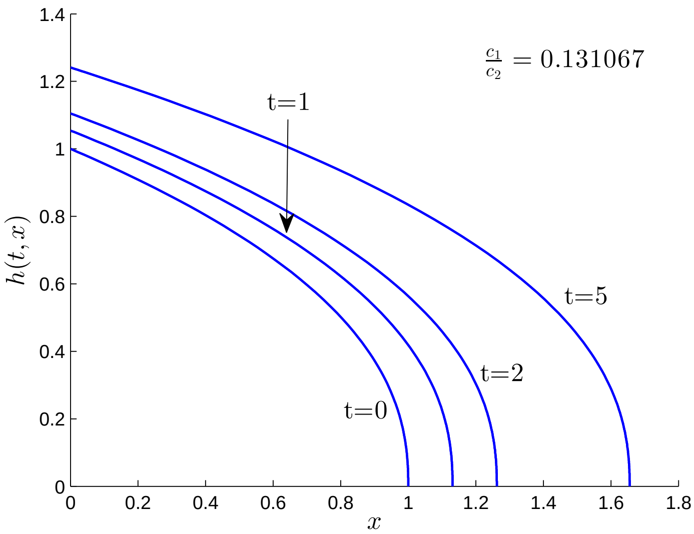

FIGURE 3.6.10: Fracture half-width given by (3.6.179) plotted against x at $t = 0, 1, 2, 5$ when $\Gamma = 1$, $c_3 = 0$ and strong leak-off at the interface.

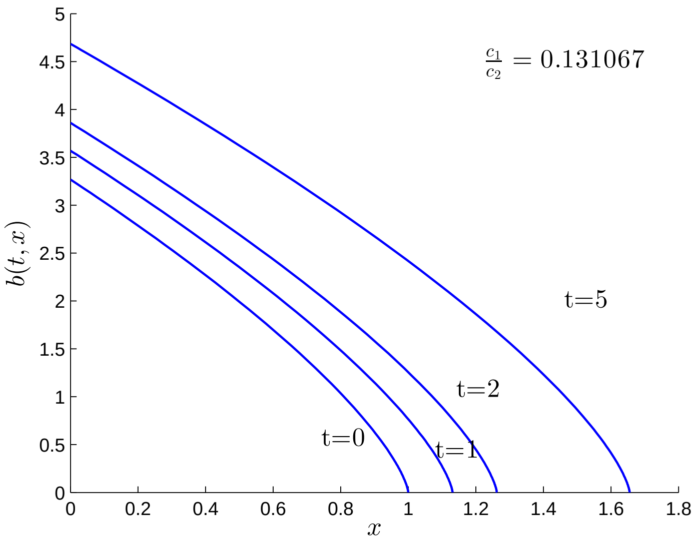

FIGURE 3.6.11: Leak-off depth given by (3.6.180) plotted against x at $t = 0, 1, 2, 5$ when $\Gamma = 1$, $c_3 = 0$ and strong leak-off at the interface.

3.6.7 Moderate leak-off at the interface: $\Omega \sim 1$ and $\Gamma \sim 1$

Consider the case of moderate fluid leak-off into the rock-mass

$$\Omega \frac{c_1}{c_2}\frac{dF(\xi)}{d\xi} + \frac{d}{d\xi}\left(F^3(\xi)\frac{dF(\xi)}{d\xi}\right) - \frac{1}{\Gamma}\frac{F(\xi)}{G(\xi)} = 0, \tag{3.6.193}$$

$$\frac{c_1}{c_2}\frac{dG(\xi)}{d\xi} + \frac{F(\xi)}{G(\xi)} = 0, \tag{3.6.194}$$

$$F(1) = 0, \quad G(1) = 0, \quad F^3\frac{dF}{d\xi} \to 0 \quad \text{as} \quad \xi \to 1. \tag{3.6.195}$$

Once $S(u)$ and$R(u)$ are obtained, the invariant solution for $L(t)$, $V(t)$, $h(t, x)$ and $b(t, x)$ are given by

$$L(t) = 1 + \frac{c_1}{c_2}t, \tag{3.6.196}$$

$$h(t, x) = F(\xi), \tag{3.6.197}$$

$$b(t, x) = G(\xi), \tag{3.6.198}$$

$$p(t, x) = F(\xi) + \sigma_{zz}^{\infty}. \tag{3.6.199}$$

With $\Omega \sim 1$ and $\Gamma \sim 1$, the asymptotic solutions of (3.6.193) and (3.6.194) as $\xi \to 1$ are as given in (3.6.152)

$$F(\xi) \sim \left(3\Omega\frac{c_1}{c_2}\right)^{\frac{1}{3}}(1-\xi)^{\frac{1}{3}}, \tag{3.6.200}$$

$$G(\xi) \sim \left(\frac{81\Omega}{8}\right)^{\frac{1}{6}}\left(\frac{c_1}{c_2}\right)^{-\frac{1}{3}}(1-\xi)^{\frac{2}{3}}. \tag{3.6.201}$$

3.6.7.1 Fracture half-width and leak-off depth

The half-width of the fracture $h(t, x)$ and the leak-off depth $b(t, x)$ for moderate fluid leak-off at the interface are plotted in Figures 3.6.12 and 3.6.13, respectively. It can be seen from Figure 3.6.12 that the rate of propagation for the fracture half-width when there is moderate fluid leak-off is small. The rate of growth of the fracture half-width is the smallest for the case of moderate fluid leak-off at the fluid-rock interface. This is expected since an equivalent fluid of the fluid entering the fracture is lost at the interface and very little fluid is left to drive the fracture propagation.

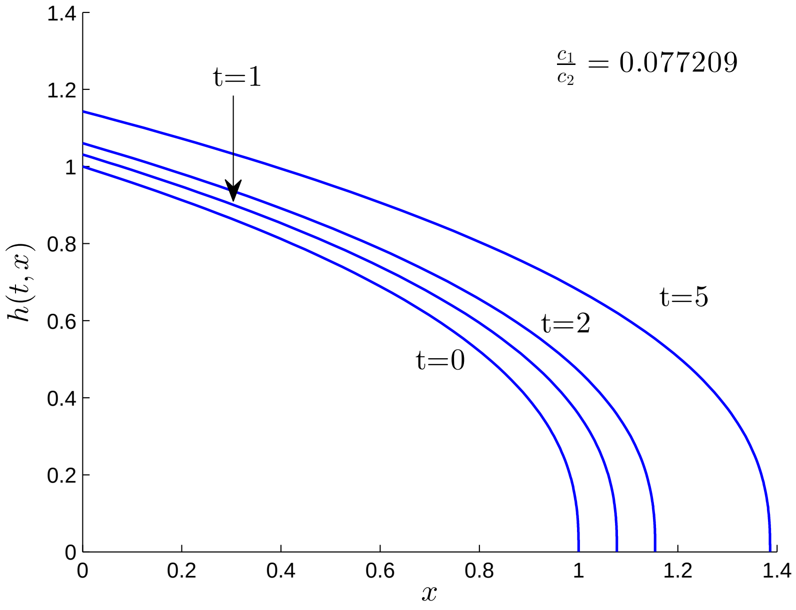

FIGURE 3.6.12: Fracture half-width given by (3.6.197) plotted against x at $t = 0, 1, 2, 5$ when $\Omega = \Gamma = 1$, $c_3 = 0$ and moderate leak-off at the interface.

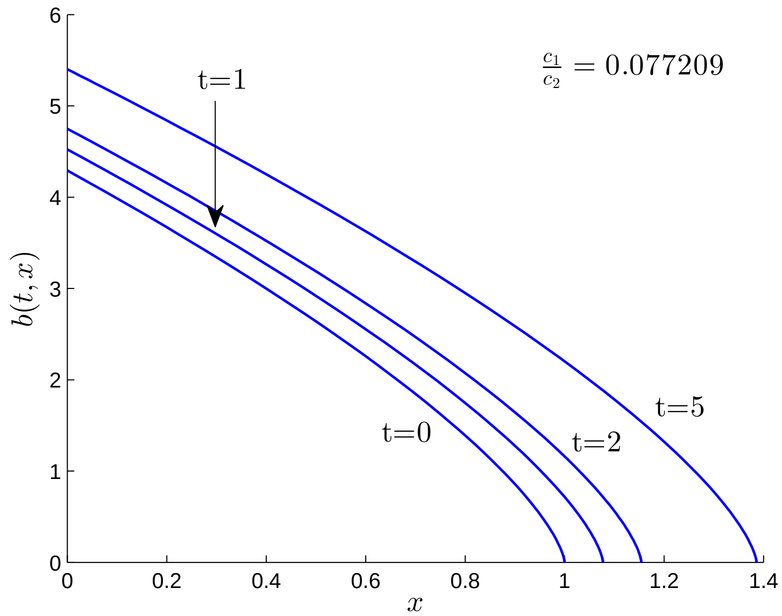

FIGURE 3.6.13: Leak-off depth given by (3.6.198) plotted against x at $t = 0, 1, 2, 5$ when $\Omega = \Gamma = 1$, $c_3 = 0$ and weak leak-off at the interface.

3.6.8 Length of the fracture

The length of the fracture $L(t)$, when $c_3 = 0$, grows almost linearly with time, the rate of growth depending on the ratio $\frac{c_1}{c_2} > 0$. The ratio $\frac{c_1}{c_2}$ was obtained analytically for the case of weak leak-off at the fluid-rock interface and numerically for strong and moderate fluid leak-off at the fracture interface. The ratio $\frac{c_1}{c_2}$ has the least value for the case of moderate fluid leak-off and the highest value for weak leak-off. Figure 3.6.14 clearly illustrates the growth of the length of the fracture $L(t)$ for the three distinct cases of fluid leak-off. As shown in Figure 3.6.14, the fracture length for weak leak-off plotted in (i) grows the strongest. For the case of strong fluid leak-off, the growth of the length of the fracture with time is illustrated by (ii). The growth of the fracture length when there is moderate fluid leak-off is depicted in (iii). For this case, the length of the fracture $L(t)$ increases steadily with time. Similar to case $c_3 \neq 0$, the growth rate for the fracture length when there is weak leak-off at the interface is expected to be greater than when there is strong fluid leak-off since for weak leak-off, only a small proportion of the injected fluid is lost at the fracture walls. The growth rate for the length of the fracture when there is strong fluid leak-off at the interface is greater than when there is moderate fluid leak-off since for strong leak-off, the fluid flux at the fracture entry is much more than the fracture volume. The moderate fluid leak-off case has the least growth rate of fracture length since much of the fluid flux entering the fracture, which is approximately equal to the fracture volume, is lost at the fracture walls.

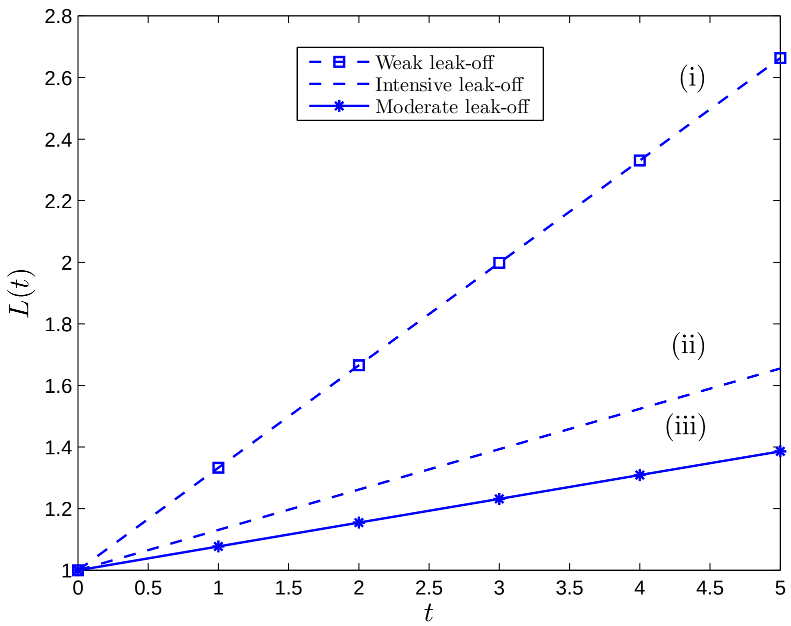

FIGURE 3.6.14: Length of the fracture $L(t)$ plotted against t for (i) weak fluid leak-off, (ii) strong fluid leak-off and (iii) moderate leak-off of fluid at the interface.

3.7 Conclusions

In this chapter, a two-dimensional fluid-driven fracture propagating in a permeable rock formation is considered. The momentum equation together with the conservation of mass equation are used to describe the flow of fluid inside the fracture and the Darcy's fluid flow model is used to describe the flow of fluid in the encompassing rock formation. The momentum equation was simplified by comparing the order of magnitude of the terms in the x and z direction. The conservation of mass equation remained unchanged after comparing the order of magnitude of its terms. Using the boundary conditions, a nonlinear diffusion equation governing the evolution of the half-width of the fracture $h(t, x)$ and a first order partial differential equation governing the leak-off depth $b(t, x)$ were derived. The system of equations governing the physical mechanisms were represented in terms of dimensionless variables. The resulting system of equations contained dimensionless parameters Ω and Γ. Using the definition of Ω and Γ, the fluid leak-off at the fracture interface was classified into three forms, namely, weak, strong and moderate leak-off. When $\Omega \sim 1$ and $\Gamma \gg 1$, there is weak leak-off at the fracture interface and when $\Omega \ll 1$ and $\Gamma \sim 1$, there is strong leak-off at the fracture interface. Lastly, when $\Omega \sim 1$ and $\Gamma \sim 1$, there is moderate leak-off at the fracture interface.
Lie symmetry analysis was used to reduce the system consisting of the nonlinear diffusion equation and Darcy's fluid flow model to a system consisting of a nonlinear second order ordinary differential equation and a first order ordinary differential equation, respectively, for the two cases considered, namely, $c_3 \neq 0$ and case $c_3 = 0$. For the case $c_3 \neq 0$, the solution was generated by a Lie point symmetry of the form

$$X = (c_2 + c_3 t)\frac{\partial}{\partial t} + (c_1 + 2c_3 x)\frac{\partial}{\partial x} + c_3 b\frac{\partial}{\partial b} + c_3 h\frac{\partial}{\partial h}, \tag{3.7.1}$$

where

$$\frac{c_3}{c_2} = \frac{1}{S^3(0)}. \tag{3.7.2}$$

The value of the ratio $\frac{c_3}{c_2}$ decreases from the weak leak-off to moderate leak-off case. Graphical solutions for the half-width of the fracture and leak-off depth are given for each case of fluid leak-off. Of interest was that the half-width of the fracture increased even when there was strong fluid leak-off at the fracture interface. The half-width of the fracture for the case of weak leak-off was growing more than the other cases of fluid leak-off and the case of moderate leak-off was growing the least. These results were however expected since for the case of weak leak-off, the fluid discharging into the rock-mass formation is far less than what is being pumped into the fracture hence more fluid is there to drive the propagation of the fracture unlike in the strong and moderate case were little fluid is responsible to drive the fracture propagation.

Figure 3.6.7 shows that the length of the fracture was growing the fastest for the case of weak leak-off at all times $t > 0$ and the case of moderate fluid leak-off had the least growth. The length of the fracture was growing quadratically with time for case $c_3 \neq 0$. When $c_3 \neq 0$, analytical solutions to compare with numerical solutions could not be found.

In the case $c_3 = 0$, the solution was generated by a Lie point symmetry of the form

$$X = c_2 \frac{\partial}{\partial t} + c_1 \frac{\partial}{\partial x}. \tag{3.7.3}$$

The propagation behaviour of the fracture half-width for when $c_3 = 0$ is similar to when $c_3 \neq 0$ for all three distinct cases of fluid leak-off at the interface. However, when $c_3 = 0$, we found an analytical solution for the case of weak leak-off. The corresponding numerical solution was found to be in good agreement with the analytical solution as presented in Table 3.1. The numerical and analytical solutions agree to 2 decimal places except when x is 0.2 or 0.4. In Figure 3.6.14, the growth of the length of the fracture is shown. The fracture length grew linearly with time when $c_3 = 0$ with the fracture length for the case in which there is weak leak-off growing the fastest.

Chapter 4

TWO-DIMENSIONAL HYDRAULIC FRACTURE WITH NON-DARCY FLOW IN PERMEABLE ROCK-MASS

4.1 Introduction

In this chapter, we study a two-dimensional hydraulic fracture propagating in a porous medium with non-Darcy fluid flow in the rock-mass formation. Darcy flow model assumes laminar flow and neglects inertial effects. In a case of high velocity flow, the flow model exhibits a nonlinear relationship between the pressure gradient and the leak-off velocity. A lot of models have been proposed to correct the deviation induced by inertial effects from Darcy's flow model. An extensive review of a non-Darcy fluid flow in a permeable medium is covered in [45–49]. The two most historically used criterion for identifying the beginning of non-Darcy fluid flow are: the Reynolds and Forchheimer number. In the earliest work on criterion for non-Darcy flow, the Reynolds number was used to identify turbulent flow in pipes. A lot of researchers likened non-Darcy flow in a permeable medium to turbulent flow in a conduit, hence the Reynolds number was adapted to describe the non-Darcy fluid flow in a permeable medium. Figure 4.1.1 gives a classification of flow regimes, as proposed by Skjetne [50], in complex porous media for a range of Reynolds numbers. The Reynolds number is varied from low to high values and the following flow regimes are noted [50]: 1. Darcy 2. Weak inertia 3. Strong inertia (Forchheimer) 4. transition from strong inertia to turbulence 5. Turbulence. Because of the complex structure of porous media, it is difficult to define the characteristic

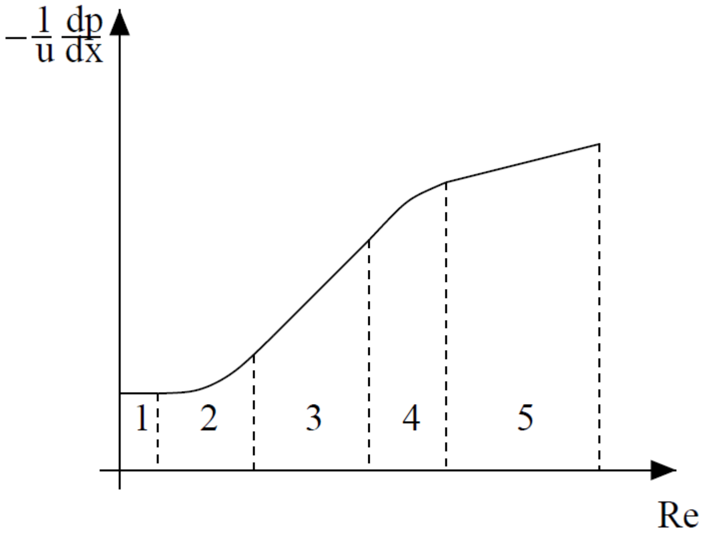

FIGURE 4.1.1: Flow regimes in a permeable medium for varied Reynolds number, adapted from [50].

length in the Reynolds number equation. However, in some cases, such as packed particles, a representative diameter is selected to be the characteristic length. This could lead to misleading conclusions. It is for this unclear determination of the characteristic length that in this research we use the Forchheimer number as a criteria to describe the non-Darcy flow in the porous media. There is no expression that is widely superior in describing the non-Darcy fluid flow in a permeable medium, however the Forchheimer model is often preferred because of its clear meaning and broad applicability. It should be noted that there is no accurate or general equation available to determine the non-Darcy flow coefficient, β, in the Forchheimer fluid flow model. It is helpful to determine the non-Darcy flow coefficient based on the problem.

In this research, we use the Forchheimer flow model to describe the non-Darcy fluid flow in the porous medium. To obtain the Forchheimer flow model, an additional term is added to Darcy's equation to account for inertial effects [21, 51, 52]. A validation of Forchheimer's model for fluid flowing through a permeable medium with converging boundaries was given in [45]. Ma and Ruth [53] performed analysis of high Forchheimer number flow in a permeable medium. The Reynolds number was defined as

$$Re = \frac{\rho \bar{U} d}{\mu}, \tag{4.1.1}$$

where d is the throat diameter, ρ, fluid density, μ, fluid viscosity and $\bar{U}$ is the mean velocity. The Forchheimer number, F_0, is

$$F_0 = \frac{\kappa \beta \rho \bar{U}}{\mu}, \tag{4.1.2}$$

where κ is the permeability, β is the non-Darcy coefficient and a characteristic of the porous medium, and ρ, μ and $\bar{U}$ are as defined earlier. When $F_0 > 1$, the inertial effects are dominant over viscous effects and non-dominant when $F_0 < 1$. The Forchheimer number is used to identify the onset of non-Darcy flow in a porous medium. Low values of the Forchheimer number describe Darcy flow while high values describe non-Darcy flow. When the non-Darcy coefficient or the fluid velocity approaches zero, the Forchheimer number tends to zero. Through experimental data, several authors derived an empirical model for correlations of the non-Darcy coefficient and the permeability of the form [54–56]

$$\beta = \frac{a}{\kappa^b}, \tag{4.1.3}$$

where a and b are constants. Generally, the non-Darcy coefficient decreases with an increase in porosity and permeability. Pascal et al. [56] gave the parameters $a = 4.8 \times 10^{12}$ and $b = 1.176$. In their paper, Ruth and Ma [57] recommended that the permeability κ in (4.1.2) be treated as a velocity dependent parameter for non-Darcy flow regimes. The Forchheimer number can be found for any type of porous material as long as the permeability κ and the non-Darcy coefficient β can be determined through experimental or empirical techniques [58]. Ma and Ruth [53] when considering high

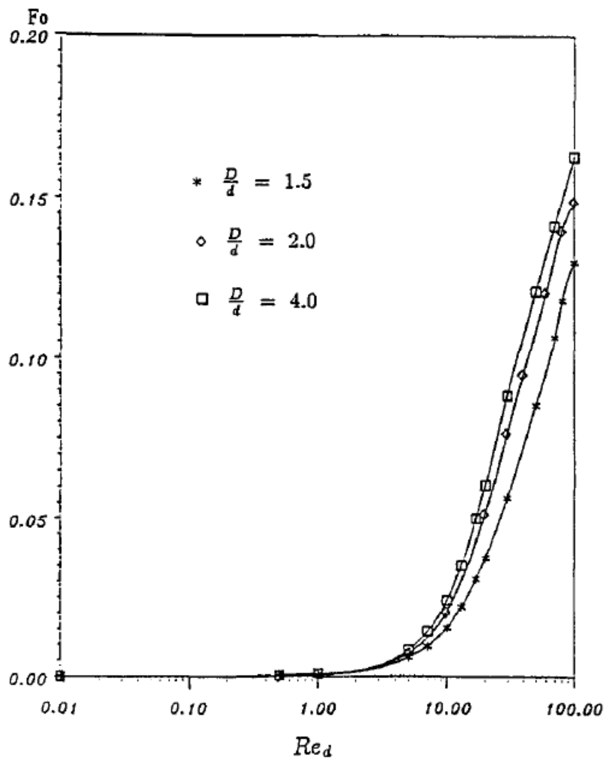

FIGURE 4.1.2: The Forchheimer number F_0 plotted against the Reynolds number Re, adapted from [53].

Forchheimer number flow in a permeable medium found that the critical Reynolds number was 3-10 while the corresponding Forchheimer number was 0.005-0.02. Several authors found the critical Reynolds number and Forchheimer number for non-Darcy flow in porous media to be in different ranges [21, 59, 60], hence consistent results cannot be achieved. Due to this inconsistency, no specific critical values are widely accepted as criterion for non-Darcy flow in porous medium. Usually the critical Reynolds number and Forchheimer number are selected based on the underlying problem. In their work, Ma and Ruth [53] when investigating the microscopic flow mechanisms of high Forchheimer number flow in a permeable medium gave a relationship between the Forchheimer number F_0 and the Reynolds number Re as depicted in Figure 4.1.2. At considerably low Reynolds number, the Forchheimer number is almost zero. As the Reynolds number increased beyond 1, a quadratic relationship is observed. Figure 4.1.3 shows flow regimes in a permeable medium for varied velocity. The red line gives a relationship between

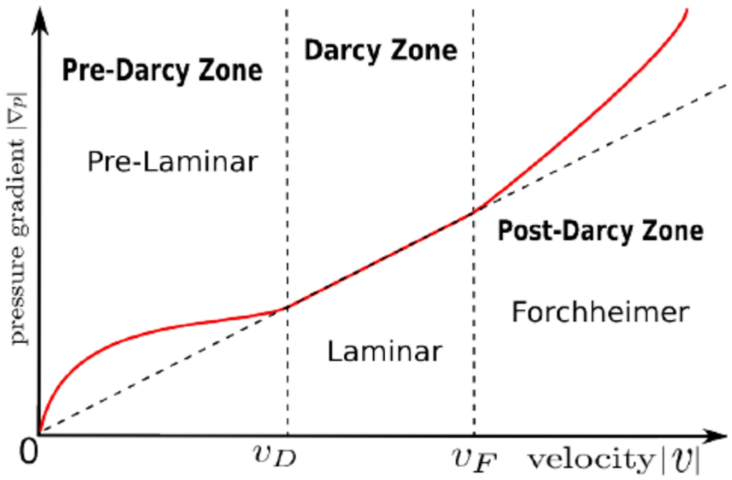

FIGURE 4.1.3: Schematic representation of flow regimes in porous media, adapted from [49].

the pressure gradient and the fluid velocity for the indicated flow zones. The pre-Darcy zone occurs for low velocity flow. It is also referred to as non-Darcy flow. But for this Masters research, non-Darcy flow refers to high velocity flow. High velocity flow occurs in the Post-Darcy Zone. It should be noted that for both Pre-Darcy and Post-Darcy zone, which are non-Darcy, there is a nonlinear relationship between the pressure gradient and the fluid velocity. For the Darcy zone, the red line depicts a linear relationship. Figure 4.1.3 solidifies the need to consider other flow models when modeling fluid flow in a porous medium for high and low velocity.

4.2 Fluid flow in the porous medium

Since we are interested in high velocity flows in the rock media there is an inclusion of an inertia term to equation (3.3.7) and the resulting model called the Forchheimer model is given by

$$-\nabla p_d = \frac{\mu}{\kappa}\mathbf{v} + \beta\rho\,|\mathbf{v}|\,\mathbf{v}, \qquad |\mathbf{v}| = \sqrt{u^2+v^2}, \tag{4.2.1}$$

where p_d is the fluid pressure, μ is the dynamic viscosity, κ is the rock permeability, β is the non-Darcy coefficient, $\mathbf{v} = (u, v)$ is the fluid velocity and ρ, the fluid density. In (4.2.1), the left hand side is the total pressure gradient which is equal to the sum of a linear and a square term in leak-off velocity. The square term accounts for additional pressure drop when there is high velocity.

For a one directional flow in a porous medium, $\mathbf{v} = (0, v)$ in the z-direction. Equation (4.2.1) becomes

$$-\frac{\partial p_d}{\partial z} = \frac{\mu}{\kappa}\frac{\partial b}{\partial t} + \beta\rho\left(\frac{\partial b}{\partial t}\right)^2. \tag{4.2.2}$$

Integrate (4.2.2) from $z = h$ to $z = h + b$ to obtain

$$\frac{\Lambda h}{b} = \frac{\mu}{\kappa}\frac{\partial b}{\partial t} + \beta\rho\left(\frac{\partial b}{\partial t}\right)^2. \tag{4.2.3}$$

In the next section we non-dimensionalize (4.2.3) using the dimensionless variables introduced in Section 3.5. The mass balance equation is also derived and the problem statement is outlined.

4.3 Analysis of the dimensionless system of equations

We rewrite (4.2.3) in terms of the dimensionless variables introduced in Section 3.5. Substituting the dimensionless variables into (4.2.3), we obtain

$$\frac{\kappa\Lambda}{\mu}\frac{HT}{B^2}\frac{\bar{h}}{\bar{b}} = \frac{\partial\bar{b}}{\partial\bar{t}} + \frac{\beta\rho\kappa}{\mu}\frac{B}{T}\left(\frac{\partial\bar{b}}{\partial\bar{t}}\right)^2. \tag{4.3.1}$$

Dropping the overhead bars and using $B^2 = \frac{\Lambda\kappa HT}{\mu}$, (4.3.1) becomes

$$\frac{h}{b} = \frac{\partial b}{\partial t} + F_0\left(\frac{\partial b}{\partial t}\right)^2, \tag{4.3.2}$$

where $F_0 = \frac{\beta\rho\kappa}{\mu}\frac{B}{T}$ is the Forchheimer number. When β approaches zero, F_0 tends to zero and the pressure gradient can be calculated using Darcy's law. Solving the quadratic equation (4.3.2) we obtain since $\frac{\partial b}{\partial t} > 0$,

$$\frac{\partial b}{\partial t} = \frac{1}{F_0}\left[\left(\frac{1}{4} + F_0\frac{h}{b}\right)^{\frac{1}{2}} - \frac{1}{2}\right], \quad F_0 > 0. \tag{4.3.3}$$

The similarity parameters Ω and Γ are ratios as discussed in Section 3.5. As with the previous section three cases of strength of leak-off are considered. The global mass balance equation is given by (3.5.23). The problem statement is therefore to solve the system of partial differential equations

$$\Omega\frac{\partial h}{\partial t} - h^3\frac{\partial^2 h}{\partial x^2} - 3h^2\left(\frac{\partial h}{\partial x}\right)^2 + \frac{1}{\Gamma}\frac{\partial b}{\partial t} = 0, \tag{4.3.4}$$

$$\frac{h}{b} = \frac{\partial b}{\partial t} + F_0\left(\frac{\partial b}{\partial t}\right)^2, \tag{4.3.5}$$

for $h(t,x)$, $b(t,x)$ and $L(t)$ subject to the boundary conditions

$$h(L(t),t) = 0, \qquad b(L(t),t) = 0, \tag{4.3.6}$$

and the mass balance law

$$\Omega\frac{dV}{dt} = -2h^3(0,t)\frac{\partial h(0,t)}{\partial x} - 2\left(\frac{1}{\Gamma}\right)\int_0^{L(t)}\frac{\partial b}{\partial t}\mathrm{d}x, \tag{4.3.7}$$

where

$$L(0) = 1, \quad h(0,0) = 1 \quad \text{and} \quad V(t) = 2\int_0^{L(t)} h(t,x)\mathrm{d}x. \tag{4.3.8}$$

In the next section we derive a group invariant solution for $h(t,x)$, $b(t,x)$ and $L(t)$. We start by looking for the symmetry generators of the system of equations (4.3.4)-(4.3.5).

4.4 Lie point symmetries and group invariant solutions

We first derive the Lie point symmetries for the coupled differential equation (4.3.4) and (4.3.5). The Lie point symmetries will be used to construct a group invariant solution for $h(t,x)$ and $b(t,x)$. We will use Sym [61], a Mathematica software package to obtain the Lie point symmetries. The Sym package was implemented to verify the Lie symmetries derived in Chapter 3. The Lie point symmetry generator

$$X = \xi^1(t,x,b,h)\frac{\partial}{\partial t} + \xi^2(t,x,b,h)\frac{\partial}{\partial x} + \eta^1(t,x,b,h)\frac{\partial}{\partial b} + \eta^2(t,x,b,h)\frac{\partial}{\partial h} \tag{4.4.1}$$

(4.3.4) and (4.3.5) is derived by solving the determining equations

$$X^{[2]}\left(\Omega h_t - h^3 h_{xx} - 3h^2(h_x)^2 + \frac{1}{\Gamma}b_t\right)\Bigg|_{\substack{\Omega h_t - h^3 h_{xx} - 3h^2(h_x)^2 + \frac{1}{\Gamma}b_t = 0 \\ b_t + \frac{1}{2F_0} - \frac{1}{F_0}\left(\frac{1}{4}+F_0\frac{h}{b}\right)^{\frac{1}{2}} = 0}} = 0, \quad F_0 > 0, \tag{4.4.2}$$

$$X^{[2]}\left(b_t + \frac{1}{2F_0} - \frac{1}{F_0}\left(\frac{1}{4}+F_0\frac{h}{b}\right)^{\frac{1}{2}}\right)\Bigg|_{\substack{\Omega h_t - h^3 h_{xx} - 3h^2(h_x)^2 + \frac{1}{\Gamma}b_t = 0 \\ b_t + \frac{1}{2F_0} - \frac{1}{F_0}\left(\frac{1}{4}+F_0\frac{h}{b}\right)^{\frac{1}{2}} = 0}} = 0, \quad F_0 > 0, \tag{4.4.3}$$

for ξ^1, ξ^2, η^1 and η^2 where $X^{[2]}$ is the second prolongation of the Lie point symmetry generator X. The Lie point symmetries obtained are the same to those obtained for the case of Darcy flow given by (3.6.7) and (3.6.8). Hence the group invariant solutions for the half-width of the fracture, $h(t,x)$, and leak-off depth, $b(t,x)$, are

$$h(t,x) = (c_2 + c_3 t) f(\xi), \tag{4.4.4}$$

$$b(t,x) = (c_2 + c_3 t) g(\xi), \tag{4.4.5}$$

where f and g are an arbitrary functions of ξ. The variable ξ is given by

$$\xi = \frac{c_1 + 2c_3 x}{2c_3(c_2 + c_3 t)^2}. \tag{4.4.6}$$

Case: $c_3 \neq 0$

We will now express (4.3.4), (4.3.5) and the boundary conditions (4.3.6) and (4.3.7) in terms of ξ, $f(\xi)$ and $g(\xi)$. We substitute (4.4.4) and (4.4.5) into (4.3.4) and (4.3.5) for $h(t,x)$ and $b(t,x)$ to obtain

$$\Omega\left(c_3 f(\xi) - 2c_3\xi\frac{df(\xi)}{d\xi}\right) - \frac{d}{d\xi}\left(f^3(\xi)\frac{df(\xi)}{d\xi}\right) + \frac{1}{\Gamma}\left(c_3 g(\xi) - 2c_3\xi\frac{dg(\xi)}{d\xi}\right) = 0, \tag{4.4.7}$$

$$\frac{f(\xi)}{g(\xi)} = c_3 g(\xi) - 2c_3\xi\frac{dg(\xi)}{d\xi} + F_0\left[c_3^2 g^2(\xi) - 4c_3^2\xi g(\xi)\frac{dg(\xi)}{d\xi} + 4c_3^2\xi^2\left(\frac{dg(\xi)}{d\xi}\right)^2\right]. \tag{4.4.8}$$

Since equation (4.4.7) and (4.4.8) do not depend on c_1, we choose $c_1 = 0$ such that $\xi = 0$ when $x = 0$. Equation (4.4.6) becomes

$$\xi = \frac{x}{(c_2 + c_3 t)^2}. \tag{4.4.9}$$

The boundary conditions (4.3.6) becomes

$$f(\xi_0) = 0, \quad g(\xi_0) = 0 \quad \text{at} \quad \xi_0 = \frac{L(t)}{(c_2 + c_3 t)^2}. \tag{4.4.10}$$

The fracture length is thus derived as

$$L(t) = \left(1 + \frac{c_3}{c_2}t\right)^2. \qquad (4.4.11)$$

We represent the mass balance equation (4.3.7) in terms of ξ, $f(\xi)$ and $g(\xi)$. Equation (4.3.7) becomes

$$\Omega\frac{dV}{dt} = -2(c_2+c_3t)^2 f^3(0)\frac{df(0)}{d\xi} - 6c_3(c_2+c_3t)^2\left(\frac{1}{\Gamma}\right)\int_0^{\frac{1}{c_2^2}} g(\xi)d\xi. \qquad (4.4.12)$$

We now evaluate the left side of the mass balance equation. Substituting (4.4.4) into (4.3.8) we obtain

$$V(t) = 2(c_2+c_3t)^3\int_0^{\frac{1}{c_2^2}} f(\xi)d\xi. \qquad (4.4.13)$$

Differentiating (4.4.13) with respect to t gives

$$\frac{dV}{dt} = 6c_3(c_2+c_3t)^2\int_0^{\frac{1}{c_2^2}} f(\xi)d\xi. \qquad (4.4.14)$$

Substituting (4.4.14) into (4.4.12) and dividing through by $2(c_2+c_3t)^2$ yields

$$f^3(0)\frac{df(0)}{d\xi} = -3c_3\left[\Omega\int_0^{\frac{1}{c_2^2}} f(\xi)d\xi + \frac{1}{\Gamma}\int_0^{\frac{1}{c_2^2}} g(\xi)d\xi\right]. \qquad (4.4.15)$$

The mathematical formulation of the non-Darcy fluid flow problem is summarized as follows

$$\Omega\left(c_3f(\xi) - 2c_3\xi\frac{df(\xi)}{d\xi}\right) - \frac{d}{d\xi}\left(f^3(\xi)\frac{df(\xi)}{d\xi}\right) + \frac{1}{\Gamma}\left(c_3g(\xi) - 2c_3\xi\frac{dg(\xi)}{d\xi}\right) = 0, \qquad (4.4.16)$$

$$c_3g(\xi) - 2c_3\xi\frac{dg(\xi)}{d\xi} + F_0\left[c_3^2g^2(\xi) - 4c_3^2\xi g(\xi)\frac{dg(\xi)}{d\xi} + 4c_3^2\xi^2\left(\frac{dg(\xi)}{d\xi}\right)^2\right] - \frac{f(\xi)}{g(\xi)} = 0, \qquad (4.4.17)$$

$$f(\xi_0) = 0, \quad g(\xi_0) = 0, \qquad (4.4.18)$$

$$f^3(0)\frac{df(0)}{d\xi} = -3c_3\left[\Omega\int_0^{\frac{1}{c_2^2}} f(\xi)d\xi + \frac{1}{\Gamma}\int_0^{\frac{1}{c_2^2}} g(\xi)d\xi\right]. \qquad (4.4.19)$$

The invariant solutions are

$$L(t) = \left(1 + \frac{c_3}{c_2}t\right)^2, \qquad (4.4.20)$$

$$V(t) = V_0(c_2+c_3t)^3, \quad V_0 = 2\int_0^{\frac{1}{c_2^2}} f(\xi)d\xi, \qquad (4.4.21)$$

$$h(t,x) = (c_2+c_3t)f(\xi), \qquad (4.4.22)$$

$$b(t,x) = (c_2 + c_3 t) g(\xi), \tag{4.4.23}$$

$$p_f(t,x) = \sigma_{zz}^{\infty} + h(t,x), \tag{4.4.24}$$

where $0 < \xi < \frac{1}{c_2^2}$.

To simplify the problem statement we make change of variables

$$u = \frac{x}{L(t)}, \quad \xi = \frac{1}{c_2^2} u, \quad f(\xi) = \left(\frac{c_3}{c_2^4}\right)^{\frac{1}{3}} S(u), \quad g(\xi) = \frac{1}{c_3} R(u), \tag{4.4.25}$$

where the range of u is $0 \leq u \leq 1$. Expressed in terms of the similarity variables $S(u)$ and $R(u)$, the problem is therefore to solve the system of ordinary differential equation as follows

$$\Omega\left(S(u) - 2u\frac{dS(u)}{du}\right) - \frac{d}{du}\left(S^3(u)\frac{dS(u)}{du}\right) + \frac{1}{\Gamma}\left(\frac{c_3}{c_2}\right)^{-\frac{4}{3}}\left(R(u) - 2u\frac{dR(u)}{du}\right) = 0, \tag{4.4.26}$$

$$R(u) - 2u\frac{dR(u)}{du} + F_0\left[R^2(u) - 4uR(u)\frac{dR(u)}{du} + 4u^2\left(\frac{dR(u)}{du}\right)^2\right] - \left(\frac{c_3}{c_2}\right)^{\frac{4}{3}}\frac{S(u)}{R(u)} = 0, \tag{4.4.27}$$

subject to the boundary conditions

$$S(1) = 0, \quad R(1) = 0, \tag{4.4.28}$$

$$S^3(0)\frac{dS(0)}{du} = -3\left[\Omega\int_0^1 S(u)du + \left(\frac{c_3}{c_2}\right)^{-\frac{4}{3}}\frac{1}{\Gamma}\int_0^1 R(u)du\right]. \tag{4.4.29}$$

The invariant solutions are of the form

$$L(t) = \left(1 + \frac{c_3}{c_2}t\right)^2, \tag{4.4.30}$$

$$V(t) = V_0\left(1 + \frac{c_3}{c_2}t\right)^3, \quad V_0 = 2\left(\frac{c_3}{c_2}\right)^{\frac{1}{3}}\int_0^1 S(u)du, \tag{4.4.31}$$

$$h(t,x) = \left(1 + \frac{c_3}{c_2}t\right)\frac{S(u)}{S(0)}, \tag{4.4.32}$$

$$b(t,x) = \left(1 + \frac{c_3}{c_2}t\right)S^3(0)R(u), \tag{4.4.33}$$

$$p_f(t,x) = \sigma_{zz}^{\infty} + h(t,x), \tag{4.4.34}$$

where

$$S(0) = \left(\frac{c_3}{c_2}\right)^{-\frac{1}{3}}. \tag{4.4.35}$$

We have now completed the mathematical formulation for a hydraulic fracture with non-Darcy fluid flow in the porous rock-mass. The system of differential equation (4.4.26)-(4.4.27) as well as the invariant solutions (4.4.30)-(4.4.34) depend on the ratio $\frac{c_3}{c_2}$ and not on the constants c_2 and c_3 separately.

The general asymptotic solution for equations (4.4.26) and (4.4.27) as $\xi \to 1$ can be derived. We look for an asymptotic solution of the form

$$S(u) \sim a(1-u)^s, \quad R(u) \sim b(1-u)^r \quad \text{as} \quad u \to 1, \tag{4.4.36}$$

where a, b, s and r are all real constants. We substitute (4.4.36) into (4.4.26) and (4.4.27) to obtain

$$\begin{aligned} &\Omega a(1-2s)(1-u)^s + 2\Omega as(1-u)^{s-1} - a^4 s(4s-1)(1-u)^{4s-2} \\ &\quad - \left(\frac{1}{\Gamma}\right)\left(\frac{c_3}{c_2}\right)^{-\frac{4}{3}} \left[b(1-2r)(1-u)^r + 2br(1-u)^{r-1}\right] \sim 0, \end{aligned} \tag{4.4.37}$$

$$\begin{aligned} &-F_0 b^2(2r-1)^2(1-u)^{2r} + 4F_0 b^2 r(2r-1)(1-u)^{2r-1} - 4F_0 r^2 b^2 (1-u)^{2r-2} + \\ &\quad \left(\frac{c_3}{c_2}\right)^{\frac{4}{3}} \frac{a}{b}(1-u)^{s-r} + (2r-1)b(1-u)^r - 2rb(1-u)^{r-1} \sim 0, \end{aligned} \tag{4.4.38}$$

as $u \to 1$. The dominant terms balance each other in (4.4.37) and (4.4.38) provided

$$s - 1 = 4s - 2 \quad \text{and} \quad s - r = 2r - 2, \tag{4.4.39}$$

that is, provided

$$s = \frac{1}{3} \quad \text{and} \quad r = \frac{7}{9}. \tag{4.4.40}$$

Equations (4.4.37) and (4.4.38) become

$$\frac{1}{3}\Omega a(1-u) + \frac{2}{3}\Omega a - a^4\frac{1}{9} - \left(\frac{1}{\Gamma}\right)\left(\frac{c_3}{c_2}\right)^{-\frac{4}{3}} \left[-\frac{5}{9}b(1-u)^{\frac{19}{9}} + \frac{14}{9}b(1-u)^{\frac{10}{9}}\right] \sim 0, \tag{4.4.41}$$

$$\begin{aligned} &-\frac{25}{81}F_0 b^2(1-u)^2 + \frac{140}{81}F_0 b^2(1-u) - \frac{196}{81}F_0 b^2 + \left(\frac{c_3}{c_2}\right)^{\frac{4}{3}}\left(\frac{a}{b}\right) + \frac{5}{9}b(1-u)^{\frac{11}{9}} \\ &\quad -\frac{14}{9}b(1-u)^{\frac{2}{9}} \sim 0, \end{aligned} \tag{4.4.42}$$

as $u \to 1$. Letting $u \to 1$ and solving for a and b yields

$$a = 6^{\frac{1}{3}}\Omega^{\frac{1}{3}}, \quad b = \left(\frac{1}{F_0}\right)^{\frac{1}{3}} \left(\frac{81 \times 6^{\frac{1}{3}}\Omega^{\frac{1}{3}}}{196}\right)^{\frac{1}{3}} \left(\frac{c_3}{c_2}\right)^{\frac{4}{9}}, \quad F_0 > 0. \tag{4.4.43}$$

Observe that

$$S^3(1)\frac{\mathrm{d}S}{\mathrm{d}u}(1) = 0, \tag{4.4.44}$$

and therefore there is no leak-off at the fracture tip. The asymptotic solutions are

$$S(u) \sim (6\Omega)^{\frac{1}{3}}(1-u)^{\frac{1}{3}}, \quad R(u) \sim \left(\frac{1}{F_0}\right)^{\frac{1}{3}} \left(\frac{81 \times (6\Omega)^{\frac{1}{3}}}{196}\right)^{\frac{1}{3}} \left(\frac{c_3}{c_2}\right)^{\frac{4}{9}} (1-u)^{\frac{7}{9}} \quad \text{as} \quad u \to 1, \tag{4.4.45}$$

with $F_0 > 0$. We note that the least dominant terms in equation (4.4.37) are the first term and the terms from leak-off. A balance is then made between the two remaining terms in (4.4.37). Thus, the general asymptotic result given by (4.4.45) also holds when there is weak leak-off and moderate fluid leak-off at the fracture interface. We will only determine the asymptotic solution for the case of strong leak-off. The asymptotic result is used when numerical integration is applied to (4.4.26) and (4.4.27).

We investigate the three cases of fluid leak-off arising as a result of the presence of the two dimensionless parameters Ω and Γ. The boundary value problem (4.4.26)-(4.4.34) will be solved in terms of the independent variable u and dependent variables $S(u)$ and $R(u)$ for each of the three cases of fluid leak-off.

4.4.1 Weak leak-off at the interface: $\Omega \sim 1$ and $\Gamma \gg 1$

The boundary value problem becomes

$$\Omega \left[S(u) - 2u\frac{dS(u)}{du}\right] - \frac{d}{du}\left(S^3(u)\frac{dS(u)}{du}\right) = 0, \tag{4.4.46}$$

$$R(u) - 2u\frac{dR(u)}{du} + F_0\left[R^2(u) - 4uR(u)\frac{dR(u)}{du} + 4u^2\left(\frac{dR(u)}{du}\right)^2\right] - \left(\frac{c_3}{c_2}\right)^{\frac{4}{3}}\frac{S(u)}{R(u)} = 0, \tag{4.4.47}$$

$$S(1) = 0, \quad R(1) = 0, \tag{4.4.48}$$

$$S^3(0)\frac{dS(0)}{du} = -3\int_0^1 S(u)du. \tag{4.4.49}$$

Once $S(u)$ and $R(u)$ are obtained, the invariant solution follows from (4.4.30) to (4.4.34).

With $\Omega \sim 1$ and $\Gamma \gg 1$, the asymptotic solutions of (4.4.46) and (4.4.47) as $u \to 1$, which are true for any value of $\frac{c_3}{c_2} > 0$ are given in (4.4.45) as

$$S(u) \sim (6\Omega)^{\frac{1}{3}}(1-u)^{\frac{1}{3}} \quad \text{as} \quad u \to 1, \tag{4.4.50}$$

$$R(u) \sim \left(\frac{1}{F_0}\right)^{\frac{1}{3}} \left(\frac{81 \times (6\Omega)^{\frac{1}{3}}}{196}\right)^{\frac{1}{3}} \left(\frac{c_3}{c_2}\right)^{\frac{4}{9}} (1-u)^{\frac{7}{9}} \quad \text{as} \quad u \to 1, \quad F_0 > 0. \tag{4.4.51}$$

4.4.1.1 Fracture half-width and leak-off depth

In Figure 4.4.1, the half-width of the fracture $h(t,x)$ is plotted against x for t=0, 1, 2, 5 when $c_3 \neq 0$ and F_0=0.001, 0.1, 1. The value of the ratio $\frac{c_3}{c_2}$ was obtained numerically as part of the solution. When there is weak leak-off of fluid at the fracture interface, the variation of F_0 does not affect the ratio $\frac{c_3}{c_2}$ since in each of the graphs in Figure 4.4.1 the ratio $\frac{c_3}{c_2}$ agrees to four decimal places. Therefore, the speed of propagation is unchanged in each of the graphs. The rate of growth of the fracture half-width also remains unchanged with an increase in the Forchheimer number. The leak-off depth $b(t,x)$ when there is weak fluid leak-off at the fracture interface is plotted in Figure 4.4.2 for varied values of the Forchheimer number. It is seen from Figure 4.4.2 that an increase in the Forchheimer number leads to a decrease in the rate of leak-off across the fracture. The half-width of the fracture is unaffected by the Forchheimer number because the leaked-off fluid is significantly small hence the dynamics in the porous medium has little effect to the propagation of the fracture half-width. The asymptotic result of $S(u)$ as $u \to 1$ when there is weak fluid leak-off at the fracture walls does not depend on the Forchheimer number, F_0. However, the asymptotic result for $R(u)$ as $u \to 1$ in (4.4.51) is inversely proportional to the Forchheimer number, F_0.

4.4.2 Strong leak-off at the interface: $\Omega \ll 1$ and $\Gamma \sim 1$

Consider now the case of strong leak-off into the rock-mass. The boundary value problem becomes

$$\frac{d}{du}\left(S^3(u)\frac{dS(u)}{du}\right) - \left(\frac{1}{\Gamma}\right)\left(\frac{c_3}{c_2}\right)^{-\frac{4}{3}}\left(R(u) - 2u\frac{dR(u)}{du}\right) = 0, \tag{4.4.52}$$

$$R(u) - 2u\frac{dR(u)}{du} + F_0\left[R^2(u) - 4uR(u)\frac{dR(u)}{du} + 4u^2\left(\frac{dR(u)}{du}\right)^2\right] - \left(\frac{c_3}{c_2}\right)^{\frac{4}{3}}\frac{S(u)}{R(u)} = 0, \tag{4.4.53}$$

$$S(1) = 0, \quad R(1) = 0, \tag{4.4.54}$$

$$S^3(0)\frac{dS(0)}{du} = -3\left(\frac{c_3}{c_2}\right)^{-\frac{4}{3}}\int_0^1 R(u)du. \tag{4.4.55}$$

The invariant solutions follows from (4.4.30) to (4.4.34).

We seek the asymptotic solutions of (4.4.52) and (4.4.53) of the form

$$S(u) \sim a(1-u)^n, \quad R(u) \sim b(1-u)^r \quad \text{as} \quad u \to 1, \tag{4.4.56}$$

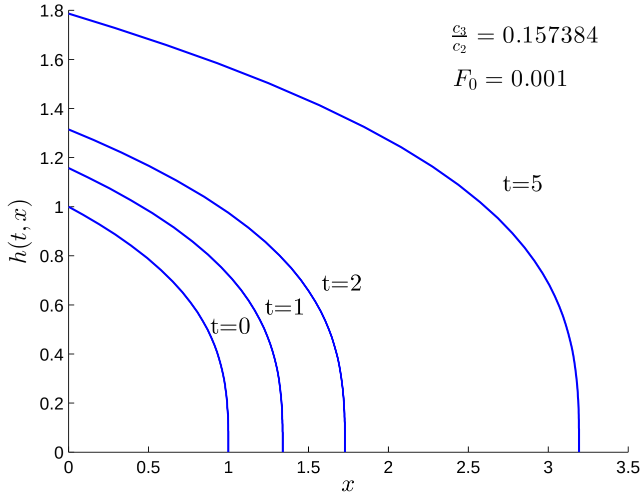

(I)

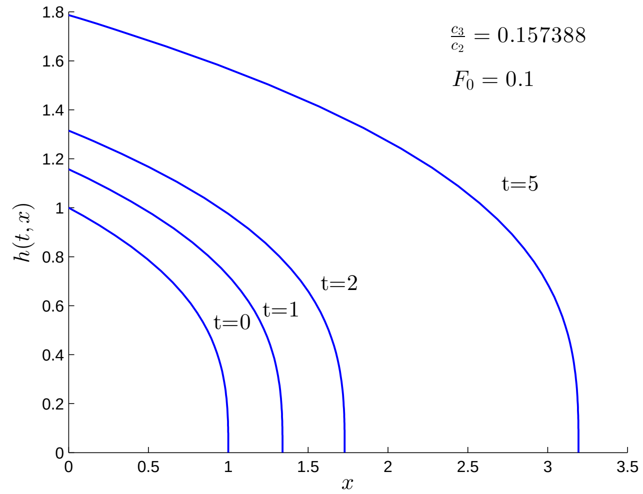

(II)

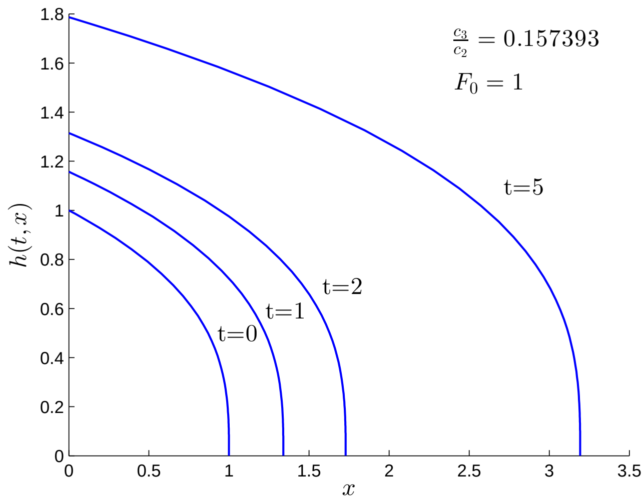

(III)

FIGURE 4.4.1: Fracture half-width plotted against x at times t=0, 1, 2, 5 for weak fluid leak-off at the interface when $\Omega = 1$, $c_3 \neq 0$ and F_0=0.001, 0.1, 1.

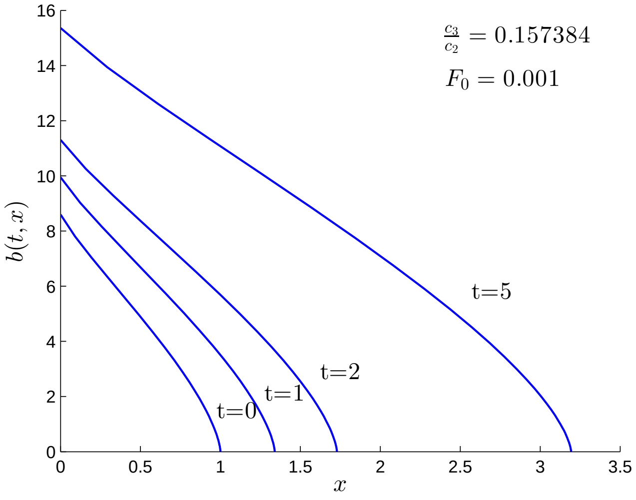

(I)

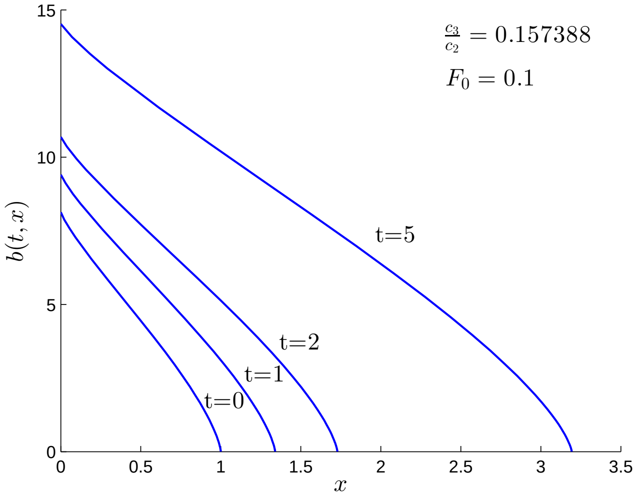

(II)

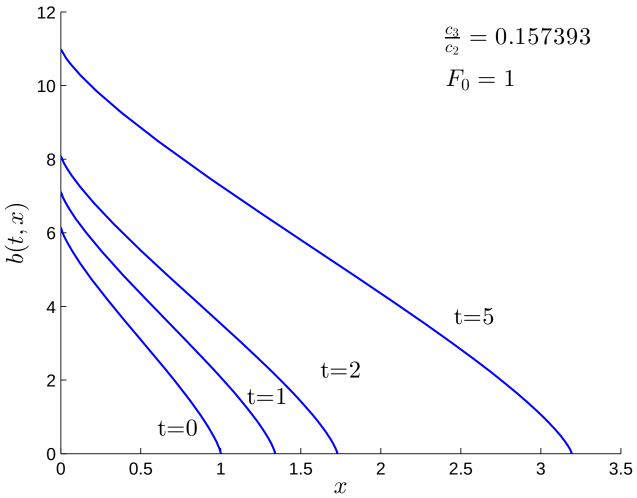

(III)

FIGURE 4.4.2: Leak-off depth plotted against x at times t=0, 1, 2, 5 for weak fluid leak-off at the interface when $\Omega = 1$, $c_3 \neq 0$ and F_0=0.001, 0.1, 1.

where a, n, b and r are constants. We substitute (4.4.56) into (4.4.52) to obtain

$$a^4 n(4n-1)(1-u)^{4n-2} - \left(\frac{1}{\Gamma}\right)\left(\frac{c_3}{c_2}\right)^{-\frac{4}{3}} \left[(1-2r)b(1-u)^r + 2br(1-u)^{r-1}\right] \sim 0, \tag{4.4.57}$$

as $u \to 1$. In order for the dominant terms in (4.4.57) to balance each other it is required that

$$4n-2 = r-1 \Longrightarrow r = 4n-1. \tag{4.4.58}$$

Similarly, as $u \to 1$, (4.4.53) becomes, using (4.4.56)

$$\begin{aligned} -F_0 b^2(2r^2-1)^2(1-u)^{2r} + 4F_0 b^2 r(4r-1)(1-u)^{2r-1} - 4F_0 r^2 b^2 (1-u)^{2r-2} \\ + \left(\frac{c_3}{c_2}\right)^{\frac{4}{3}} \frac{a}{b}(1-u)^{n-r} + (2r-1)b(1-u)^r - 2rb(1-u)^{r-1} \sim 0. \end{aligned} \tag{4.4.59}$$

In order for the dominant terms in (4.4.59) to balance each other it is required that

$$n - r = 2r - 2. \tag{4.4.60}$$

Solving (4.4.58) and (4.4.60) for n and r yield

$$n = \frac{5}{11} \quad \text{and} \quad r = \frac{9}{11}. \tag{4.4.61}$$

Equation (4.4.57) becomes

$$a^4\left(\frac{45}{121}\right) - \left(\frac{1}{\Gamma}\right)\left(\frac{c_3}{c_2}\right)^{-\frac{4}{3}} \left[\left(-\frac{7}{11}\right)b(1-u) + 2b\left(\frac{9}{11}\right)\right] \sim 0, \tag{4.4.62}$$

as $u \to 1$. Letting $u = 1$, we obtain

$$b = \left(\frac{5}{22}\right)\left(\frac{c_3}{c_2}\right)^{\frac{4}{3}} \Gamma a^4. \tag{4.4.63}$$

With (4.4.61), (4.4.59) becomes

$$\begin{aligned} -\frac{49}{121}F_0 b^2(1-u)^{\frac{18}{11}} + \frac{252}{121}F_0 b^2(1-u)^{\frac{7}{11}} - \frac{324}{121}F_0 b^2(1-u)^{-\frac{4}{11}} + \left(\frac{c_3}{c_2}\right)^{\frac{4}{3}} \frac{a}{b}(1-u)^{-\frac{4}{11}} \\ + \frac{7}{11}b(1-u)^{\frac{9}{11}} - \frac{18}{11}b(1-u)^{-\frac{2}{11}} \sim 0, \end{aligned} \tag{4.4.64}$$

as $u \to 1$, and therefore

$$-\frac{49}{121}F_0 b^2(1-u)^2 - \frac{252}{121}F_0 b^2(1-u) - \frac{324}{121}F_0 b^2 + \left(\frac{c_3}{c_2}\right)^{\frac{4}{3}} \frac{a}{b} + \frac{7}{11}b(1-u)^{\frac{13}{11}} - \frac{18}{11}b(1-u)^{\frac{2}{11}} \sim 0, \tag{4.4.65}$$

as $u \to 1$. Setting $u = 1$ and solving for a and b, with $F_0 > 0$, we obtain

$$a = \left(\frac{121}{324}\right)^{\frac{1}{11}} \left(\frac{22}{5}\right)^{\frac{3}{11}} \left(\frac{1}{F_0}\right)^{\frac{1}{11}} \left(\frac{c_3}{c_2}\right)^{-\frac{8}{33}} \left(\frac{1}{\Gamma}\right)^{\frac{3}{11}}, \quad F_0 > 0, \tag{4.4.66}$$

$$b = \left(\frac{121}{324}\right)^{\frac{4}{11}} \left(\frac{22}{5}\right)^{\frac{1}{11}} \left(\frac{1}{F_0}\right)^{\frac{4}{11}} \left(\frac{c_3}{c_2}\right)^{\frac{12}{33}} \left(\frac{1}{\Gamma}\right)^{\frac{23}{11}} \quad F_0 > 0. \tag{4.4.67}$$

Observe that there is no leak-off at the fracture tip since

$$S^3(1)\frac{\mathrm{d}S}{\mathrm{d}u}(1) = 0. \tag{4.4.68}$$

The asymptotic solutions of (4.4.52) and (4.4.53) as $u \to 1$ are

$$S(u) \sim \left(\frac{121}{324}\right)^{\frac{1}{11}} \left(\frac{22}{5}\right)^{\frac{3}{11}} \left(\frac{1}{F_0}\right)^{\frac{1}{11}} \left(\frac{c_3}{c_2}\right)^{-\frac{8}{33}} \left(\frac{1}{\Gamma}\right)^{\frac{3}{11}} (1-u)^{\frac{5}{11}}, \quad F_0 > 0, \tag{4.4.69}$$

$$R(u) \sim \left(\frac{121}{324}\right)^{\frac{4}{11}} \left(\frac{22}{5}\right)^{\frac{1}{11}} \left(\frac{1}{F_0}\right)^{\frac{4}{11}} \left(\frac{c_3}{c_2}\right)^{\frac{12}{33}} \left(\frac{1}{\Gamma}\right)^{\frac{23}{11}} (1-u)^{\frac{9}{11}}, \quad F_0 > 0. \tag{4.4.70}$$

4.4.2.1 Fracture half-width and leak-off depth

The half-width $h(t, x)$ for the case of strong leak-off at the fracture interface is plotted in Figure 4.4.3 for varying values of the Forchheimer number F_0. As shown in Figure 4.4.3 (I)-(III), the value of the ratio $\frac{c_3}{c_2}$ increases with an increase in the Forchheimer number, F_0. Therefore, the rate of growth of the fracture half-width increases with an increase in F_0, the rate of growth being the weakest when $F_0 = 0.001$, and the strongest when $F_0 = 1$. The half-width of the fracture grows with time, even when there is strong leak-off at the interface. In Figure 4.4.4, the leak-off depth is plotted against x at times t=0, 1, 2, 5 for F_0=0.001, 0.1, 1. It is seen that an increase in the Forchheimer number decreases the rate of fluid leak-off across the fracture. For the case of strong fluid leak-off, the asymptotic result for both $S(u)$ and $R(u)$ as $u \to 1$ depend on the Forchheimer number, F_0. Both the asymptotic results are inversely proportional to the Forchheimer number.

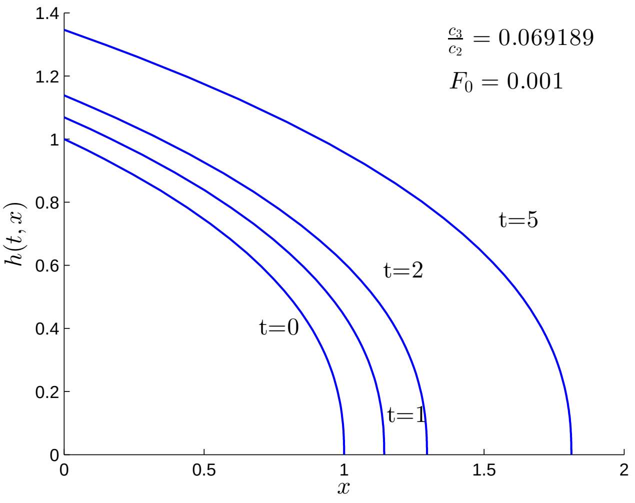

(i)

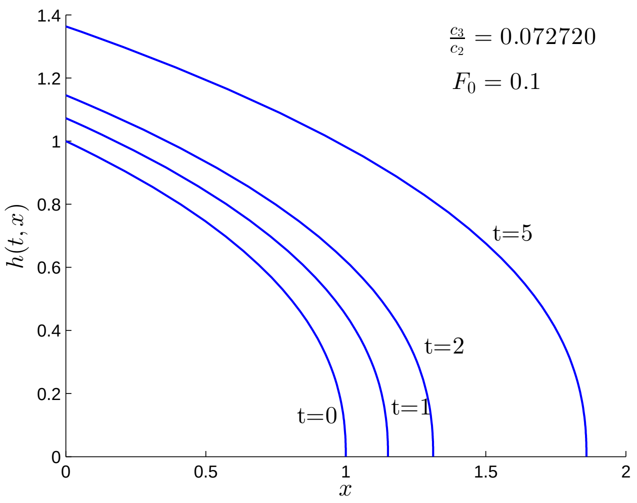

(ii)

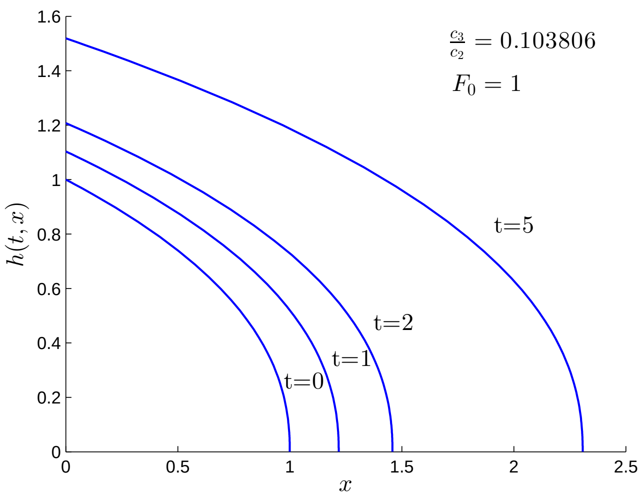

(iii)

FIGURE 4.4.3: Fracture half-width plotted against x at times t=0, 1, 2, 5 for strong fluid leak-off at the interface when $\Gamma = 1$, $c_3 \neq 0$ and F_0=0.001, 0.1, 1.

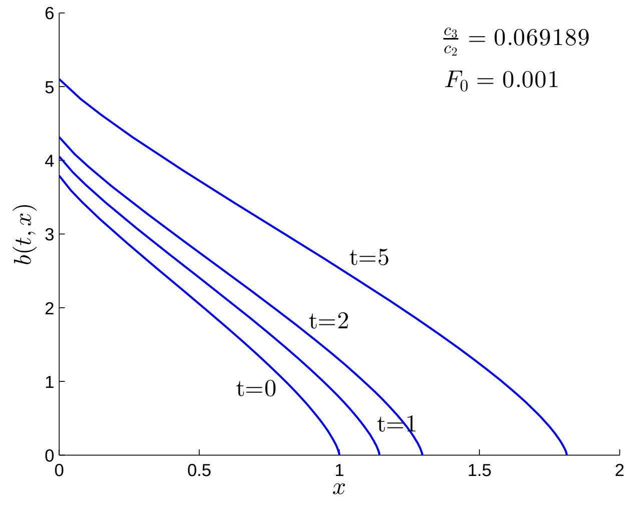

(I)

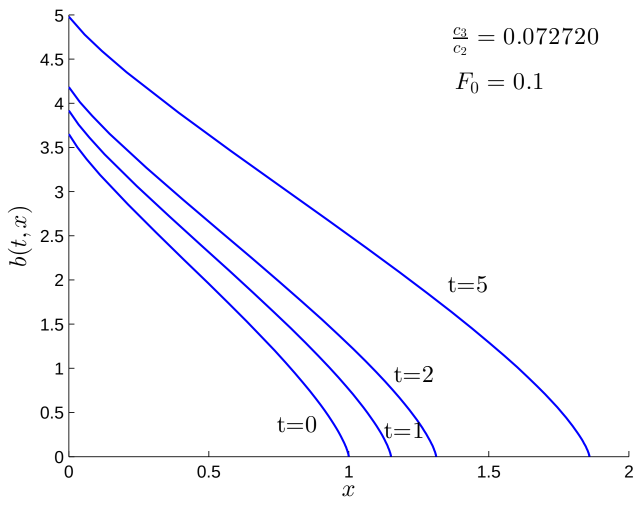

(II)

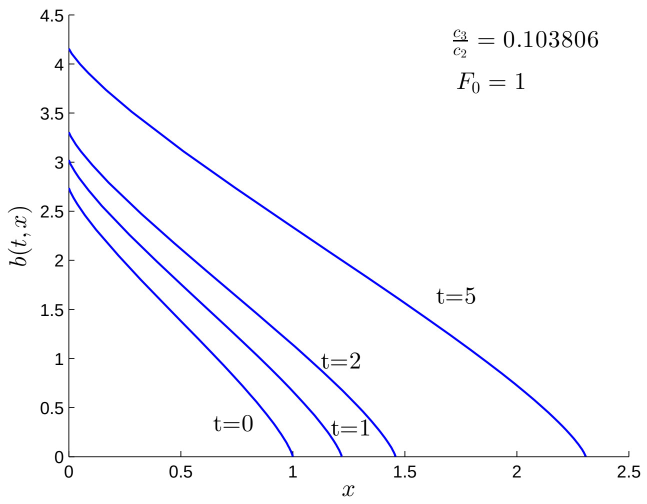

(III)

FIGURE 4.4.4: Leak-off depth plotted against x at times t=0, 1, 2, 5 for strong fluid leak-off at the interface when $\Gamma = 1$, $c_3 \neq 0$ and F_0=0.001, 0.1, 1.

4.4.3 Moderate leak-off at the interface: $\Omega \sim 1$ and $\Gamma \sim 1$

We consider the case of moderate fluid leak-off into the rock-mass

$$\Omega \left[S(u) - 2u\frac{dS(u)}{du} \right] - \frac{d}{du}\left(S^3(u)\frac{dS(u)}{du} \right) + \left(\frac{1}{\Gamma}\right)\left(\frac{c_3}{c_2}\right)^{-\frac{4}{3}} \left(R(u) - 2u\frac{dR(u)}{du} \right) = 0, \tag{4.4.71}$$

$$R(u) - 2u\frac{dR(u)}{du} + F_0\left[R^2(u) - 4uR(u)\frac{dR(u)}{du} + 4u^2\left(\frac{dR(u)}{du}\right)^2 \right] - \left(\frac{c_3}{c_2}\right)^{\frac{4}{3}} \frac{S(u)}{R(u)} = 0, \tag{4.4.72}$$

$$S(1) = 0, \quad R(1) = 0, \tag{4.4.73}$$

$$S^3(0)\frac{dS(0)}{du} = -3\left[\int_0^1 S(u)du + \left(\frac{c_3}{c_2}\right)^{-\frac{4}{3}} \int_0^1 R(u)du \right]. \tag{4.4.74}$$

Once $S(u)$ and $R(u)$ are obtained, the solutions for $L(t)$, $V(t)$, $h(t,x)$ and $b(t,x)$ follow from (4.4.30) to (4.4.34).

With $\Omega \sim 1$ and $\Gamma \sim 1$, the asymptotic solutions of (4.4.71) and (4.4.72) as $u \to 1$ are as given in (4.4.45)

$$S(u) \sim (6\Omega)^{\frac{1}{3}}(1-u)^{\frac{1}{3}} \quad \text{as} \quad u \to 1, \tag{4.4.75}$$

$$R(u) \sim \left(\frac{1}{F_0}\right)^{\frac{1}{3}} \left(\frac{81 \times (6\Omega)^{\frac{1}{3}}}{196}\right)^{\frac{1}{3}} \left(\frac{c_3}{c_2}\right)^{\frac{4}{9}} (1-u)^{\frac{7}{9}} \quad \text{as} \quad u \to 1, \quad F_0 > 0. \tag{4.4.76}$$

4.4.3.1 Fracture half-width and leak-off depth

Figure 4.4.5 shows the evolution of the half-width of the fracture when there is moderate leak-off of fluid at the fracture walls for varied values of the Forchheimer number F_0. Similar to the case of strong fluid leak-off, the rate of growth of the fracture half-width increases as the Forchheimer number increases. The ratio $\frac{c_3}{c_2}$ increase with an increase in the Forchheimer number. The corresponding leak-off depth is plotted in Figure 4.4.6. Similar to the two preceding cases of fluid leak-off, the leak-off depth at the fracture entry decreases with an increase in the Forchheimer number. When there is moderate fluid leak-off at the fracture walls the asymptotic solution for $S(u)$ as $u \to 1$ is independent of the Forchheimer number, F_0. The asymptotic solution for $R(u)$ as $u \to 1$ depends on the Forchheimer number F_0.

The half-width of the fracture grows the least for moderate fluid leak-off and the most for strong fluid leak-off for all the values of the Forchheimer number considered.

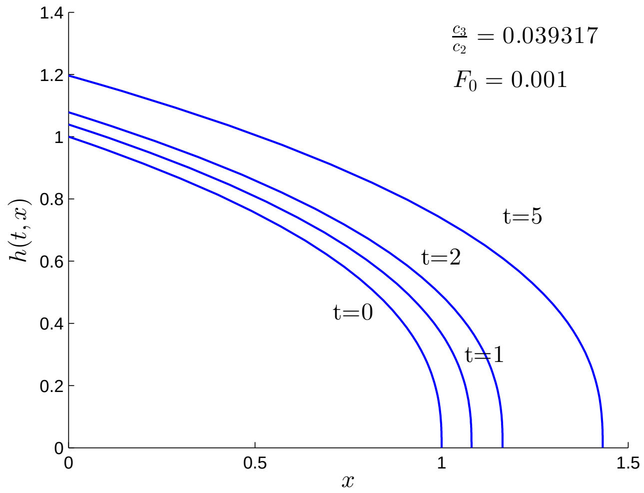

(I)

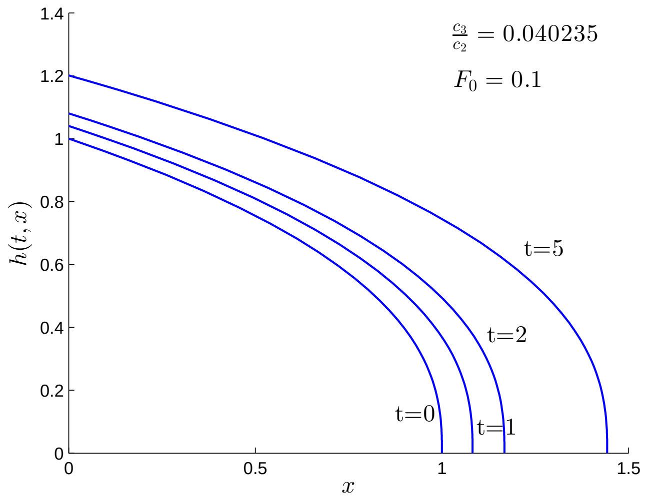

(II)

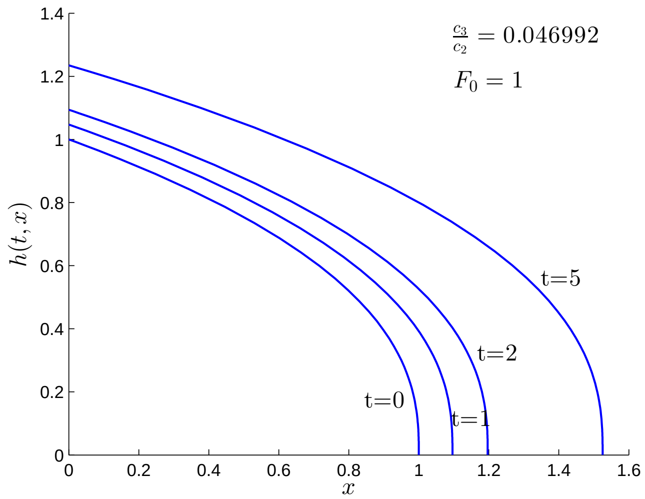

(III)

FIGURE 4.4.5: Fracture half-width plotted against x at times t=0, 1, 2, 5 for moderate fluid leak-off at the interface when $\Omega = \Gamma = 1$, $c_3 \neq 0$ and F_0=0.001, 0.1, 1.

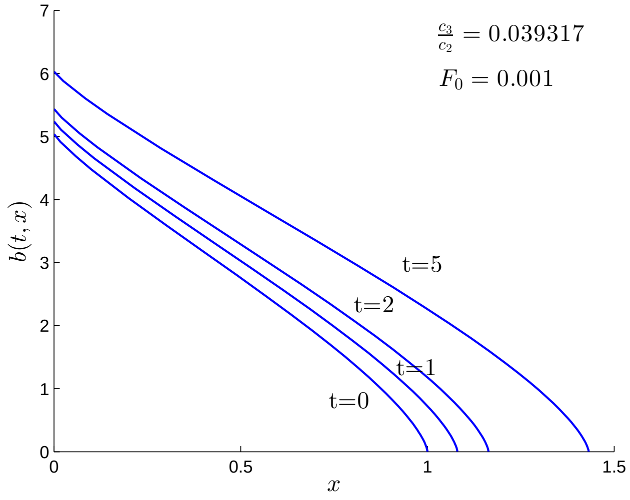

(I)

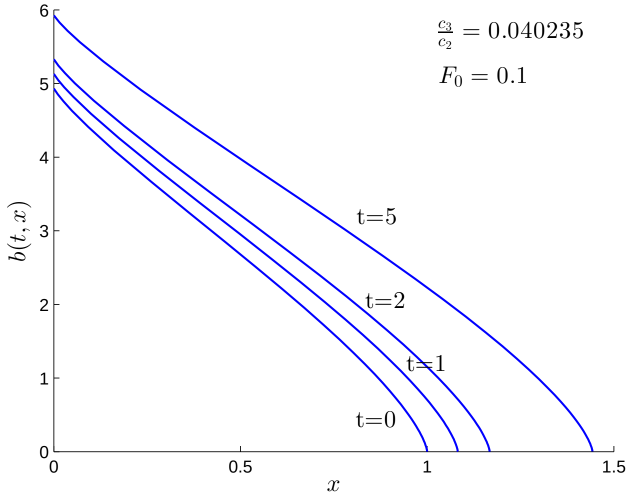

(II)

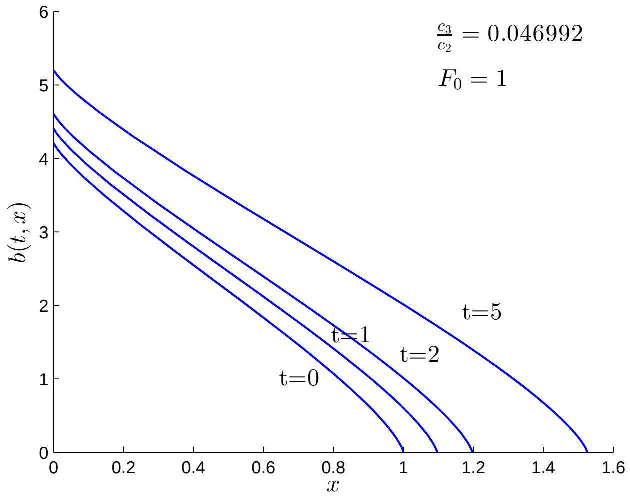

(III)

FIGURE 4.4.6: Leak-off depth plotted against x at times t=0, 1, 2, 5 for moderate fluid leak-off at the interface when $\Omega = \Gamma = 1$, $c_3 \neq 0$ and F_0=0.001, 0.1, 1.

4.4.4 Length of the fracture

The fracture length $L(t)$ for the case of weak fluid leak-off into the rock-mass formation does not change with an increase in the value of the Forchheimer number. The graphs for the length of the fracture are therefore not displayed for this case. In Figure 4.4.7, the graphs when there is strong fluid leak-off at the fracture walls are plotted. It is clear from Figure 4.4.7 that the graph plotted in (i) grows the strongest. The fracture length for this case increases quadratically with time t. When F_0 is equal to 0.001 or 1, the fracture length $L(t)$ grows almost linearly with time. This is only because the time interval considered is small. For sufficiently large time range $L(t)$ will behave quadratically. The time range needed to show quadratic behaviour decreases as F_0 increases. The weakest rate of growth of the fracture length occurs when F_0=0.001. Expectedly, the increase in the value of the Forchheimer number results in an increase in the rate of growth of the fracture length for the case of of strong fluid leak-off and moderate fluid leak-off. When there is moderate fluid leak-off at the fluid-rock interface, the growth of the fracture length is depicted in Figure 4.4.8. Similarly, the fracture length $L(t)$ grows the strongest for high values of the Forchheimer number and the weakest for small values of Forchheimer number. In Figure 4.4.9, the graphs of the fracture length

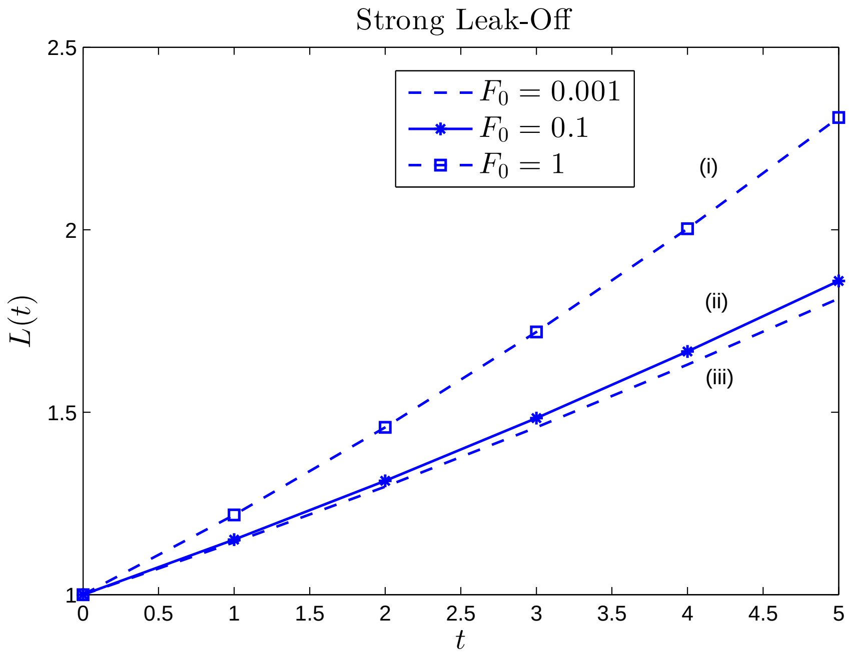

FIGURE 4.4.7: Length of the fracture $L(t)$ plotted against t for strong fluid leak-off at the interface when F_0=0.001, 0.1, 1.

$L(t)$ for the three distinct cases of fluid leak-off at the fracture interface are plotted. The Forchheimer number, F_0, is equal to 1. Expectedly, the rate of growth of the fracture length is strongest when there is weak fluid leak-off at the fracture interface. This result is however not true for all the values of Forchheimer number considered. In Figure 4.4.9, the graph of the fracture length for when there is strong leak-off at the fracture is depicted in (ii). Lastly, the growth of the length of the fracture when there is moderate fluid leak-off at the interface is plotted in (iii).

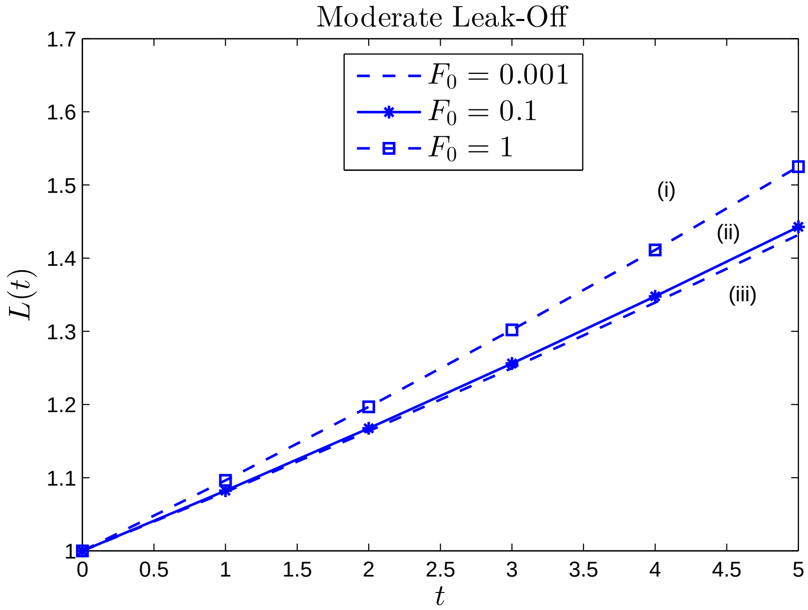

FIGURE 4.4.8: Length of the fracture $L(t)$ plotted against t for moderate fluid leak-off at the interface when F_0=0.001, 0.1, 1.

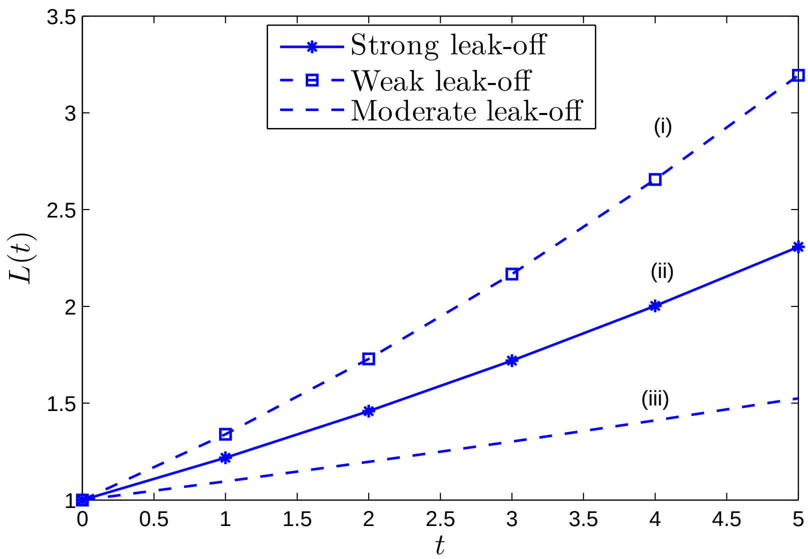

FIGURE 4.4.9: Length of the fracture $L(t)$ plotted against t for (i) weak fluid leak-off, (ii) strong fluid leak-off and (iii) moderate leak-off of fluid at the interface when F_0=1.

Case: $c_3 = 0$

When $c_3 = 0$, the Lie point symmetry generator is given by (3.6.117), then the solutions $h(t,x)$ and $b(t,x)$ are

$$h(t,x) = f(\xi), \tag{4.4.77}$$

$$b(t,x) = g(\xi), \tag{4.4.78}$$

where

$$\xi = x - \frac{c_1}{c_2}t. \tag{4.4.79}$$

The system of partial differential equations (4.3.4), (4.3.5) and the boundary conditions (4.3.6), after substituting (4.4.77) and (4.4.78), becomes

$$\Omega\frac{c_1}{c_2}\frac{df(\xi)}{d\xi} + \frac{d}{d\xi}\left(f^3(\xi)\frac{df(\xi)}{d\xi}\right) + \frac{1}{\Gamma}\frac{c_1}{c_2}\frac{dg(\xi)}{d\xi} = 0, \tag{4.4.80}$$

$$F_0\left(\frac{c_1}{c_2}\right)^2\left(\frac{dg(\xi)}{d\xi}\right)^2 - \frac{c_1}{c_2}\frac{dg(\xi)}{d\xi} - \frac{f(\xi)}{g(\xi)} = 0, \tag{4.4.81}$$

$$f(\xi) = 0, \quad g(\xi) = 0 \quad \text{at} \quad \xi = L(t) - \frac{c_1}{c_2}t, \tag{4.4.82}$$

where $L(t)$ the length of the fracture is

$$L(t) = 1 + \frac{c_1}{c_2}t. \tag{4.4.83}$$

Using (4.4.83), the boundary conditions in (4.4.82) becomes

$$f(1) = 0, \qquad g(1) = 0. \tag{4.4.84}$$

We now derive the general asymptotic solution for equations (4.4.80) and (4.4.81) as $\xi \to 1$. We look for an asymptotic solution of the form

$$f(\xi) \sim a(1-\xi)^{\alpha}; \quad g(\xi) \sim b(1-\xi)^{\beta} \quad \text{as} \quad \xi \to 1, \tag{4.4.85}$$

where a, b, α and β are all real constants. We substitute (4.4.85) into (4.4.80) and (4.4.81) to obtain

$$\Omega\frac{c_1}{c_2}a\alpha(1-\xi)^{\alpha-1} - a^4\alpha(4\alpha-1)(1-\xi)^{4\alpha-2} + \frac{1}{\Gamma}\frac{c_1}{c_2}\beta b(1-\xi)^{\beta-1} \sim 0, \tag{4.4.86}$$

$$F_0\left(\frac{c_1}{c_2}\right)^2\beta^2 b^2(1-\xi)^{2\beta-2} + \left(\frac{c_1}{c_2}\right)\beta b(1-\xi)^{\beta-1} - \frac{a}{b}(1-\xi)^{\alpha-\beta} \sim 0, \tag{4.4.87}$$

as $\xi \to 1$. The dominant terms balance each other in (4.4.86) and (4.4.87) provided

$$\alpha - 1 = 4\alpha - 2 \quad \text{and} \quad \alpha - \beta = 2\beta - 2, \tag{4.4.88}$$

that is, provided

$$\alpha = \frac{1}{3} \quad \text{and} \quad \beta = \frac{7}{9}. \tag{4.4.89}$$

Substituting (4.4.89) into (4.4.86) and (4.4.87) yield

$$\frac{1}{3}\frac{c_1}{c_2}\Omega a - \frac{1}{9}a^4 + \frac{1}{\Gamma}\frac{c_1}{c_2}\frac{7}{9}b(1-\xi)^{\frac{4}{9}} \sim 0, \quad \text{as} \quad \xi \to 1, \tag{4.4.90}$$

$$F_0\left(\frac{c_1}{c_2}\right)^2\left(\frac{7}{9}\right)^2 b^2 + \frac{c_1}{c_2}\frac{7}{9}b(1-\xi)^{\frac{2}{9}} - \frac{a}{b} \sim 0, \quad \text{as} \quad \xi \to 1. \tag{4.4.91}$$

Letting $\xi = 1$ and solving for a and b we obtain

$$a = 3^{\frac{1}{3}}\Omega^{\frac{1}{3}}\left(\frac{c_1}{c_2}\right)^{\frac{1}{3}}, \quad b = \left(\frac{3^{13}}{7^6}\times\Omega\right)^{\frac{1}{9}}\left(\frac{1}{F_0}\right)^{\frac{1}{3}}\left(\frac{c_1}{c_2}\right)^{-\frac{5}{9}}, \quad F_0 > 0. \tag{4.4.92}$$

The general asymptotic solutions of (4.4.80) and (4.4.81) as $\xi \to 1$ are

$$f(\xi) \sim \left(3\Omega\frac{c_1}{c_2}\right)^{\frac{1}{3}}(1-\xi)^{\frac{1}{3}}, \tag{4.4.93}$$

$$g(\xi) \sim \left(\frac{3^{13}}{7^6}\times\Omega\right)^{\frac{1}{9}}\left(\frac{1}{F_0}\right)^{\frac{1}{3}}\left(\frac{c_1}{c_2}\right)^{-\frac{5}{9}}(1-\xi)^{\frac{7}{9}}, \quad F_0 > 0. \tag{4.4.94}$$

From (4.4.93),

$$f^3\frac{df}{d\xi} \sim -\left(3^{\frac{1}{4}}\Omega\frac{c_1}{c_2}\right)^{\frac{4}{3}}(1-\xi)^{\frac{1}{3}}. \tag{4.4.95}$$

Therefore, $f^3\frac{df}{d\xi} \to 0$ as $\xi \to 1$ and the fluid flux disappears at the fracture nose. The problem is therefore to solve

$$\Omega\frac{c_1}{c_2}\frac{df(\xi)}{d\xi} + \frac{d}{d\xi}\left(f^3(\xi)\frac{df(\xi)}{d\xi}\right) + \frac{1}{\Gamma}\frac{c_1}{c_2}\frac{dg(\xi)}{d\xi} = 0, \tag{4.4.96}$$

$$F_0\left(\frac{c_1}{c_2}\right)^2\left(\frac{dg(\xi)}{d\xi}\right)^2 - \frac{c_1}{c_2}\frac{dg(\xi)}{d\xi} - \frac{f(\xi)}{g(\xi)} = 0, \tag{4.4.97}$$

Subject to

$$f(1) = 0, \quad g(1) = 0, \quad f^3\frac{df}{d\xi} \to 0 \quad \text{as} \quad \xi \to 1, \tag{4.4.98}$$

where

$$L(t) = 1 + \frac{c_1}{c_2}t. \tag{4.4.99}$$

$$h(t,x) = f(\xi), \tag{4.4.100}$$

$$b(t,x) = g(\xi), \tag{4.4.101}$$

$$p(t,x) = f(\xi) + \sigma_{zz}^{\infty}. \tag{4.4.102}$$

The boundary value problem for the case $c_3 = 0$ will now be solved for each of the three cases discussed. Again, the general asymptotic solution will hold when there is weak leak-off and moderate fluid leak-off at the fluid-rock interface. We only need to determine the asymptotic solution when there is strong fluid leak-off at the interface.

4.4.5 Weak leak-off at the interface: $\Omega \sim 1$ and $\Gamma \gg 1$

Consider the case of weak fluid leak-off

$$\Omega \frac{c_1}{c_2} \frac{df(\xi)}{d\xi} + \frac{d}{d\xi}\left(f^3(\xi)\frac{df(\xi)}{d\xi}\right) = 0, \tag{4.4.103}$$

$$F_0 \left(\frac{c_1}{c_2}\right)^2 \left(\frac{dg(\xi)}{d\xi}\right)^2 - \frac{c_1}{c_2}\frac{dg(\xi)}{d\xi} - \frac{f(\xi)}{g(\xi)} = 0, \tag{4.4.104}$$

$$f(1) = 0, \quad g(1) = 0, \quad f^3 \frac{df}{d\xi} \to 0 \quad \text{as} \quad \xi \to 1. \tag{4.4.105}$$

Once $f(\xi)$ and $g(\xi)$ are obtained, the invariant solutions for $L(t)$, $h(t,x)$, $b(t,x)$ and $p(t,x)$ follow from (4.4.99)-(4.4.102). With $\Omega \sim 1$ and $\Gamma \gg 1$, the asymptotic solutions of (4.4.103) and (4.4.104) as $\xi \to 1$ are as given in (4.4.93) and (4.4.94)

$$f(\xi) \sim \left(3\Omega\frac{c_1}{c_2}\right)^{\frac{1}{3}} (1-\xi)^{\frac{1}{3}}, \tag{4.4.106}$$

$$g(\xi) \sim \left(\frac{3^{13}}{7^6} \times \Omega\right)^{\frac{1}{9}} \left(\frac{1}{F_0}\right)^{\frac{1}{3}} \left(\frac{c_1}{c_2}\right)^{-\frac{5}{9}} (1-\xi)^{\frac{7}{9}}, \quad F_0 > 0. \tag{4.4.107}$$

4.4.5.1 Fracture half-width and leak-off depth

Figure 4.4.10 shows the propagation of the half-width of the fracture for different values of Forchheimer number. The rate of growth of the fracture half-width remained unchanged with an increase in the Forchheimer number when there is weak leak-off of fluid at the interface. The amount of fluid that has leaked-off into the rock-mass is too small to influence the propagation of the fracture. The ratio $\frac{c_1}{c_2}$ also remained unchanged with the increase in the Forchheimer number. The leak-off depth plotted in Figure 4.4.11 at times t=0, 1, 2, 5 exhibits the expected behaviour, that is, the rate of fluid leak-off across the fracture decreases as a result of an increase in the Forchheimer number, F_0. Only the asymptotic result for $g(\xi)$ as ξ tends to 1 depends on the Forchheimer number F_0.

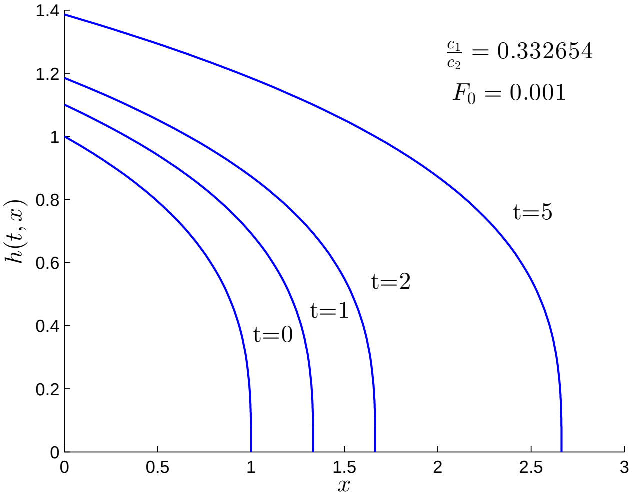

(I)

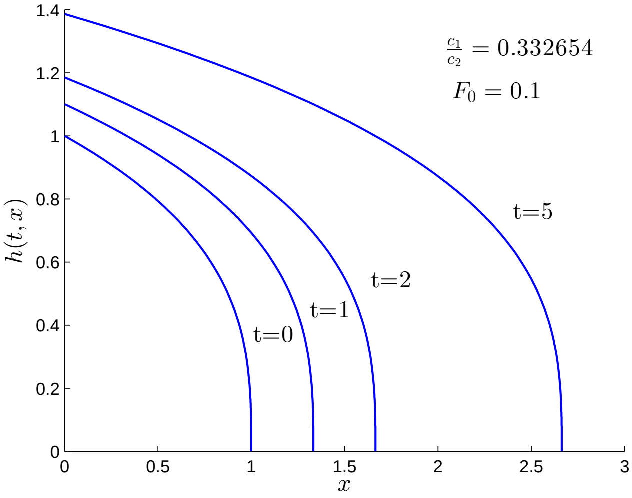

(II)

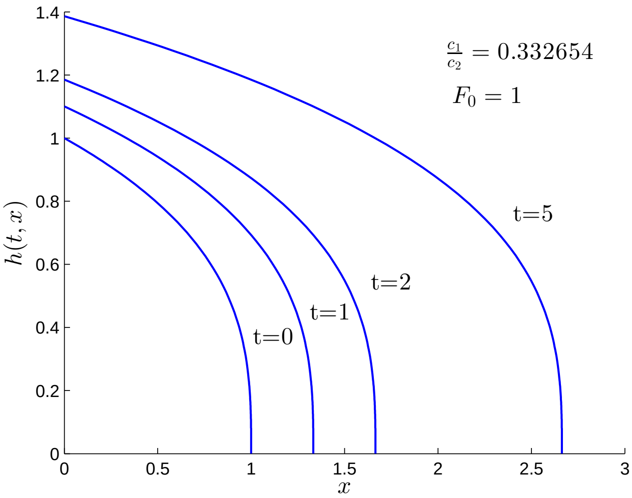

(III)

FIGURE 4.4.10: Fracture half-width plotted against x at times t=0, 1, 2, 5 for weak fluid leak-off at the interface when $\Omega = 1$, $c_3 = 0$ and F_0=0.001, 0.1, 1.

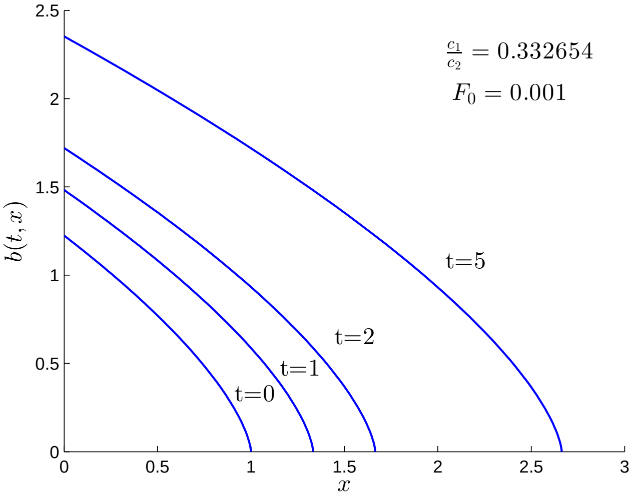

(I)

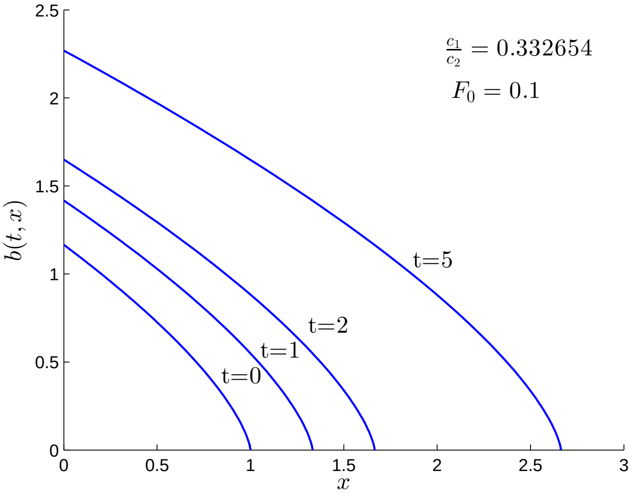

(II)

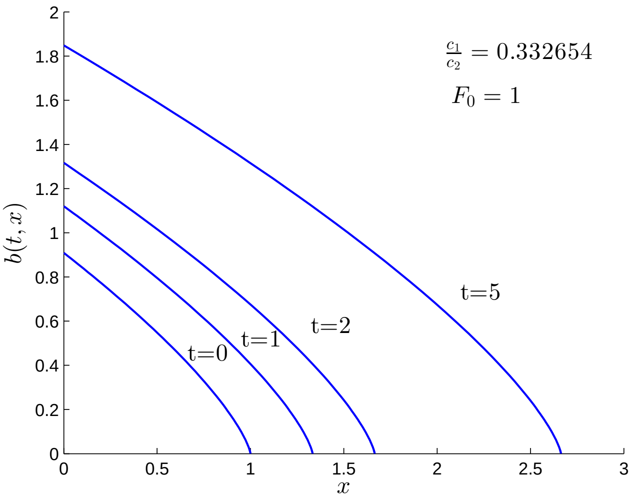

(III)

FIGURE 4.4.11: Leak-off depth plotted against x at times t=0, 1, 2, 5 for weak fluid leak-off at the interface when $\Omega = 1$, $c_3 = 0$ and F_0=0.001, 0.1, 1.

4.4.6 Strong leak-off at the interface: $\Omega \ll 1$ and $\Gamma \sim 1$

We now investigate the case of strong leak-off into the rock-mass. The boundary value problem becomes

$$\frac{d}{d\xi}\left(f^3(\xi)\frac{df(\xi)}{d\xi}\right) + \left(\frac{1}{\Gamma}\right)\left(\frac{c_1}{c_2}\right)\frac{dg(\xi)}{d\xi} = 0, \tag{4.4.108}$$

$$F_0\left(\frac{c_1}{c_2}\right)^2\left(\frac{dg(\xi)}{d\xi}\right)^2 - \frac{c_1}{c_2}\frac{dg(\xi)}{d\xi} - \frac{f(\xi)}{g(\xi)} = 0, \tag{4.4.109}$$

$$f(1) = 0, \quad g(1) = 0, \quad f^3\frac{df}{d\xi} \to 0 \quad \text{as} \quad \xi \to 1. \tag{4.4.110}$$

The invariant solutions are

$$L(t) = 1 + \frac{c_1}{c_2}t. \tag{4.4.111}$$

$$h(t,x) = f(\xi), \tag{4.4.112}$$

$$b(t,x) = g(\xi), \tag{4.4.113}$$

$$p(t,x) = f(\xi) + \sigma_{zz}^{\infty}. \tag{4.4.114}$$

We now seek to understand the behavior of $f(\xi)$ and $g(\xi)$ as ξ tends to 1. We look for the asymptotic behavior of $f(\xi)$ near $\xi = 1$ of the form

$$f(\xi) \sim a(1-\xi)^{\alpha} \qquad \text{as} \qquad \xi \to 1, \tag{4.4.115}$$

where a and α are constants. Since $g(1) = 0$, we also have

$$g(\xi) \sim b(1-\xi)^{\beta} \qquad \text{as} \qquad \xi \to 1, \tag{4.4.116}$$

where b and β are constants. Substituting (4.4.115) and (4.4.116) into (4.4.108), we obtain

$$\alpha(4\alpha-1)a^4(1-\xi)^{4\alpha-2} - \left(\frac{1}{\Gamma}\right)\left(\frac{c_1}{c_2}\right)\beta b(1-\xi)^{\beta-1} \sim 0, \tag{4.4.117}$$

as $\xi \to 1$. In order for the dominant terms in (4.4.117) to balance each other, it is required that

$$4\alpha - 2 = \beta - 1, \tag{4.4.118}$$

which implies

$$\beta = 4\alpha - 1. \tag{4.4.119}$$

Using (4.4.115) and (4.4.116), (4.4.109) becomes

$$F_0\left(\frac{c_1}{c_2}\right)^2\beta^2 b^2(1-\xi)^{2\beta-2} + \frac{c_1}{c_2}\beta b(1-\xi)^{\beta-1} - \frac{a}{b}(1-\xi)^{\alpha-\beta} \sim 0, \tag{4.4.120}$$

as $\xi \to 1$. In order for the dominant terms in (4.4.120) to balance each other, it is required that

$$2\beta - 2 = \alpha - \beta, \tag{4.4.121}$$

which after substituting (4.4.119) gives

$$\alpha = \frac{5}{11}. \tag{4.4.122}$$

Substituting equation (4.4.122) into (4.4.119) gives

$$\beta = \frac{9}{11}. \tag{4.4.123}$$

Using (4.4.122) and (4.4.123) in (4.4.117) yield

$$a^4\left(\frac{45}{121}\right) - \left(\frac{1}{\Gamma}\right)\left(\frac{c_1}{c_2}\right)\left(\frac{9}{11}\right) b \sim 0, \tag{4.4.124}$$

and therefore solving for b gives

$$b = \left(\frac{5}{11}\right)\left(\frac{c_1}{c_2}\right)^{-1}\Gamma a^4. \tag{4.4.125}$$

Substituting (4.4.122) and (4.4.123) into (4.4.120), we get

$$F_0\left(\frac{c_1}{c_2}\right)^2\left(\frac{9}{11}\right)^2 b^2 + \frac{c_1}{c_2}\left(\frac{9}{11}\right) b(1-\xi)^{\frac{2}{11}} - \frac{a}{b} \sim 0, \tag{4.4.126}$$

as $\xi \to 1$. Setting $\xi = 1$, gives

$$F_0\left(\frac{c_1}{c_2}\right)^2\left(\frac{9}{11}\right)^2 b^3 - a = 0. \tag{4.4.127}$$

Using (4.4.125), we obtain

$$a = \left(\frac{1}{F_0}\right)^{\frac{1}{11}}\left(\frac{c_1}{c_2}\right)^{-\frac{1}{11}}\left(\frac{9}{11}\right)^{-\frac{2}{11}}\left(\frac{5}{11}\right)^{-\frac{3}{11}}\left(\frac{1}{\Gamma}\right)^{\frac{3}{11}}, \quad F_0 > 0, \tag{4.4.128}$$

$$b = \left(\frac{1}{F_0}\right)^{\frac{4}{11}}\left(\frac{c_1}{c_2}\right)^{-\frac{15}{11}}\left(\frac{9}{11}\right)^{-\frac{8}{11}}\left(\frac{5}{11}\right)^{-\frac{1}{11}}\left(\frac{1}{\Gamma}\right)^{\frac{1}{11}}, \quad F_0 > 0. \tag{4.4.129}$$

The asymptotic solutions of (4.4.108) and (4.4.109) as $\xi \to 1$ are

$$f(\xi) \sim \left(\frac{1}{F_0}\right)^{\frac{1}{11}}\left(\frac{c_1}{c_2}\right)^{-\frac{1}{11}}\left(\frac{9}{11}\right)^{-\frac{2}{11}}\left(\frac{5}{11}\right)^{-\frac{3}{11}}\left(\frac{1}{\Gamma}\right)^{\frac{3}{11}}(1-\xi)^{\frac{5}{11}}, \quad F_0 > 0, \tag{4.4.130}$$

$$g(\xi) \sim \left(\frac{1}{F_0}\right)^{\frac{4}{11}}\left(\frac{c_1}{c_2}\right)^{-\frac{15}{11}}\left(\frac{9}{11}\right)^{-\frac{8}{11}}\left(\frac{5}{11}\right)^{-\frac{1}{11}}\left(\frac{1}{\Gamma}\right)^{\frac{1}{11}}(1-\xi)^{\frac{9}{11}} \quad F_0 > 0. \tag{4.4.131}$$

4.4.6.1 Fracture half-width and leak-off depth

In Figure 4.4.12, the fracture half-width $h(t,x)$ is plotted for a range of values of the Forchheimer number. The increase in the Forchheimer number led to an increase in the rate of growth of the half-width of the fracture for the case of moderate fluid leak-off. The value of the ratio $\frac{c_1}{c_2}$ increased with an increase in the Forchheimer number. Figure 4.4.13 depicts the leak-off depth $b(t,x)$ for strong fluid leak-off. Similar to the preceding cases of fluid leak-off, an increase in the Forchheimer number leads to a decrease in the rate of fluid leak-off across the fracture. Both the asymptotic results in (4.4.130) and (4.4.131) depends on the Forchheimer number.

4.4.7 Moderate leak-off at the interface: $\Omega \sim 1$ and $\Gamma \sim 1$

Consider the case of moderate fluid leak-off into the rock-mass

$$\Omega \frac{c_1}{c_2}\frac{df(\xi)}{d\xi} + \frac{d}{d\xi}\left(f^3(\xi)\frac{df(\xi)}{d\xi}\right) + \left(\frac{1}{\Gamma}\right)\left(\frac{c_1}{c_2}\right)\frac{dg(\xi)}{d\xi} = 0, \tag{4.4.132}$$

$$F_0\left(\frac{c_1}{c_2}\right)^2\left(\frac{dg(\xi)}{d\xi}\right)^2 - \frac{c_1}{c_2}\frac{dg(\xi)}{d\xi} - \frac{f(\xi)}{g(\xi)} = 0, \tag{4.4.133}$$

$$f(1) = 0, \quad g(1) = 0, \quad f^3\frac{df}{d\xi} \to 0 \quad \text{as} \quad \xi \to 1. \tag{4.4.134}$$

The solution for $L(t)$, $h(t,x)$, $b(t,x)$ and $p(t,x)$ follows from (4.4.99)-(4.4.102) . The asymptotic solutions of (4.4.132) and (4.4.133) as $\xi \to 1$ with $\Omega \sim 1$ and $\Gamma \sim 1$ are as given in (4.4.93) and (4.4.94)

$$f(\xi) \sim \left(3\Omega\frac{c_1}{c_2}\right)^{\frac{1}{3}}(1-\xi)^{\frac{1}{3}}, \qquad g(\xi) \sim \left(\frac{3^{13}}{7^6}\times\Omega\right)^{\frac{1}{9}}\left(\frac{1}{F_0}\right)^{\frac{1}{3}}\left(\frac{c_1}{c_2}\right)^{-\frac{5}{9}}(1-\xi)^{\frac{7}{9}}, \quad F_0 > 0. \tag{4.4.135}$$

4.4.7.1 Fracture half-width and leak-off depth

Figure 4.4.14 shows the propagation of the fracture half-width for when there is moderate fluid leak-off at the fluid-rock interface. The rate of propagation is strong for high Forchheimer number and weak for low Forchheimer number. The value of the ratio $\frac{c_1}{c_2}$ increases with an increase in the value of the Forchheimer number F_0. The corresponding leak-off depth $b(t,x)$ is plotted in Figure 4.4.15. It is found that the rate of leak-off decreases with an increase in the value of the Forchheimer number across the fracture. Only the asymptotic result for $f(\xi)$ as ξ tends to 1 does not depend on the Forchheimer number F_0.

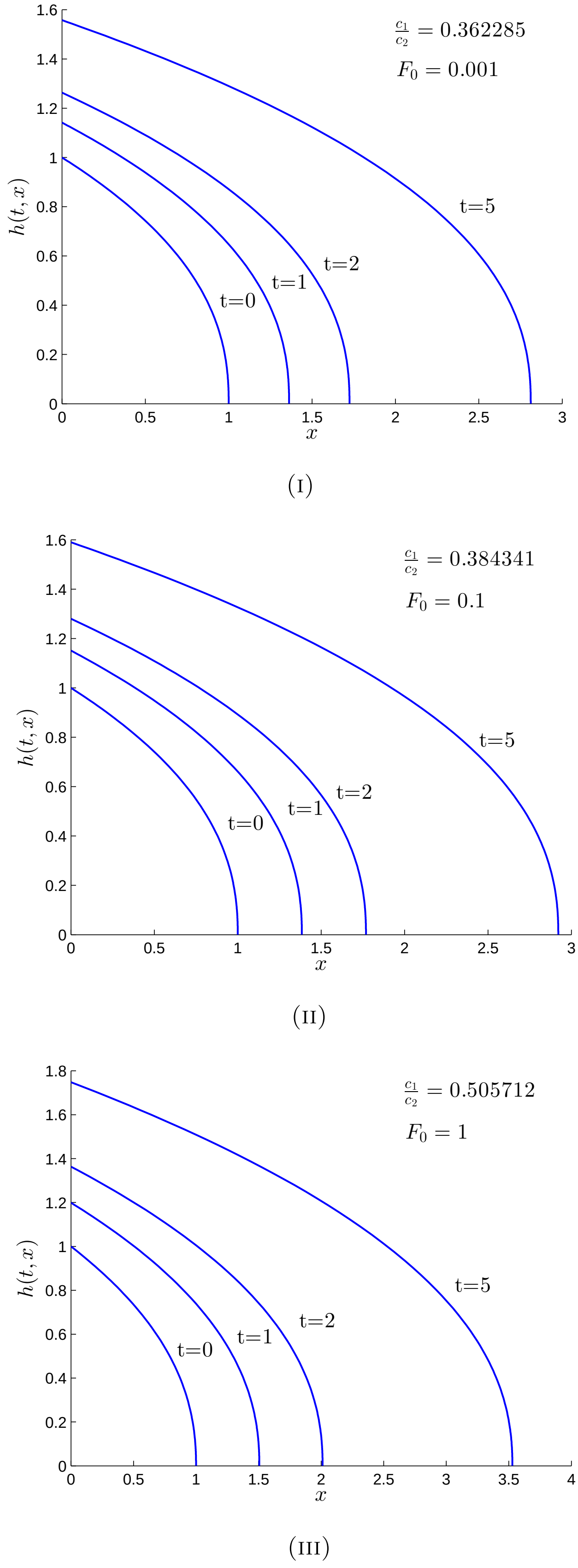

FIGURE 4.4.12: Fracture half-width plotted against x at times t=0, 1, 2, 5 for strong fluid leak-off at the interface when $\Gamma = 1$, $c_3 = 0$ and F_0=0.001, 0.1, 1.

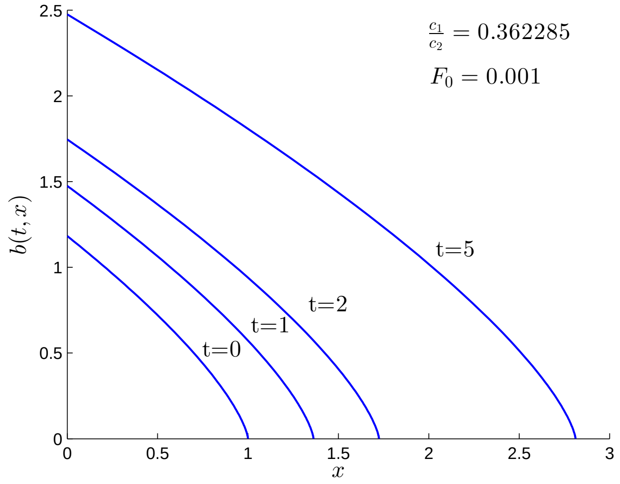

(I)

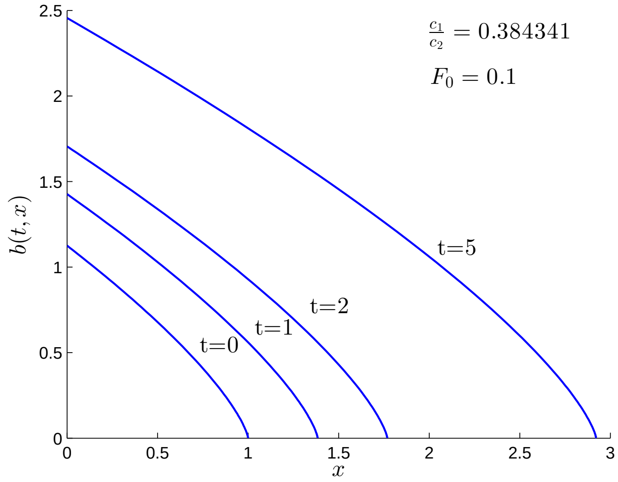

(II)

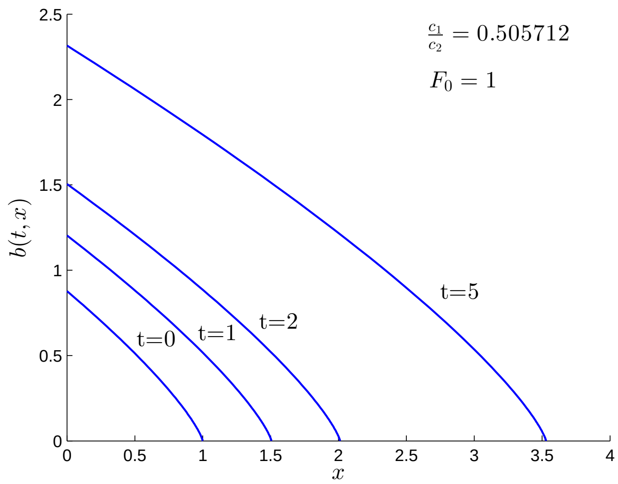

(III)

FIGURE 4.4.13: Leak-off depth plotted against x at times t=0, 1, 2, 5 for strong fluid leak-off at the interface when $\Gamma = 1$, $c_3 = 0$ and F_0=0.001, 0.1, 1.

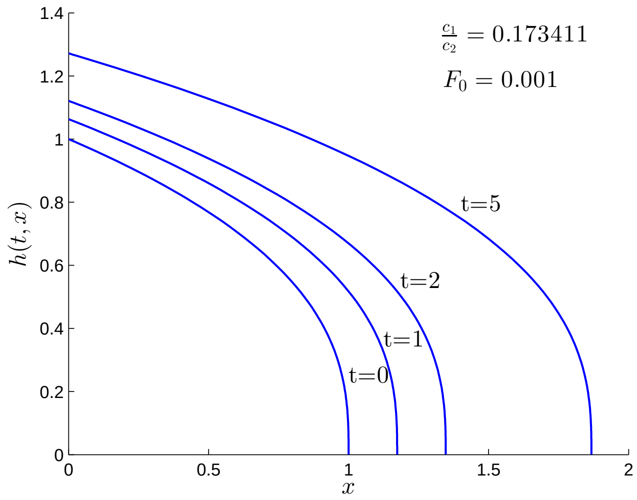

(I)

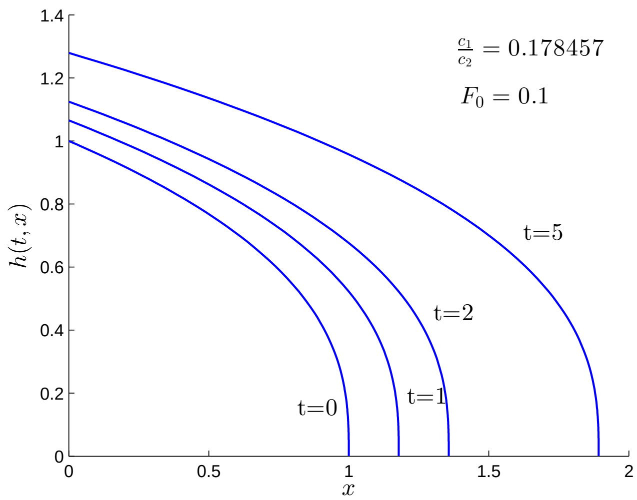

(II)

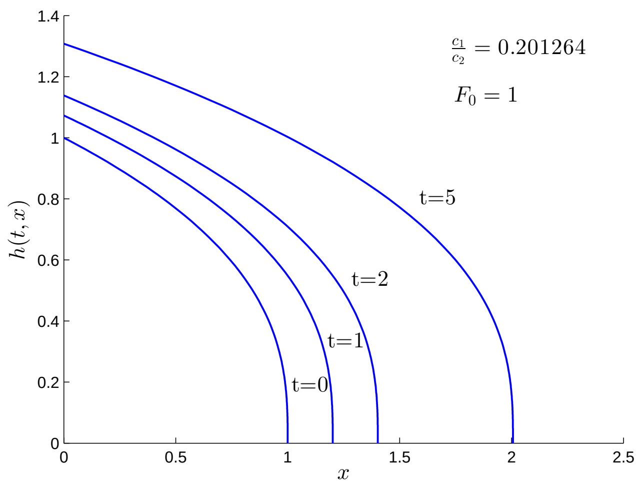

(III)

FIGURE 4.4.14: Fracture half-width plotted against x at times t=0, 1, 2, 5 for moderate fluid leak-off at the interface when $\Omega = \Gamma = 1$, $c_3 = 0$ and F_0=0.001, 0.1, 1.

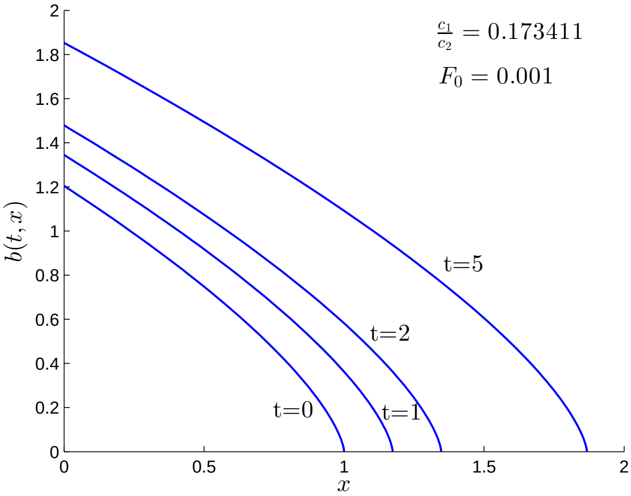

(I)

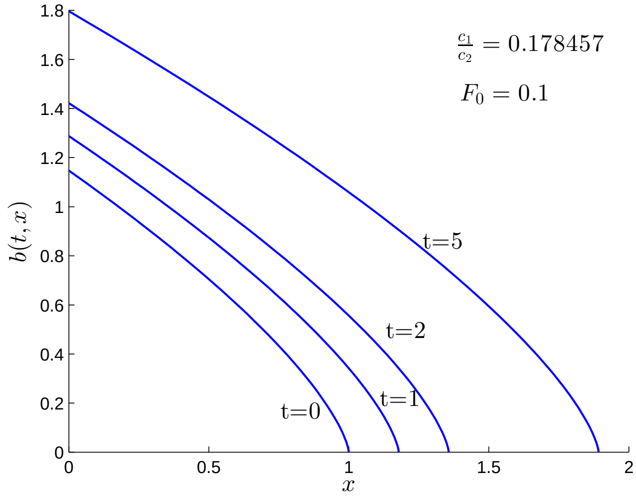

(II)

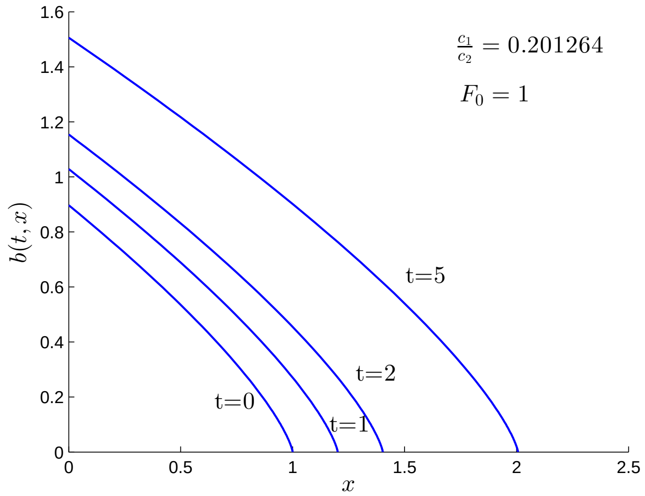

(III)

FIGURE 4.4.15: Leak-off depth plotted against x at times t=0, 1, 2, 5 for moderate fluid leak-off at the interface when $\Omega = \Gamma = 1$, $c_3 = 0$ and F_0=0.001, 0.1, 1.

4.4.8 Length of the fracture

The fracture length $L(t)$, when $c_3 = 0$, grows linearly with time, the rate of growth depending on the ratio $\frac{c_1}{c_2} > 0$. The values of the ratio were obtained numerically for all cases of fluid leak-off at the interface. The length of the fracture does not change with an increase in the value of the Forchheimer number when there is weak fluid leak-off at the interface. Therefore, for this case, the growth of the fracture is not shown.

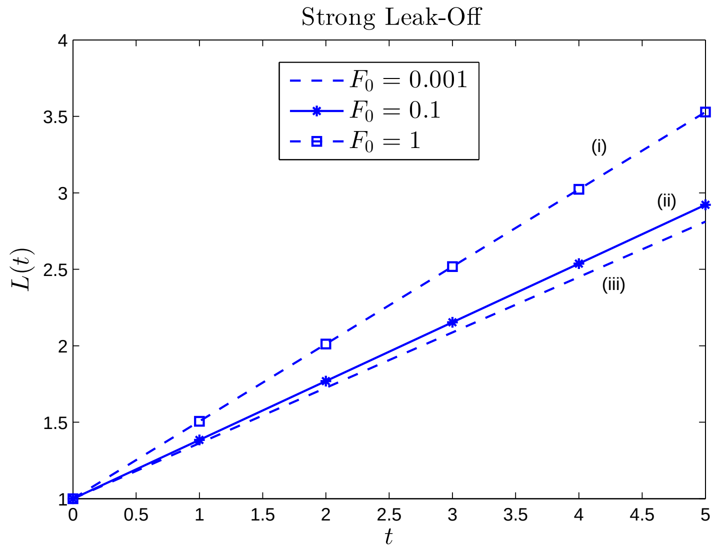

FIGURE 4.4.16: Length of the fracture $L(t)$ plotted against t for strong fluid leak-off at the interface when F_0=0.001, 0.1, 1.

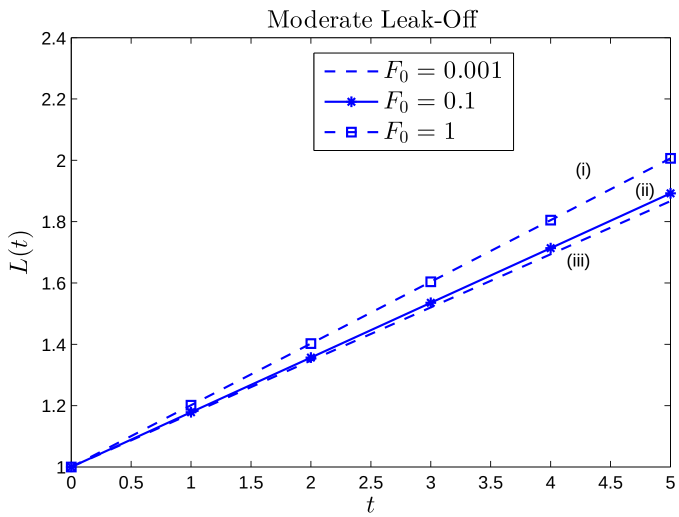

FIGURE 4.4.17: Length of the fracture $L(t)$ plotted against t for moderate fluid leak-off at the interface when F_0=0.001, 0.1, 1.

In Figure 4.4.16, the length of the fracture when there is strong fluid leak-off is plotted for F_0=0.001, 0.1, 1. The rate of growth of the fracture length is strong for $F_0 = 1$ and weak for $F_0 = 0.001$. The growth of the length of the fracture with time when there is moderate fluid leak-off into the permeable medium is illustrated in Figure 4.4.17. An increase in the Forchheimer number results in an increase in the rate of growth of the fracture. However, the rate of growth of the fracture length when there is strong leak-off is stronger than the rate of growth when there is weak fluid leak-off at the fracture interface for all values of the Forchheimer number. In Figure 4.4.18, the three cases of fluid leak-off at the interface are plotted for F_0=1. Uncharacteristically, the fracture length for the case of strong fluid leak-off plotted in (i) grows the strongest. This was unanticipated since a large volume of fluid is expected to discharge into the permeable medium at the fracture interface. When there is weak leak-off at the fluid-rock interface, the growth of the fracture length with time is shown in (ii). Lastly, the growth of the fracture length when there is moderate leak-off of fluid at the fluid-rock interface is depicted in (iii). The distinguishing feature in Figure 4.4.18 is that the rate of growth of the fracture length when there is strong fluid leak-off at the interface is the greatest and not weak leak-off. Since $\Omega \ll 1$, there is more fluid to drive the propagation of the fracture for the case of strong fluid leak-off when fluid velocity is relatively high.

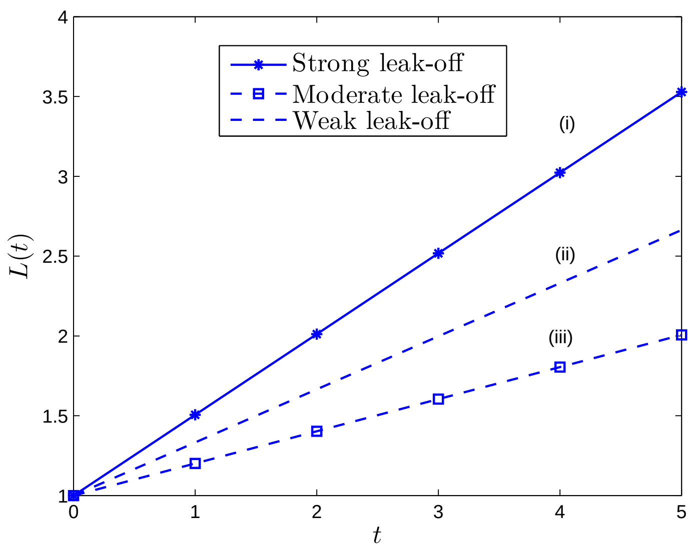

FIGURE 4.4.18: Length of the fracture $L(t)$ plotted against t for (i) strong fluid leak-off, (ii) weak fluid leak-off and (iii) moderate leak-off of fluid at the interface when F_0=1.

4.5 Conclusions

In this chapter, we have considered a two-dimensional fluid-driven fracture propagation in a elastic porous medium. Again, the conservation of mass equation and the momentum equation are used to describe the fluid flow inside the fracture. Without change of boundary conditions, we adopted the nonlinear diffusion equation governing the evolution of the half-width of the fracture. The distinguishing characteristic in Chapter 4 is that the flow of fluid in the porous media is non-Darcy. Hence, the Forchheimer model was used to describe the flow of fluid in the encompassing rock formation. By non-dimensionalizing the fluid flow models, we obtained a dimensionless parameter, F_0, which we termed the Forchheimer number.

The classification of fluid leak-off at the fracture walls remained the same as discussed in Section 3.5. Lie point symmetry analysis was used to reduce the nonlinear diffusion equation and Forchheimer flow model into a system of ordinary differential equations. The Lie point symmetry generator was found to be the same as the case of Darcy fluid flow model in Chapter 3. The boundary equations were stated in terms of the transformed variables. The boundary value problem was further classified into two cases: $c_3 \neq 0$ and $c_3 = 0$. The resulting system of ordinary differential equations for when $c_3 \neq 0$ could not be solved analytically hence the asymptotic behaviour of the similarity dependent variables $S(u)$ and $R(u)$ at the fracture tip was considered to integrate backward with distinct values of the Forchheimer number to obtain numerical solutions. A general asymptotic solution was obtained. Both the asymptotic results for the case of weak fluid leak-off and moderate fluid leak-off were obtained from the general asymptotic solution with the use of the definition of Ω and Γ for the respective cases of fluid leak-off. It was found that for the case of weak leak-off, an increase Forchheimer number had no effect on the half-width of the fracture. Nonetheless, an increase in the Forchheimer number decreased the leak-off depth. It was also found that for both the case of strong and moderate fluid leak-off, the half-width of the fracture increased with an increase in the Forchheimer number but the leak-off depth decreased across the fracture with an increase in the Forchheimer number. The effect of a non-Darcy flow is therefore to decrease the rate of fluid leak-off while increasing the rate of growth of the half-width of the fracture.

The half-width of the fracture grew the most for large Forchheimer number and the least for small Forchheimer number. When $c_3 = 0$, invariant solutions of the traveling wave form are obtained. The rate of growth of the fracture length and half-width also increases as F_0 increases, while the rate of leak-off is decreased, similar to when $c_3 \neq 0$.

Chapter 5

CONCLUSIONS

The objective of this research was to study the propagation of a two-dimensional hydraulic fracture in a permeable medium with non-Darcy fluid flow in the encompassing rock-mass. The fracture is propagated by injection of high pressured fluid at the fracture entry. During the fracturing time process, some proportion of the fracturing fluid discharge into the rock-mass formation at the fracture interface. Lubrication approximation was one of the two main important assumptions in formulating the mathematical model governing the fracture propagation. Using Lubrication approximation, the momentum equation describing the flow of fluid in the fracture was simplified. The other important assumption is the PKN approximation. The PKN approximation is a simpler formulation in which the net pressure and the fracture half-width are related linearly with the proportionality constant depending on the material properties of the rock. It aided in closing the system of differential equations and in the determination of the characteristic fluid velocity along the fracture. The elasticity equation can be modeled using the more robust formulation which is the Cauchy principal integral derived from linear elastic fracture mechanics. The flow of fluid into the permeable medium was identified as Darcy and non-Darcy fluid flow. The Forchheimer model was used to describe the flow of fluid in the event of non-Darcy fluid flow.

The mathematical formulation resulted in a system of partial differential equations relating the half-width of the fracture and the leak-off velocity. We have demonstrated in this study that invariant solutions can be derived for a fluid-driven pre-existing fracture with Darcy and non-Darcy fluid flow in the permeable rock by the adoption of the lubrication approximation, the PKN elasticity hypothesis and by using Lie point symmetries obtained from the system of partial differential equations. The first of the system of two equations that was derived is a nonlinear diffusion equation, which after non-dimensionalizing contained two dimensionless parameters describing the strength of fluid leak-off at the fracture interface. The dimensionless parameters can be chosen to identify the strength of fluid leak-off at fracture interface as weak, strong or finite. These three cases of fluid leak-off were considered. Using Lie symmetry analysis, the system of nonlinear partial differential equations was reduced to a system of nonlinear ordinary differential equations. The resulting differential equation contained the ratio $\frac{c_3}{c_2}$ which was to be determined numerically as part of the solution. The system of differential equations governing the fracture propagation with fluid leak-off at the fracture interface admitted two Lie point symmetries which, however, were not sufficient to integrate completely the system to obtain an exact analytical solution. When the fluid flow in the porous medium is Darcy and $c_3 \neq 0$, the boundary value problem was in terms of two dependent variables S and R. Numerical results were obtained for all the three cases of fluid leak-off at the fracture walls. For each of the three cases of fluid leak-off the value of the ratio $\frac{c_3}{c_2}$ was obtained. High values of the ratio were associated with strong rate of growth of the fracture length and half-width. Solutions were also obtained for $c_3 = 0$. The boundary value problem for this case also contained a ratio, $\frac{c_1}{c_2}$. The group invariant solution was of the traveling wave form. An Analytical solution was derived for the case of weak leak-off when $c_3 = 0$. Comparison of the analytical solutions to the numerical results is showed in Table 3.1. The numerical solution was in good agreement with the analytical solution. In both cases, $c_3 \neq 0$ and $c_3 = 0$, the fracture length always increased even when there was strong fluid leak-off at the fracture interface. For the times considered, the extent of fluid leak-off into the porous rock for the case of weak leak-off is not as wide as for the case of finite and strong leak-off. This pattern was observed for both $c_3 \neq 0$ and $c_3 = 0$.

When considering a fluid-driven fracture propagating in an elastic permeable medium with non-Darcy flow, the solution depended essentially on the parameter F_0 termed the Forchheimer number. This parameter was varied to obtain different mathematical models which were solved numerically. Again, the three cases of fluid leak-off at the fracture interface were considered. For the case of non-Darcy fluid flow, we could not obtain analytical solution. In all the values of the Forchheimer number considered the half-width of the fracture was not affected by a change in the Forchheimer number when there was weak fluid leak-off at the fracture walls for both the case $c_3 \neq 0$ and $c_3 = 0$. However, the leak-off depth decreased with an increase in the Forchheimer number for all the three distinct cases of fluid leak-off. The propagation of the half-width of the fracture for when there is strong and finite fluid leak-off increased with an increase in the value of the Forchheimer number with the strongest rate of growth occurring when there is strong fluid leak-off at the interface. This occurred for both $c_3 \neq 0$ and $c_3 = 0$. These solutions may be helpful in improving production forecasting in the petroleum and mining industry when there is high velocity during the fracturing process.

In this research we have used the PKN model to relate the excess fluid pressure $p(t, x)$

and the fracture half-width $h(t, x)$, as a consequence, the width-averaged fluid velocity vanishes at the fracture tip and therefore the fluid flux also vanishes at the tip of the fracture. Also, at the fracture tip, the gradient of the fracture half-width satisfies $\frac{\partial h}{\partial x} \to -\infty$. When using the PKN model, the net pressure vanishes at the tip of the fracture hence it is not possible to define the stress intensity factor. Thus, future work can be done, for example we can use the more sophisticated Cauchy principal value formulation for the elasticity equation where the rock's response to the injected fluid is taken into account. In this work, conservation laws for the nonlinear diffusion equation were not considered.

Appendix A

Lie point symmetry analysis

In this section, we show the complete derivation of the Lie point symmetries of the partial differential equations (3.5.20) and (3.5.21)

$$\Omega \frac{\partial h}{\partial t} - \frac{\partial}{\partial x}\left(h^3 \frac{\partial h}{\partial x}\right) + \frac{1}{\Gamma}\frac{h}{b} = 0, \tag{A.1}$$

$$\frac{\partial b}{\partial t} - \frac{h}{b} = 0, \tag{A.2}$$

where Ω and Γ are dimensionless parameters. To derive the Lie point symmetries we will require that both Ω and Γ be non-zero. Equations (A.1) and (A.2) can be expressed in the form

$$\Omega h_t - h^3 h_{xx} - 3h^2 (h_x)^2 + \frac{1}{\Gamma}\frac{h}{b} = 0, \tag{A.3}$$

$$b_t - \frac{h}{b} = 0. \tag{A.4}$$

We derive the Lie point symmetry generator

$$X = \xi^1(t,x,b,h)\frac{\partial}{\partial t} + \xi^2(t,x,b,h)\frac{\partial}{\partial x} + \eta^1(t,x,b,h)\frac{\partial}{\partial b} + \eta^2(t,x,b,h)\frac{\partial}{\partial h}, \tag{A.5}$$

of (A.1) and (A.2) by solving the determining equations

$$X^{[2]}\left(\Omega h_t - h^3 h_{xx} - 3h^2(h_x)^2 + \frac{1}{\Gamma}\frac{h}{b}\right)\Bigg|_{\substack{\Omega h_t - h^3 h_{xx} - 3h^2(h_x)^2 + \frac{1}{\Gamma}\frac{h}{b} = 0 \\ b_t - \frac{h}{b} = 0}} = 0, \tag{A.6}$$

$$X^{[2]}\left(b_t - \frac{h}{b}\right)\Bigg|_{\substack{\Omega h_t - h^3 h_{xx} - 3h^2(h_x)^2 + \frac{1}{\Gamma}\frac{h}{b} = 0 \\ b_t - \frac{h}{b} = 0}} = 0, \tag{A.7}$$

for $\xi^1(t,x,b,h)$, $\xi^2(t,x,b,h)$, $\eta^1(t,x,b,h)$ and $\eta^2(t,x,b,h)$ where $X^{[2]}$ is the second prolongation of the Lie point symmetry generator X given by

$$X^{[2]} = X + \zeta_1^1\frac{\partial}{\partial b_t} + \zeta_2^1\frac{\partial}{\partial b_x} + \zeta_{12}^1\frac{\partial}{\partial b_{tx}} + \zeta_{22}^1\frac{\partial}{\partial b_{xx}} + \zeta_1^2\frac{\partial}{\partial h_t} + \zeta_2^2\frac{\partial}{\partial h_x} + \ldots \\ \zeta_{12}^2\frac{\partial}{\partial h_{tx}} + \zeta_{22}^2\frac{\partial}{\partial h_{xx}}, \tag{A.8}$$

and ζ_{xi}^α and $\zeta_{x^ix^j}^\alpha$ are defined by

$$\zeta_{xi}^\alpha \quad = \quad D_{x^i}(\eta^\alpha) - u_{x^j}^\alpha D_{x^i}(\xi^j), \qquad \alpha, i = 1,2 \tag{A.9}$$

$$\zeta_{x^ix^j}^\alpha \quad = \quad D_{x^i}(\eta^\alpha) - u_{jl}^\alpha D_{x^i}(\xi^l), \qquad \alpha, i = 1,2 \tag{A.10}$$

with summation over the index j from 1 to 2 in equation (A.9) and l from 1 to 2 in equation (A.10). The total derivative operator with respect to the independent variable t and x is defined by

$$D_t = \frac{\partial}{\partial t} + b_t\frac{\partial}{\partial b} + h_t\frac{\partial}{\partial h} + b_{tx}\frac{\partial}{\partial b_x} + h_{tx}\frac{\partial}{\partial h_x} + b_{tt}\frac{\partial}{\partial b_t} + h_{tt}\frac{\partial}{\partial h_t}, \tag{A.11}$$

$$D_x = \frac{\partial}{\partial x} + b_x\frac{\partial}{\partial b} + h_x\frac{\partial}{\partial h} + b_{xt}\frac{\partial}{\partial b_t} + h_{xt}\frac{\partial}{\partial h_t} + b_{xx}\frac{\partial}{\partial b_x} + h_{xx}\frac{\partial}{\partial h_x}. \tag{A.12}$$

From the determining equations (A.6) and (A.7), we obtain

$$\zeta_t^2 - 3h^2\zeta_x^2 - h^3\zeta_{xx}^2 - 3h^2h_{xx}\eta^2 - 6hh_x^2\eta^2 + \frac{1}{b}\eta^2\Big|_{\substack{h_t = h^3h_{xx} + 3h^2(h_x)^2 - \frac{h}{b} \\ b_t = \frac{h}{b}}} = 0, \tag{A.13}$$

$$\zeta_t^1 - \frac{1}{b}\eta^2 + \frac{h}{b^2}\eta^1\Big|_{\substack{h_t = h^3h_{xx} + 3h^2(h_x)^2 - \frac{h}{b} \\ b_t = \frac{h}{b}}} = 0. \tag{A.14}$$

Now, we calculate the expressions of ζ_t^1, ζ_t^2, ζ_x^2 and ζ_{xx}^2 according to equations (A.9) and (A.10)

$$\zeta_t^1 = D_t(\eta^1) - b_tD_t(\xi^1) - b_xD_t(\xi^2), \tag{A.15}$$

$$\zeta_t^2 = D_t(\eta^2) - h_tD_t(\xi^1) - h_xD_t(\xi^2), \tag{A.16}$$

$$\zeta_x^2 = D_x(\eta^2) - h_tD_x(\xi^1) - h_xD_x(\xi^2), \tag{A.17}$$

$$\zeta_{xx}^2 = D_x(\zeta_x^2) - h_{xt}D_x(\xi^1) - h_{xx}D_x(\xi^2). \tag{A.18}$$

Expanding (A.15)-(A.18) using (A.11) and (A.12), we obtain

$$\zeta_t^1 = \eta_t^1 + \eta_b^1b_t + \eta_h^1h_t - b_t\left(\xi_b^1 + \xi_h^1h_t + \xi_t^1\right) - b_x\left(\xi_b^2b_t + \xi_h^2h_t + \xi_t^2\right), \tag{A.19}$$

$$\zeta_t^2 = \eta_t^2 + \eta_b^2 b_t + \eta_h^2 h_t - h_t\left(\xi_b^1 b_t + \xi_h^1 h_t + \xi_t^1\right) - h_x\left(\xi_b^2 b_t + \xi_h^2 h_t + \xi_t^2\right), \tag{A.20}$$

$$\zeta_x^2 = \eta_x^2 + \eta_b^2 b_x + \eta_h^2 h_x - h_t\left(\xi_b^1 b_x + \xi_h^1 h_x + \xi_x^1\right) - h_x\left(\xi_b^2 b_x + \xi_h^2 h_x + \xi_x^2\right), \tag{A.21}$$

$$\begin{aligned}
\zeta_{xx}^2 = {} & \eta_{xx}^2 + h_{xx}\eta_h^2 + b_{xx}\eta_b^2 + h_x\eta_{xh}^2 + b_x\eta_{xb}^2 - 2h_{tx}\left(h_x\xi_h^1 + b_x\xi_b^1 + \xi_x^1\right) \\
& - 2h_{xx}\left(h_x\xi_h^2 + b_x\xi_b^2 + \xi_x^2\right) + h_x\left(h_x\eta_{hh}^2 + b_x\eta_{bh}^2 + \eta_{xh}^2\right) \\
& + b_x\left(h_x\eta_{bh}^2 + b_x\eta_{bb}^2 + \eta_{xb}^2\right) - h_t\left(h_{xx}\xi_h^1 + b_{xx}\xi_b^1 + h_x\xi_{xh}^1 + b_x\xi_{xb}^1 + \xi_{xx}^1\right) \\
& + h_t\left[h_x\left(h_x\xi_{hh}^1 + b_x\xi_{bh}^1 + \xi_{xh}^1\right) + b_x\left(h_x\xi_{bh}^1 + b_x\xi_{bb}^1 + \xi_{xb}^1\right)\right] \\
& - h_x\left(h_{xx}\xi_h^2 + b_{xx}\xi_b^2 + h_x\xi_{xh}^2 + h_x + b_x\xi_{xb}^2 + \xi_{xx}^2\right) \\
& + h_x\left[h_x\left(h_x{\xi^2}_{hh} + b_x\xi_{bh}^2 + \xi_{xh}^2\right) + b_x\left(h_x\xi_{bh}^2 + b_x\xi_{bb}^2 + \xi_{xb}^2\right)\right].
\end{aligned} \tag{A.22}$$

Substituting the expressions for ζ_t^1, ζ_t^2, ζ_x^2 and ζ_{xx}^2 into (A.13) and (A.14), we obtain

$$\begin{aligned}
& \eta_t^2 + \eta_b^2 b_t + \eta_h^2 h_t - 3h^2\left[\eta_x^2 + \eta_b^2 b_x + \eta_h^2 h_x - h_t\left(\xi_b^1 b_x + \xi_h^1 h_x + \xi_x^1\right) - h_x\left(\xi_b^2 b_x + \xi_h^2 h_x + \xi_x^2\right)\right] \\
& - h_t\left(\xi_b^1 b_t + \xi_h^1 h_t + \xi_t^1\right) - h_x\left(\xi_b^2 b_t + \xi_h^2 h_t + \xi_t^2\right) - 3h^2 h_{xx}\eta^2 - 6hh_x^2\eta^2 + \frac{1}{b}\eta^2 - h^3\eta_{xx}^2 - h^3 h_{xx}\eta_h^2 \\
& - h^3 b_{xx}\eta_b^2 - h^3 h_x\eta_{xh}^2 - h^3 b_x\eta_{xb}^2 + 2h^3 h_{tx}\left(h_x\xi_h^1 + b_x\xi_b^1 + \xi_x^1\right) + 2h^3 h_{xx}\left(h_x\xi_h^2 + b_x\xi_b^2 + \xi_x^2\right) \\
& - h^3 h_x\left(h_x\eta_{hh}^2 + b_x\eta_{bh}^2 + \eta_{xh}^2\right) + h^3 h_t\left(h_{xx}\xi_h^1 + b_{xx}\xi_b^1 + h_x\xi_{xh}^1 + b_x\xi_{xb}^1 + \xi_{xx}^1\right) \\
& - h^3 h_t\left[h_x\left(h_x\xi_{hh}^1 + b_x\xi_{bh}^1 + \xi_{xh}^1\right) + b_x\left(h_x\xi_{bh}^1 + b_x\xi_{bb}^1 + \xi_{xb}^1\right)\right] - h^3 b_x\left(h_x\eta_{bh}^2 + b_x\eta_{bb}^2 + \eta_{xb}^2\right) \\
& + h^3 h_x\left(h_{xx}\xi_h^2 + b_{xx}\xi_b^2 + h_x\xi_{xh}^2 + h_x + b_x\xi_{xb}^2 + \xi_{xx}^2\right) \\
& - h^3 h_x\left[h_x\left(h_x{\xi^2}_{hh} + b_x\xi_{bh}^2 + \xi_{xh}^2\right) + b_x\left(h_x\xi_{bh}^2 + b_x\xi_{bb}^2 + \xi_{xb}^2\right)\right] = 0,
\end{aligned} \tag{A.23}$$

$$\eta_t^1 + \eta_b^1 b_t + \eta_h^1 h_t - b_t\left(\xi_b^1 + \xi_h^1 h_t + \xi_t^1\right) - b_x\left(\xi_b^2 b_t + \xi_h^2 h_t + \xi_t^2\right) - \frac{1}{b}\eta^2 + \frac{h}{b^2}\eta^1 = 0. \tag{A.24}$$

From (A.3) and (A.4),

$$h_t = h^3 h_{xx} + 3h^2(h_x)^2 - \frac{h}{b}, \tag{A.25}$$

$$b_t = \frac{h}{b}. \tag{A.26}$$

Substituting (A.25) and (A.26) into (A.23) and (A.24) we obtain

$$
\begin{aligned}
&2h_x h_{xxx}\xi^1_h h^6 + h_x^2 h_{xx}\xi^1_{hh} h^6 + b_{xx} h_{xx}\xi^1_b h^6 + 2b_x h_{xxx}\xi^1_b h^6 + 2b_x h_x h_{xx}\xi^1_{bh} h^6 + b_x^2 h_{xx}\xi^1_{bb} h^6 \\
&+ 2h_{xxx}\xi^1_x h^6 + 2h_x h_{xx}\xi^1_{xh} h^6 + 2b_x h_{xx}\xi^1_{xb} h^6 + h_{xx}\xi^1_{xx} h^6 + 21h_x^2 h_{xx}\xi^1_h h^5 + 3h_x^4\xi^1_{hh} h^5 \\
&+ 3h_x^2 b_{xx}\xi^1{}_b h^5 + 24b_x h_x h_{xx}\xi^1_b h^5 + 6b_x h_x^3\xi^1_{bh} h^5 + 3b_x^2 h_x^2\xi^1_{bb} h^5 + 24h_x h_{xx}\xi^1_x h^5 + 6h_x^3\xi^1_{xh} h^5 \\
&+ 6b_x h_x^2\xi^1_{xb} h^5 + 3h_x^2\xi^1_{xx} h^5 + 21h_x^4\xi^1_h h^4 + \frac{2b_x h_x\xi^1_h h^4}{b^2} + \frac{h_{xx}\xi^1_h h^4}{b} - \frac{h_x^2\xi^1{}_{hh} h^4}{b} + 30b_x h_x{}^3\xi^1_b h^4 \\
&+ \frac{2b_x^2\xi^1_b h^4}{b^2} - \frac{b_{xx}\xi^1_b h^4}{b} + \frac{h_{xx}\xi^1_b h^4}{b} - \frac{2b_x h_x\xi^1{}_{bh} h^4}{b} - \frac{b_x{}^2\xi^1_{bb} h^4}{b} + 30h_x^3\xi^1_x h^4 + \frac{2b_x\xi^1_x h^4}{b^2} \\
&- \frac{2h_x\xi^1_{xh} h^4}{b} - \frac{2b_x\xi^1_{xb} h^4}{b} - \frac{\xi^1_{xx} h^4}{b} - \frac{2h_x^2\xi^1_h h^3}{b} + 2h_x h_{xx}\xi^2_h h^3 - h_x^2\eta^2_{hh} h^3 + h_x^3\xi^2_{hh} h^3 - b_{xx}\eta^2_b h^3 \\
&+ \frac{3h_x^2\xi^1_b h^3}{b} - \frac{8b_x h_x\xi^1_b h^3}{b} + h_x b_{xx}\xi^2{}_b h^3 + 2b_x h_{xx}\xi^2_b h^3 - 2b_x h_x\eta^2_{bh} h^3 + 2b_x h_x^2\xi^2_{bh} h^3 - b_x^2\eta^2_{bb} h^3 \\
&+ b_x^2 h_x\xi^2_{bb} h^3 - \frac{8h_x\xi^1_x h^3}{b} + 2h_{xx}\xi^2_x h^3 - 2h_x\eta^2_{xh} h^3 + 2h_x^2\xi^2_{xh} h^3 - 2b_x\eta^2_{xb} h^3 + 2b_x h_x\xi^2_{xb} h^3 \\
&- \eta^2_{xx} h^3 + h_x\xi^2_{xx} h^3 - h_{xx}\xi^1{}_t h^3 - 3\eta^2 h_{xx} h^2 - 3h_x^2\eta^2_h h^2 - \frac{\xi^1_h h^2}{b^2} + 3h_x^3\xi^2_h h^2 - 6b_x h_x\eta^2_b h^2 \\
&- \frac{\xi^1_b h^2}{b^2} + 6b_x h_x^2\xi^2_b h^2 - 6h_x\eta^2_x h^2 + 6h_x^2\xi^2_x h^2 - 3h_x^2\xi^1_t h^2 - 6\eta^2 h_x{}^2 h - \frac{\eta^1 h}{b^2} - \frac{\eta^2_h h}{b} + \frac{h_x\xi^2_h h}{b} \\
&- \frac{\eta^2_b h}{b} + \frac{h_x\xi^2_b h}{b} + \frac{\xi^1_t h}{b} + \frac{\eta^2}{b} + \eta^2_t - h_x\xi^2_t = 0,
\end{aligned}
\tag{A.27}
$$

$$
\begin{aligned}
&\frac{\eta^2}{b} - \frac{h\eta^1}{b^2} - \frac{h^2\xi^1_h}{b^2} - \frac{h^2\xi^1_b}{b^2} + \frac{h^4\xi^1_h h_{xx}}{b} - h^3\xi^2_h b_x h_{xx} + \frac{3h^3\xi^1_h h_x{}^2}{b} - 3h^2 b_x\xi^2_h h_x^2 \\
&- \frac{h\eta^1_h}{b} - \frac{h\eta^1_b}{b} + \frac{h\xi^1_t}{b} + \frac{hb_x\xi^2_h}{b} + \frac{h\xi^2_b b_x}{b} - b_x\xi^2_t + h^3\eta^1_h h_{xx} + 3h^2\eta^1_h h_x^2 + \eta^1_t = 0.
\end{aligned}
\tag{A.28}
$$

Since the functions ξ^1, ξ^2, η^1 and η^2 do not depend on the derivatives of b and h, the terms in (A.27) and (A.28) are classified according to partial derivatives of b and h and their product. In this way, equations (A.27) and (A.28) are decomposed into two overdetermined systems of equations in which there are less unknown variables than equations. We now equate the coefficients of the partial derivatives of b, h and their product in (A.27) to zero to obtain

$$h_x h_{xxx}: \quad \xi^1_h = 0, \tag{A.29}$$

$$b_x h_{xxx}: \quad \xi^1_b = 0, \tag{A.30}$$

$$h_{xxx}: \quad \xi^1_x = 0, \tag{A.31}$$

$$b_{xx} h_{xx}: \quad \xi^1_b = 0, \tag{A.32}$$

$$b_x h_x h_{xx}: \quad 24h^5\xi^1_b + 2h^6\xi^1_{bh} = 0, \tag{A.33}$$

$$h_x^2 h_{xx}: \quad 21h^5\xi^1_h + h^6\xi^1_{hh} = 0, \tag{A.34}$$

$$h_x^2 h_{xx}: \quad \xi_b^1 = 0, \tag{A.35}$$

$$b_x^2 h_{xx}: \quad \xi_{bb}^1 = 0, \tag{A.36}$$

$$h_x h_{xx}: \quad 2h^3\xi_h^2 + 24h^5\xi_x^1 + +2h^6\xi_{xh}^1 = 0, \tag{A.37}$$

$$h_x b_{xx}: \quad \xi_b^2 = 0, \tag{A.38}$$

$$b_x h_{xx}: \quad 2h^3\xi_b^2 + 2h^6\xi_{xb}^1 = 0, \tag{A.39}$$

$$h_{xx}: \quad 2h^3\xi_x^2 + h^6\xi_{xx}^1 - 3h^2\eta^2 + \frac{h^4}{b}\xi_h^1 + \frac{h^4}{b}\xi_b^1 - h^3\xi_t^1 = 0, \tag{A.40}$$

$$b_{xx}: \quad h^3\eta_b^2 + \frac{h^4}{b}\xi_b^1 = 0, \tag{A.41}$$

$$b_x h_x^3: \quad 30h^4\xi_b^1 + 6h^5\xi_{bh}^1 = 0, \tag{A.42}$$

$$b_x^2 h_x^2: \quad \xi_{bb}^1 = 0, \tag{A.43}$$

$$b_x h_x^2: \quad 6h^2\xi_b^2 + 2h^3\xi_{bh}^2 + 6h^2\xi_{xb}^1 = 0, \tag{A.44}$$

$$b_x^2 h_x: \quad \xi_{bb}^2 = 0, \tag{A.45}$$

$$b_x h_x: \quad \frac{2h^4}{b^2}\xi_h^1 - 6h^2\eta_b^2 - \frac{8h^3}{b}\xi_b^1 - 2h^3\eta_{bh}^2 - \frac{2h^4}{b^2}\xi_{bh}^1 + 2h^3\xi_{xb}^2 = 0, \tag{A.46}$$

$$h_x^4: \quad 21h^4\xi_h^1 + 3h^5\xi_{hh}^1 = 0, \tag{A.47}$$

$$h_x^3: \quad 3h^2\xi_h^2 + h^3\xi_{hh}^2 + 30h^4\xi_x^1 + 6h^5\xi_{xh}^1 = 0, \tag{A.48}$$

$$h_x^2: \quad 6h^2\xi_x^2 + 2h^3\xi_{xh}^2 + 3h^5\xi_{xx}^1 - 3h^2\xi_t^1 + \frac{3h^3}{b}\xi_b^1 - 6h\eta^2 - 3h^2\eta_h^2 - \frac{2h^3}{b}\xi_h^1 - h^3\eta_{hh}^2 - \frac{h^4}{b}\xi_{hh}^1 = 0, \tag{A.49}$$

$$b_x^2: \quad \frac{2h^4}{b^2}\xi_b^1 - h^3\eta_{bb}^2 - \frac{h^4}{b}\xi_{bb}^1 = 0, \tag{A.50}$$

$$h_x: \quad \frac{h}{b}\xi_h^2 + \frac{h}{b}\xi_b^2 - \frac{8h^3}{b}\xi_x^1 - 2h^3\eta_{xh}^2 - \frac{2h^4}{b}\xi_{xh}^1 + h^3\xi_{xx}^2 - \xi_t^2 - 6h^2\eta_x^2 = 0, \tag{A.51}$$

$$b_x: \quad \frac{2h^4}{b^2}\xi_x^1 - 2h^3\eta_{xb}^2 - \frac{2h^4}{b}\xi_{xb}^1 = 0, \tag{A.52}$$

$$1: \quad \frac{\eta^2}{b} - \frac{h}{b^2}\eta^1 - \frac{h}{b}\eta_h^2 - \frac{h^2}{b^2}\xi_h^1 - \frac{h}{b}\eta_b^2 - \frac{h^2}{b^2}\xi_b^1 - h^3\eta_{xx}^2 - \frac{h^4}{b}\xi_{xx}^1 + \eta_t^2 + \frac{h}{b}\xi_t^1 = 0, \tag{A.53}$$

and in (A.28) to obtain

$$b_x h_{xx}: \quad \xi_h^2 = 0, \tag{A.54}$$

$$h_{xx}: \quad h^3\eta_h^1 + \frac{h^4}{b}\xi_h^1 = 0, \tag{A.55}$$

$$h_x^2: \quad 3h^2\eta_h^1 + \frac{3h^3}{b}\xi_h^1 = 0, \tag{A.56}$$

$$b_x: \quad \frac{h}{b}\xi_h^2 + \frac{h}{b}\xi_b^2 - \xi_t^2 = 0, \tag{A.57}$$

$$1: \quad \frac{\eta^2}{b} - \frac{h}{b^2}\eta^1 - \frac{h}{b}\eta_h^1 - \frac{h^2}{b^2}\xi_h^1 - \frac{h}{b}\eta_b^1 - \frac{h^2}{b^2}\xi_b^1 + \eta_t^1 + \frac{h}{b}\xi_t^1 = 0. \tag{A.58}$$

From (A.29)-(A.32), we have

$$\xi^1_h = 0, \quad \xi^1_b = 0, \quad \text{and} \quad \xi^1_x = 0, \tag{A.59}$$

which implies

$$\xi^1 = \xi^1(t). \tag{A.60}$$

Equation (A.38) and (A.54) implies

$$\xi^2 = \xi^2(t, x). \tag{A.61}$$

Equations (A.33)-(A.39) are identically satisfied. Equations (A.40)-(A.53) reduces to

$$h_{xx}: \quad 2h^3\xi^2_x - 3h^2\eta^2 - h^3\xi^1_t = 0, \tag{A.62}$$

$$b_{xx}: \quad \eta^2_b = 0, \tag{A.63}$$

$$h^2_x: \quad 6h^2\xi^2_x - 3h^2\xi^1_t - 6h\eta^2 - 3h^2\eta^2_h - h^3\eta^2_{hh} = 0, \tag{A.64}$$

$$h_x: \quad h^3\xi^2_{xx} - 2h^3\eta^2_{xh} - \xi^2_t - 6h^2\eta^2_x = 0, \tag{A.65}$$

$$1: \quad \frac{\eta^2}{b} - \frac{h}{b^2}\eta^1 - \frac{h}{b}\eta^2_h - h^3\eta^2_{xx} + \eta^2_t + \frac{h}{b}\xi^1_t = 0, \tag{A.66}$$

and equations (A.56)-(A.58) reduces to

$$h^2_x: \quad \eta^1_h = 0, \tag{A.67}$$

$$b_x: \quad \xi^2_t = 0, \tag{A.68}$$

$$1: \quad \frac{\eta^2}{b} - \frac{h}{b^2}\eta^1 - \frac{h}{b}\eta^1_b + \eta^1_t + \frac{h}{b}\xi^1_t = 0. \tag{A.69}$$

From equations (A.63), (A.67) and (A.68), we get

$$\eta^1 = \eta^1(t, x, h) \quad \eta^2 = \eta^2(t, x, h), \quad \text{and} \quad \xi^2 = \xi^2(x). \tag{A.70}$$

Equation (A.62) gives

$$\eta^2 = \frac{h}{3}\left(2\xi^2_x - \xi^1_t\right). \tag{A.71}$$

We now differentiate η^2 with respect to x and then with respect to h to obtain

$$\eta^2_x = \frac{2h}{3}\xi^2_{xx} \quad \text{and} \quad \eta^2_{xh} = \frac{2}{3}\xi^2_{xx}. \tag{A.72}$$

Substituting η^2_x and η^2_{xh} given by (A.72) into (A.65) gives

$$\xi^2_{xx} = 0. \tag{A.73}$$

Integrating (A.73) twice, we obtain

$$\xi^2(x) = a_1 x + a_2, \tag{A.74}$$

where a_1 and a_2 are arbitrary constants. Substituting $\xi^2_x = a_1$ into (A.71) gives

$$\eta^2 = \frac{h}{3}\left(2a_1 - \xi^1_t\right), \tag{A.75}$$

which implies that $\eta^2 = \eta^2(t,h)$ since ξ^1 is a function of t. We differentiate η^2 with respect to t and h to obtain

$$\eta^2_t = \frac{h}{3}\xi^1_{tt} \quad \text{and} \quad \eta^2_h = \frac{1}{3}\left(2a_1 - \xi^1_t\right). \tag{A.76}$$

Substituting (A.75) and (A.76) into (A.66) gives

$$\eta^1 = \frac{b^2}{3}\xi^1_{tt} + b\xi^1_t. \tag{A.77}$$

Differentiating η^1 with respect to t and b gives

$$\eta^1_t = \frac{b^2}{3}\xi^1_{ttt} + b\xi^1_{tt} \quad \text{and} \quad \eta^1_b = \frac{2b}{3}\xi^1_{tt} + \xi^1_t. \tag{A.78}$$

We substitute (A.75), (A.77) and (A.78) into (A.69) to obtain

$$\frac{b^4}{3}\xi^1_{ttt} + b^3\xi^1_{tt} - hb^2\xi^1_{tt} + \frac{2hb}{3}a_1 - \frac{4hb}{3}\xi^1_t = 0. \tag{A.79}$$

The function ξ^1 is independent of both b and h. Hence we equate the coefficients of powers of b and the product of b and h to get

$$b^4: \quad \xi^1_{ttt} = 0, \tag{A.80}$$

$$b^3: \quad \xi^1_{tt} = 0, \tag{A.81}$$

$$hb^2: \quad \xi^1_{tt} = 0, \tag{A.82}$$

$$hb: \quad \frac{2}{3}a_1 - \frac{4}{3}\xi^1_t = 0. \tag{A.83}$$

Integrating (A.80) three times gives

$$\xi^1 = \frac{a_3}{2}t^2 + a_4 t + a_5, \tag{A.84}$$

where a_3, a_4 and a_5 are arbitrary constants. Using (A.81) and (A.82), we get

$$a_3 = 0, \tag{A.85}$$

hence (A.84) becomes

$$\xi^1(t) = a_4 t + a_5. \tag{A.86}$$

Differentiating ξ^1 with respect to t gives

$$\xi^1_t = a_4. \tag{A.87}$$

Substituting (A.87) into (A.83) gives

$$a_1 = 2a_4. \tag{A.88}$$

Using (A.81), (A.87) and (A.88), equation (A.75) and (A.77) becomes

$$\eta^1 = a_4 b \quad \text{and} \quad \eta^2 = a_4 h. \tag{A.89}$$

For convenience, we let $a_2 = c_1$, $a_4 = c_3$ and $a_5 = c_2$, then we have

$$\xi^1 = c_2 + c_3 t, \tag{A.90}$$

$$\xi^2 = c_1 + 2c_3 x, \tag{A.91}$$

$$\eta^1 = c_3 b, \tag{A.92}$$

$$\eta^2 = c_3 h, \tag{A.93}$$

where c_1, c_2 and c_3 are constants. Therefore, the Lie point symmetry generator is given by

$$\begin{aligned} X &= (c_2 + c_3 t)\frac{\partial}{\partial t} + (c_1 + 2c_3 x)\frac{\partial}{\partial x} + c_3 b\frac{\partial}{\partial b} + c_3 h\frac{\partial}{\partial h} \\ &= c_2 X_1 + c_1 X_2 + c_3 X_3 \end{aligned} \tag{A.94}$$

where

$$\begin{aligned} X_1 &= \frac{\partial}{\partial t}, \\ X_2 &= \frac{\partial}{\partial x}, \\ X_3 &= t\frac{\partial}{\partial t} + 2x\frac{\partial}{\partial x} + b\frac{\partial}{\partial b} + h\frac{\partial}{\partial h}. \end{aligned} \tag{A.95}$$

The Lie point symmetries that are derived are valid for arbitrary non-zero values of Ω and Γ.

Bibliography

[1] T.L. Anderson. *Fracture Mechanics.* CRC Press, second edition. Boca Raton, Florida, 1995.

[2] A.G. Fareo and D.P. Mason. *A group invariant solution for a pre-existing fluid-driven fracture in permeable rock.* Nonlinear Analysis: Real world Applications, 12: 767–779, 2011.

[3] S.H. Emerman and D.L. Turcotte. *Transport of magma and hydrothermal solutions by laminar and turbulent fluid fracture.* Physics of the Earth and Planetary Interiors, 41:249–259, 1986.

[4] S. Mathias and M. van Reeuwijk. *Hydraulic Fracture Propagation with 3-D Leak-off.* Department of Civil and Environmental Engineering, Imperial College London, UK, 2009.

[5] G.C. Howard and C.R. Fast. *Optimum fluid characteristics for fracture extension.* In: Drilling Production and Practise, API 24:261–270, 1957.

[6] I. Vlahou and M. Worster. *Freeze fracturing of elastic porous media: a mathematical model.* PhD thesis, Department of Applied Mathematics, University of Cambridge, UK, 2015.

[7] M.S. Klamkin. *On the transformation of a class of boundary value problems into initial value problems for ordinary differential equations* . SIAM Review, 4:43–47, 1962.

[8] T. Perkins and L. Kern. *Widths of hydraulic fractures.* J.Petrol. Technol., 72(222): 937–949, December 1961.

[9] S.L. Mitchell, R. Kuske, and A.P. Peirce. *An asymptotic framework for finite hydraulic fracture including leak-off.* SIAM J. APPL. MATH., 67(2):364–386, 2007.

[10] J.C. Jaeger, N.G.W. Cook, and R.W. Zimmerman. *Fundamentals of Rock Mechanics.* Blackwell Publishing, Oxford, fourth edition, 2007.

[11] S. Khristianovic and Y. Zheltov. *Formation of vertical fractures by means of highly viscous fluids*. In:4th World Petroleum Congress, Rome, pages 579–586, 1995.

[12] D.A. Spence and P. Sharp. *Self-similar solutions for elastohydrodynamic cavity flow*. Proceedings of the Royal Society of London, Series A, Mathematical and Physical Sciences, 400:579–586, 1985.

[13] G.I. Barenblatt. *The mathematical theory of equilibrium cracks in brittle fracture*. Adv. appl. Mech., 7:55–129, 1962.

[14] A.D. Fitt, D.P. Mason, and E.A. Moss. *Group invariant solution for a pre-existing fluid-driven fracture in impermeable rock*. Z. Angew. Math. Phys., 58:1049–1067, 2008.

[15] A.G. Fareo and D.P. Mason. *A group invariant solution for a pre-existing fracture driven by power-law fluid in impermeable rock*. Comm Nonlinear Sci Numer Simulat, 18:3298–3316, 2013.

[16] A.G. Fareo and D.P. Mason. *Group invariant solution for a pre-existing fracture driven by power-law fluid in permeable rock*. International Journal of Modern Physics B. URL http://www.worldscientific.com/doi/abs/10.1142/S0217979216400105.

[17] A.M. Rubin. *Propagation of magma-filled cracks*. Annu. Rev. Earth Planet. Sci., 23:287–336, 1995.

[18] M.R.R. Kgatle and D.P. Mason. *Propagation of a linear hydraulic fracture with tortuosity*. International Journal of Non-Linear Mechanics, 61:39–53, 2014.

[19] Z. Zeng and R. Grigg. *A criterion for non-Darcy flow in porous media*. Transport in Porous Media, 63:57–69, 2006.

[20] J. Douglas Jr., P.J. Paes-Leme, and T. Giorgi. *Generalized Forchheimer flow in porous media*. Army High Performance Computing Research Center, 1993.

[21] J.S. Andrade Jr., U.M.S. Costa, M.P. Almeida, H.A. Makse, and H.E. Stanley. *Inertial effects on fluid flow through disordered porous media*. Physical Review Letters, 82:5249–5252, 1999.

[22] S.A. Holditch and R.A. Morse. *The effects of non-Darcy flow on the behavior of hydraulically fractured gas wells*. Journal of Petroleum Technology, 28:1–169, 1976.

[23] Y. Wu, B. Lai, J. L. Miskimins, P. Fakcharoenphol, and Y. Di. *Analysis of multiphase non-Darcy flow in a porous media*. Transport in Porous Media, 88:205–223, 2011.

[24] Z. Chai, B. Shi, J. Lu, and Z. Guo. *Non-Darcy flow in disordered porous media: A lattice Boltzmann study.* Computers and Fluids, 39:2069–2077, 2010.

[25] A.F. Miguel. *Non-Darcy porous media flow in no-slip and slip regimes.* Thermal Science, 16:167–176, 2012.

[26] P. Macini, E. Mesini, and R. Viola. *Laboratory measurements of non-Darcy flow coefficients in natural and artificial unconsolidated porous media.* Journal of Petroleum Science and Engineering, 77:365–374, 2011.

[27] P. Basak. *Analytical solutions for two-regime flows in well flow problems.* Journal of Hydrology, 38:147–159, 1978.

[28] D.J. Acheson. *Elementary Fluid Dynamics* . Clarendon Press, Oxford , 1990.

[29] R.B. Bird, R.C. Armstrong, and O. Hassager. *Dynamics of polymeric fluids.* John Wiley and Sons, Inc, New York, 1987.

[30] V.R. Tagirova. *Hydraulic fracture crack propagation driven by a non-Newtonian fluid.* Vestnik Moskovskogo Universiteta, Matematika Mekhanika, 64:33–41, 2009.

[31] P. Forchheimer. *Wasserbewegung durch boden.* Zeit. Ver. Deutsch. Ing., 45:1781–1788, 1901.

[32] M.R. Tek. *Development of a generalized Darcy equation.* Trans. AIME, 210:367–377, 1957.

[33] M.R. Tek, K.H. Coats, and D.L. Katz. *The effect of turbulence on flow of natural gas through porous reservoirs.* Trans. AIME, 225:799–806, 1963.

[34] J. Geertsma. *Estimating the coefficient of internal resistance in fluid flow through porous media.* Soc. Pet. Eng. J., 14:445–450, 1974.

[35] N.N. Smirnov and V.P. Tagirova. *Self-similar solutions of the problem of formation of a hydraulic fracture in a porous medium.* Izvestiya Rossiiskoi Akademii Nauk, 42:70–82, 2007.

[36] G. Bluman and S. Kumei. *Symmetries and Differential Equations.* Springer-Verlag, New York, 1989.

[37] G. Bluman and S. Anco. *Symmetries and Integration Methods for Differential Equations.* Springer-Verlag, New York, 2002.

[38] N.H. Ibragimov and R.L. Anderson. *One-parameter Transformation Groups.* CRC Handbook of Lie Group Analysis of Differential Equations, CRC Press, Boca Raton, In N.H.Ibragimov, editor, 1:Symmetries, Exact Solutions and Conservation Laws: 7–14, 1994.

[39] N.H. Ibragimov. *Elementary Lie Group Analysis and Ordinary Differential Equations.* John Wiley and Sons, Chichester, 1999.

[40] D.A. Mendelsohn. *A review of hydraulic fracture modelling - Part I: General concepts, 2D models and motivation for 3D modelling.* ASME J. Energy Resour. Technol, 106:369–376, 1984.

[41] A.D. Fitt, A.D. Kelly, and C.P. Please. *Crack propagation models for rock fracture in a geothermal energy reservoir.* SIAM Journal on Applied Mathematics, 55:1592–1608, 1995.

[42] R.P. Gillespie. *Integration.* Oliver and Boyd, Edinburgh, 1959.

[43] A.G. Fareo. *Group invariant solutions for a pre-existing fracture driven by a non-Newtonian fluid in permeable and impermeable rock.* PhD thesis, University of the Witwatersrand, Johannesburg, South Africa, 2013.

[44] D. Newman. *Turbulent hydraulic fracture described by Prandtl's mixing length.* MSc Dissertation, University of the Witwatersrand, 2016.

[45] P. Venkataraman and P. Rao. *Validation of Forchheimer's law for flow through porous media with converging boundaries.* Journal of Hydraulic Engineering, 126: 63–71, 2000.

[46] A. Montillet. *Flow through a finite packed bed of spheres: A note on the limit of applicability of the Forchheimer-type equation.* Journal of Fluids Engineering, 126: 139–143, 2004.

[47] S. Whitaker. *The Forchheimer equation: A theoretical development.* Transport in Porous Media, 25:27–61, 1996.

[48] K. R. Krishna and D. S. Murthy. *An experimental study on flow of water through porous media in laminar, transition and turbulent regime.* International Journal of Emerging Technology and Advanced Engineering, 3:559–569, 2013.

[49] L. Bloshanskaya, A. Ibragimov, F. Siddiqui, and M. Soliman. *Productivity Index for Darcy and pre-/post-Darcy Flow (Analytical Approach).* January 2016. URL https://www.researchgate.net/publication/287948950.

[50] E. Skjetne. *High-velocity flow in porous media.* PhD thesis, Norwegian University of Science and Technology, 1995.

[51] R. Ewing, R. Lazaros, S.L. Lyons, D.V. Papavassiliou, J. Pasciak, and G.X. Qin. *Numerical well model for non-Darcy flow.* Computational Geosciences, 3:185–204, 1999.

[52] J.G.I. Hellstrom and T.S. Lundstrom. *Flow through porous media at moderate Reynolds number.* 4th International Scientific Colloquium: Modelling for Material Processing, University of Latvia, Riga, Latvia, J 2006.

[53] H. Ma and W. Ruth. *The microscopic analysis of high Forchheimer number flow in porous media.* Transport in Porous Media, 13:139–160, 1993.

[54] S.C. Jones. *Using the inertial coefficient, β, to characterize heterogeneity in reservoir rock.* SPE Annual Technical Conference and Exhibition, 1987.

[55] C.E. Cooke. *Conductivity of fracture proppants in multiple layers.* Journal of Petroleum Technology, 25:1–101, 1973.

[56] H. Pascal, R.G. Quillian, and J Kingston. *Analysis of vertical fracture length and non-Darcy flow coefficient using variable rate tests.* PE Annual Technical Conference and Exhibition, 1980.

[57] D.W. Ruth and H. Ma. *On the derivation of the Forchheimer equation by means of the averaging theorem.* Transport in Porous Media, 7, 1992.

[58] S. Wang, Q. Feng, and X. Han. *A hybrid analytical/numerical model for the characterization of preferential flow path with non-Darcy flow.* PloS one, 8, 2013.

[59] J.P. Du Plessis and J.H. Masliyah. *Mathematical modeling of flow through consolidated isotropic porous media.* Transport in Porous Media, 3:145–161, 1988.

[60] F. Thauvin and K.K. Mohanty. *Network modeling of non-Darcy flow through porous media.* Transport in Porous Media, 31:19–37, 1993.

[61] S. Dimas and D. Tsoubelis. *SYM: A new symmetry-finding package for Mathematica.* The 10th International Conference in Modern Group Analysis, In N.H. Ibragimov, C. Sophocleous, and P.A. Damianou, editors, Nicosia, University of Cyprus:64–70, 2005. URL httpS://www.math.upatras.gr/~spawn.